



UNIVERSIDAD DE INVESTIGACIÓN DE TECNOLOGÍA EXPERIMENTAL YACHAY

Escuela de Ciencias Físicas y Nanotecnología

TÍTULO: Conversion of Solar Radiation into Heat through Carbon Nanotubes with Potential Industrial Applications

Trabajo de integración curricular presentado como
requisito para la obtención
del título de Físico

Autor:

Huera Solórzano Ariel

Tutor:

Ph.D. Reinoso Jerez Carlos

Urququí, enero de 2022

SECRETARÍA GENERAL
(Vicerrectorado Académico/Cancillería)
ESCUELA DE CIENCIAS FÍSICAS Y NANOTECNOLOGÍA
CARRERA DE FÍSICA
ACTA DE DEFENSA No. UITEY-PHY-2022-00001-AD

A los 14 días del mes de enero de 2022, a las 09:00 horas, de manera virtual mediante videoconferencia, y ante el Tribunal Calificador, integrado por los docentes:

| | |
|---------------------------------------|---|
| Presidente Tribunal de Defensa | Dr. CHACON TORRES, JULIO CESAR , Ph.D. |
| Miembro No Tutor | Dr. CHIMBORAZO GUERRON, JOHNNY FABRICIO , Ph.D. |
| Tutor | Dr. REINOSO CARLOS , Ph.D. |

El(la) señor(ita) estudiante **HUERA SOLORZANO, ARIEL ALEXANDER**, con cédula de identidad No. **0603962077**, de la **ESCUELA DE CIENCIAS FÍSICAS Y NANOTECNOLOGÍA**, de la Carrera de **FÍSICA**, aprobada por el Consejo de Educación Superior (CES), mediante Resolución **RPC-SO-39-No.456-2014**, realiza a través de videoconferencia, la sustentación de su trabajo de titulación denominado: **CONVERSION OF SOLAR RADIATION INTO HEAT THROUGH CARBON NANOTUBES WITH POTENTIAL INDUSTRIAL APPLICATIONS**, previa a la obtención del título de **FÍSICO/A**.

El citado trabajo de titulación, fue debidamente aprobado por el(los) docente(s):

| | |
|-------------------|--|
| Tutor | Dr. REINOSO CARLOS , Ph.D. |
| Co - Tutor | Dr. MEDINA DAGGER, ERNESTO ANTONIO , Ph.D. |
| Co - Tutor | MSC CORREDOR GONZALEZ, LUIS GERARDO |

Y recibió las observaciones de los otros miembros del Tribunal Calificador, las mismas que han sido incorporadas por el(la) estudiante.

Previamente cumplidos los requisitos legales y reglamentarios, el trabajo de titulación fue sustentado por el(la) estudiante y examinado por los miembros del Tribunal Calificador. Escuchada la sustentación del trabajo de titulación a través de videoconferencia, que integró la exposición de el(la) estudiante sobre el contenido de la misma y las preguntas formuladas por los miembros del Tribunal, se califica la sustentación del trabajo de titulación con las siguientes calificaciones:

| Tipo | Docente | Calificación |
|--------------------------------|---|--------------|
| Miembro Tribunal De Defensa | Dr. CHIMBORAZO GUERRON, JOHNNY FABRICIO , Ph.D. | 9,2 |
| Presidente Tribunal De Defensa | Dr. CHACON TORRES, JULIO CESAR , Ph.D. | 10,0 |
| Tutor | Dr. REINOSO CARLOS , Ph.D. | 9,9 |

Lo que da un promedio de: **9.7 (Nueve punto Siete)**, sobre 10 (diez), equivalente a: **APROBADO**

Para constancia de lo actuado, firman los miembros del Tribunal Calificador, el/la estudiante y el/la secretario ad-hoc.

Certifico que *en cumplimiento del Decreto Ejecutivo 1017 de 16 de marzo de 2020, la defensa de trabajo de titulación (o examen de grado modalidad teórico práctica) se realizó vía virtual, por lo que las firmas de los miembros del Tribunal de Defensa de Grado, constan en forma digital.*

HUERA SOLORZANO, ARIEL ALEXANDER
Estudiante



Dr. CHACON TORRES, JULIO CESAR , Ph.D.
Presidente Tribunal de Defensa



Firmado electrónicamente por:
JULIO CESAR
CHACON TORRES

Dr. REINOSO CARLOS , Ph.D.
Tutor



Firmado electrónicamente por:
CARLOS ALBERTO
REINOSO JEREZ

Dr. CHIMBORAZO GUERRON, JOHNNY FABRICIO , Ph.D.
Miembro No Tutor



Firmado electrónicamente por:
**JOHNNY FABRICIO
CHIMBORAZO
GUERRON**

CIFUENTES TAFUR, EVELYN CAROLINA
Secretario Ad-hoc


EVELYN
CAROLINA
CIFUENTES TAFUR

Firmado digitalmente por
EVELYN CAROLINA
CIFUENTES TAFUR
Fecha: 2022.01.14 10:06:44
-05'00'

AUTORÍA

Yo, **ARIEL ALEXANDER HUERA SOLÓRZANO**, con cédula de identidad 0603962077, declaro que las ideas, juicios, valoraciones, interpretaciones, consultas bibliográficas, definiciones y conceptualizaciones expuestas en el presente trabajo; así cómo, los procedimientos y herramientas utilizadas en la investigación, son de absoluta responsabilidad del autor del trabajo de integración curricular. Así mismo, me acojo a los reglamentos internos de la Universidad de Investigación de Tecnología Experimental Yachay.

Urcuquí, enero de 2022.



Ariel Alexander Huera Solórzano
CI: 0603962077

AUTORIZACIÓN DE PUBLICACIÓN

Yo, **ARIEL ALEXANDER HUERA SOLÓRZANO**, con cédula de identidad 0603962077, cedo a la Universidad de Investigación de Tecnología Experimental Yachay, los derechos de publicación de la presente obra, sin que deba haber un reconocimiento económico por este concepto. Declaro además que el texto del presente trabajo de titulación no podrá ser cedido a ninguna empresa editorial para su publicación u otros fines, sin contar previamente con la autorización escrita de la Universidad.

Asimismo, autorizo a la Universidad que realice la digitalización y publicación de este trabajo de integración curricular en el repositorio virtual, de conformidad a lo dispuesto en el Art. 144 de la Ley Orgánica de Educación Superior

Urcuquí, enero de 2022.



Ariel Alexander Huera Solórzano
CI: 0603962077

Acknowledgements

When I was 6 years old, once I asked my mother how many meters there are from the earth to the sun, she looked at me and with uncertainty she asked me the following question: why are you asking me that? For along time I do not understand this question, until today, while I was writing these lines I found the answer. I asked that because within me lies an incredible passion to learn, to create and for marvel me at the beauty of our world. That is the same passion that brought me to Yachay and the one that encouraged me to study physics, but above all, the one that has led me through the most incredible people and experiences, therefore, today that one stage ends and another begins, I want to give the thank you for everything this big trip gave me.

Thank you, because the distance brought me closer to my family, to my mother Lourdes, who is the reason for everything and to whom I dedicate this achievement. I love you mom. Also, thank you for the great family that Yachay gave me, Samantha, Robert, Juan, Emerson, Adrian, Andres, Jhon, Mayra and Ricardo, really thank you guys for making this trip so special, it was like all good trips, exciting at the start, amazing in the middle and tiring at the end. Also to my professors, many, many thanks for all your effort and dedication, especially thanks to Carlos, Ernesto and Luis for everything you taught me during this process. For you I love science and I am determined to use it for the good of our society. And finally, to the entire Yachay family for showing me that we can achieve great things if we work together. I hold you all in my heart and I hope to see you again in the construction of your dreams.

Ariel Huera

Resumen

Las nanoestructuras de carbono y en especial los nanotubos de carbono se han vuelto de gran importancia debido a sus sobresalientes propiedades en áreas como la ciencia e ingeniería. En este trabajo se han identificado aplicaciones relacionadas a su alta absorción en regiones del espectro visible e infrarrojo. Esta propiedad puede ser usada para recolectar energía solar para e.g. calentar agua en el sector industrial, una forma de reducir el consumo de combustibles fósiles. El presente trabajo muestra exitosamente una nueva técnica para fabricar nanotubos de carbono multipared o MWCNTs (por sus siglas en inglés), directamente sobre una superficie de aluminio texturizada, usando el proceso de deposición química de vapor o CVD (por sus siglas en inglés). La síntesis se logró a una baja temperatura de 650 [°C] y su caracterización fue realizada usando espectroscopia Raman, la cual confirma la presencia de MWCNTs con sus principales picos en 1346 [cm⁻¹], 1582 [cm⁻¹], y 2692 [cm⁻¹] para la banda D, banda G, y banda 2D respectivamente. La microscopia electrónica de barrido o SEM (por sus siglas en inglés) fue usada para explorar el material sintetizado y la morfología presentó una estructura en forma de algodón depositada sobre la superficie de aluminio. Fotoelectrón de rayos X o XPS (por sus siglas en inglés) probó la presencia de enlace de carbono con hibridación sp² y sp³ relacionados con estructuras de nanotubos de carbono y de carbón amorfo. Finalmente, el material fabricado fue probado bajo exposición directa al sol y los resultados muestran que nuestro dispositivo calienta, en promedio, 3.44 [°C] más que otros materiales comparados. También se realizó un análisis de exergía basado en el contraste de temperatura logrado y los resultados son muy prometedores para superficies más grandes. El contraste de temperatura se puede incrementar mejorando la estructura de los CNTs y la capacidad calorífica del sustrato usado. Finalmente, este trabajo abre la posibilidad de usar este material para varias aplicaciones relacionadas a las energías renovables, las cuales pueden ser implementadas en Ecuador en un corto tiempo.

Palabras clave: Activación de superficie, nanotubos de carbono, CVD, exergía, calefacción solar, absorbedor solar.

Abstract

Carbon nanostructures and specifically carbon nanotubes have become of high importance due their outstanding properties for many different areas in science and engineering. In this work has been identified an application related to their ultra-high absorbance in the region of visible and infrared light. This property can be used to harvest solar energy to e.g. heat water for industrial processes, a path to reduce fuel consumption. The presence work successfully shows a new technique to fabricate MWCNTs directly on an activated aluminum surface using the CVD procedure. Low-temperature synthesis was achieved around 650 [°C] and their characterization was made by using Raman spectroscopy that confirms the presence of MWCNTs with their main signature at 1346 [cm⁻¹], 1582 [cm⁻¹], and 2692 [cm⁻¹] for D-band, G-band, and 2D-band correspondingly. Scanning electron microscopy was used to explore the synthesized material and morphology presenting cotton-like structures deposited on the Al surface. XPS proved the presence of sp², sp³ binding carbon hybridization related with carbon nanotubes and amorphous carbon structures. Finally, the fabricated materials were tested under direct sun exposure. The results show that our device heats, on average, 3.44 [°C] more than other materials compared. We perform an exergy analysis of the temperature contrasts achieved and results are very promising for up-scaling surface areas. Temperature contrasts can be increased by improving the CNT coverage and the heat capacities of the base substrate used. This research work opens the possibilities to use this material for several applications regarding the renewable energies that can be done in Ecuador in the very shortly.

Keywords: surface activation, carbon nanotubes, CVD, catalyst, exergy, solar heating, solar absorber.

Contents

| | |
|--|------------|
| List of Figures | xi |
| List of Tables | xvi |
| 1 Introduction | 1 |
| 1.1 Importance of the global energy transition: from conventional sources to sustainable sources | 1 |
| 1.2 Sun as a source of heat energy | 4 |
| 1.3 Heat capture technologies | 5 |
| 1.4 Problem statement | 6 |
| 1.5 General and specific Objectives | 6 |
| 1.5.1 General objective | 6 |
| 1.5.2 Specific objectives | 6 |
| 2 Theoretical/Experimental background | 7 |
| 2.1 Theoretical background | 7 |
| 2.1.1 Surface activation of aluminum (sa-Al) | 7 |
| 2.1.2 Carbon nanotubes (CNTs) | 9 |
| 2.1.3 Thermal properties of CNTs | 12 |
| 2.1.4 Solar absorption properties of CNTs | 13 |
| 2.1.5 Blackbody (BB) physics | 15 |
| 2.1.6 BB-CNTs; emission spectrum and thermal losses | 16 |
| 2.1.7 Theoretical exergy analysis | 17 |
| 2.2 Experimental background | 19 |
| 2.2.1 Making BB-CNTs; the CVD technique | 19 |
| 2.2.2 BB-CNTs; benefits and problems for practical applications | 20 |
| 2.2.3 Characterization techniques | 21 |

| | | |
|----------|---|-----------|
| 3 | Methodology | 27 |
| 3.1 | Aluminum substrate evolution | 27 |
| 3.1.1 | Preparation of aluminum substrate | 27 |
| 3.1.2 | Surface activation of aluminum (sa-Al) | 28 |
| 3.1.3 | Rinsed of sa-Al | 29 |
| 3.1.4 | Catalyst deposition | 29 |
| 3.1.5 | Calcination process | 31 |
| 3.1.6 | Low-temperature CNTs synthesis | 31 |
| 3.2 | CNTs characterization | 32 |
| 3.3 | Measuring heating of different BB reference materials | 33 |
| 3.3.1 | Temperature system setup | 34 |
| 3.3.2 | Sensors temperature calibration | 35 |
| 4 | Results & Discussion | 39 |
| 4.1 | Carbon nanotubes over surface-activated aluminum (CNT/sa-Al) | 39 |
| 4.1.1 | Surface activation of aluminum (sa-Al) | 40 |
| 4.1.2 | Rinsed of sa-Al and Catalyst deposition of Fe/Co nanoparticles | 43 |
| 4.1.3 | Low-temperature CNTs synthesis | 43 |
| 4.1.4 | Raman Spectroscopy characterization | 46 |
| 4.1.5 | Scanning Electron Microscopy (SEM) characterization | 48 |
| 4.1.6 | X-ray Photoelectron Spectrometer (XPS) characterization | 48 |
| 4.2 | Radiation heating results | 52 |
| 4.2.1 | Part 1: "(5%)CNTs-bap/sa-Al" vs "(1%)CNTs-bap/sa-Al" | 52 |
| 4.2.2 | Part 2: "CNTs-bap/sa-Al", "bap/Al", "CNTs/sa-Al" and "bC/sa-Al" | 55 |
| 4.3 | Theoretical exergy analysis | 60 |
| 5 | Conclusions & Outlook | 63 |
| 5.1 | Synthesis of solar absorber material or CNTs/sa-Al | 63 |
| 5.2 | Characterization process | 64 |
| 5.3 | Solar-thermal analysis | 64 |
| 5.4 | Theoretical exergy analysis | 65 |
| 5.5 | Outlook | 65 |
| A | Arduino code used in the temperature data collection | 67 |
| B | Temperature references values | 69 |
| C | Peak-o-Math data | 71 |
| D | Variation of cloudiness at the test side | 73 |

Bibliography

75

Abbreviations

81

List of Figures

| | | |
|------|--|----|
| 1.1 | Correlation between global temperature and CO ₂ levels during the last millennium. Adapted figure from ¹ | 2 |
| 1.2 | Global CO ₂ emissions (in tons) by fuel type, from the beginning of Industrial Revolution to 2018. Adapted figure from ² | 3 |
| 1.3 | World energy consumption in 2014. The data used to perform this graph was taken from the International Energy Agency (IEA). Adapted figure from ³ | 4 |
| 1.4 | Solar collector types; stationary and tracking ³ | 5 |
| 2.1 | Al substrate; (a) without the treatment and (b) with the surface activated treatment. | 8 |
| 2.2 | Computer-generated images of (a) SWCNTs and (b) MWCNTs. Adapted figure from ⁴ | 9 |
| 2.3 | (a) 2D graphene sheet and the chiral vectors for computer-generated images of SWCNTs; (b) zig-zag type [m = 0], (c) helical type [n ≠ m] and (d) armchair type [n = m]. The numbers in parenthesis are the chiral indices ⁴ . Modified graph. | 10 |
| 2.4 | Stone-Wales defects on CNTs structure; (a) 5-7-7-5 defect and (b) 5-8-5 defect. Modified picture ⁵ | 10 |
| 2.5 | Vacancy defects in CNTs structure; (a) Mono-vacancy and (b) Di-vacancy. | 11 |
| 2.6 | Solar radiation is absorbed and reflected by CNTs, besides its emittance generated when the system heats up. | 14 |
| 2.7 | Blackbody (BB) radiation spectra (dashed lines) and near-perfect blackbody radiation from VA-CNTs sample (solid curves) as a function of the wavelength for several temperatures. Modified graphic taken from ⁶ | 16 |
| 2.8 | CVD technique; (a) external scheme and (b) internal mechanism. | 19 |
| 2.9 | Schematic view of XPS characterization technique. | 21 |
| 2.10 | Typical setup for Raman spectrometer with a laser attached to a microscope ⁷ . Modified graph. | 23 |
| 2.11 | The three energy level diagram of Raman scattering ⁸ | 23 |
| 2.12 | Scanning Electron Microscope (SEM); (a) scheme of the instrumentation ⁹ , (b) signals generated on the sample by the primary electrons ¹⁰ and (c) SEM images of CNTs film ¹¹ . Modified graph. | 25 |

| | | |
|------|---|----|
| 3.1 | Surface structural evolution of the Al substrate; (a) process flow diagram and (b) schematics ¹² . (1) Preparation of Al sheet, (2) surface activation of Al, (3) rinsed of sa-Al, (4) catalyst deposition of Fe/Co nanoparticles (NPs), (5) calcination process and (6) CNTs synthesis. Modified graph. | 27 |
| 3.2 | Surface activation process (part 1); (a) Al sheet, (b) side view, and (c) top view of the system. | 28 |
| 3.3 | Surface activation process (part 2); Al sheet (a) size, (b) immersed in the 10% NaCl aqueous solution, (c) during the bath sonication treatment, (i) after 5 [min] and (ii) after 10 [min] of sonication process. | 29 |
| 3.4 | Rinsed and catalyst deposition process; sa-Al immersed in (a) deionized water (b) ethanol and (c) catalyst solution. | 30 |
| 3.5 | Substances used in this work; (a) for the 10% NaCl aqueous solution and (b) for the catalytic solution. | 30 |
| 3.6 | Calcination process of the sa-Al substrates loaded with the catalyst solution; (a) inside melting pots, (b) melting pots with sa-Al inside the muffle furnace, and sa-Al substrate (i) before and (ii) after the calcination. | 31 |
| 3.7 | CNTs synthesis; (a) CVD machine, (b) Al substrate before, and (c) after the synthesis. | 32 |
| 3.8 | Characterization equipment; (a) Phenon ProX Desktop SEM, (b) PHI VersaProbe III XPS, and (c) Horiba brand Raman spectra. | 32 |
| 3.9 | The 4 solar absorber devices compared in this work; (a) black anticorrosive paint [bap], (b) black carbon [bC], (c) CNTs-bap solution and (d) carbon nanotubes [CNTs]. (b, c and d) are over a surface-activated Al [sa-Al] while (a) is over an Al sheet without treatment. | 33 |
| 3.10 | Schematic representation of the materials used in the construction of the thermal insulating box. | 34 |
| 3.11 | The general scheme of the system used to perform the thermal analysis of the material proposed in this work (CNTs/sa-Al) and other 3 solar absorber devices. | 35 |
| 3.12 | Real thermal analysis system; (a) thermal insulating box and (b) general system. | 35 |
| 3.13 | Temperature measurements of boiling water, using the 5 temperature sensors during 4 [min]. | 36 |
| 4.1 | Surface structural evolution of the Al substrate in (a) and (b); (1) preparation of Al sheets, (2) surface activation of Al, (3) rinsed of sa-Al, (4) catalyst deposition of Fe/Co NPs, (5) calcination process and (6) CNTs synthesis. | 39 |
| 4.2 | Sonication process results; (a) after 5 [min] and (b) after 10 [min] of sonication time. | 41 |
| 4.3 | Surface activation process. Part 1: Morphology of Al substrate subjected to 0 wt %, 5 wt % and 10 wt % NaCl aqueous solution, during 12, 24, 36, 48 [h] in each concentration respectively. Part 2: Morphology of Al substrate subjected to a 5 [min] of sonication process in 10 wt % NaCl aqueous solution and then soaked in the same solution during 1.5, 3, 6, and 12 [h]. | 42 |
| 4.4 | Comparison between: (a) Al substrate exposed to 10 wt % NaCl aqueous solution during 48 [h] without sonication treatment, (b) Al substrate subjected to a 5 [min] of sonication process in 10 wt % NaCl aqueous solution and then soaked in the same solution during 12 [h] and (c) Al substrate without any treatment. | 42 |
| 4.5 | Catalytic solution spilling out of the beaker due to the capillary effect of the surface-activated Al substrate. | 43 |

| | | |
|------|---|----|
| 4.6 | Part 1: Al substrates subjected to 5 [min] of sonication treatment with 12 [h] of time exposition to NaCl 10 wt % NaCl aqueous solution (a) uncalcined and (b) calcinated. Part 2: Al substrate subjected to calcination process after 5 [min] of sonication treatment with a time exposure to 10 wt % NaCl aqueous solution of (c) 12 [h] and (d) 3 [h]. | 45 |
| 4.7 | (RX "A", "B" and "C") Raman spectra of undefined carbon structure. RX "D" Raman spectrum of MWCNTs. | 46 |
| 4.8 | Lorentzian-curve fitting of RX "D" | 47 |
| 4.9 | SEM images of (a) surface-activated Al and of (b, c) CNTs. | 48 |
| 4.10 | (a,b) XPS spectra of the Al substrate without (a) and with (b) surface activation. (c, d) XPS spectra of surface-activated Al impregnated with the catalytic solution without (c) and with (d) calcination process. | 50 |
| 4.11 | High resolution XPS C1s core level presenting the main binding energies | 51 |
| 4.12 | Thermal analysis of surface-activated Al substrates covered with; 1 wt % CNTs vs 5 wt % CNTs black anticorrosive paint (bap) solutions. The shadow zone represents the data section used to find the average temperature differences between these two devices. | 53 |
| 4.13 | (a) Thermal analysis zoom of surface-activated Al substrates covered with; 1 wt % CNTs vs 5 wt % CNTs black anticorrosive paint (bap) solutions | 54 |
| 4.14 | Average of temperature differences between surface-activated Al substrates covered with; 1 wt % CNTs and 5 wt % CNTs black anticorrosive paint (bap), for each day. | 54 |
| 4.15 | Day 1: (a) thermal analysis of the 4 BB references used compared in this research, as well as, thermal analysis reference system (box). (b) represent a zoom of (a). The shadow zone represents the data section used to find the average temperature differences between the devices. | 57 |
| 4.16 | Day 2: (a) thermal analysis of the 4 BB references used compared in this research, as well as, thermal analysis reference system (box). (b) represent a zoom of (a). The shadow zone represents the data section used to find the average temperature differences between the devices. | 58 |
| 4.17 | Day 3: (a) thermal analysis of the 4 BB references used compared in this research, as well as, thermal analysis reference system (box). (b) represent a zoom of (a). The shadow zone represents the data section used to find the average temperature differences between the devices. | 59 |
| 4.18 | The exergy available due to the temperature difference between the two best BB coatings. Note that there can be up to 0.023 Watts per cm ² extra due to the temperature achieved by the best coating. | 61 |
| 4.19 | Exergy as a function of the temperature T in relation with the fixed temperature of T ₀ =25 C. | 61 |
| A.1 | Arduino code - part 1 | 67 |
| A.2 | Arduino code - part 2 | 68 |
| B.1 | Temperature measurements of frozen water. This data was used in the calibration process of the temperature sensors. | 69 |
| B.2 | Temperature measurements of water at room temperature. This data was used in the calibration process of the temperature sensors. | 70 |

| | | |
|-----|---|----|
| C.1 | Positions of D, G and 2D band peak of MWCNTs synthesized under the condition of reaction (RX) | |
| | "D" - part 1 | 71 |
| C.2 | Positions of D, G and 2D band peak of MWCNTs synthesized under the condition of reaction (RX) | |
| | "D" - part 2 | 72 |
| D.1 | Variation of cloudiness at the test side; (a) cloudy and (b) free-cloud | 73 |

List of Tables

| | | |
|-----|--|----|
| 2.1 | Summary and comparison of three most common CNTs synthesis methods. Adapted table from ¹³ . . . | 11 |
| 2.2 | Thermal conductivity of different CNTs structures, calculated by physical simulations. Adapted table from ¹⁴ | 13 |
| 2.3 | Energy and Exergy differences. Adapted table from ¹⁵ | 17 |
| 2.4 | System A surrounded by the environment A_0 that is assumed to be much larger than the system. Adapted table from ¹⁵ | 18 |
| 2.5 | Summary of the articles reporting CVD production of carbon nanoarchitectures. Adapted table from ¹⁶ | 20 |
| 3.1 | Calibration factor process; at three temperature references the (a) average value of the 5 sensors temperature measures during 4 [min], (b) difference between the temperature sensor reference (S4) and the other temperature sensor, in the end, the average values are presented, these values were the calibration factors, and (c) the values of part (a) but with the calibration factors added. | 37 |
| 4.1 | Reaction conditions used to produce CNTs in the CVD machine. | 44 |
| 4.2 | XPS analysis data. | 51 |
| 4.3 | Summary of the thermal analyses performed during 3 day on CNTs-bap/sa-Al, bap/Al, CNTs/sa-Al and bC/sa-Al devices. | 60 |

Chapter 1

Introduction

1.1 Importance of the global energy transition: from conventional sources to sustainable sources

What would happen if humanity does not stop using hydrocarbon-related sources of energy? In 1896, the Swedish physicist, Svante Arrhenius, predicted, for the first time, that the increase of CO₂ in the Earth's atmosphere would also increase its temperature¹⁷. Since then, multiple investigations have confirmed this fact, one of them is the analysis of the polar caps. In other words, throughout time Earth has suffered a series of climatic changes which have been recorded at the poles of the planet, in the layers of ice that overlap year after year. Thus, by analyzing the concentration of CO₂ in the air bubbles trapped in the deeper layers of poles, we can determine the concentration of CO₂ that the Earth's atmosphere had hundreds of thousands of years ago. In this way, the deeper the ice layer that is analyzed, the more farther we access the past. On the other hand, the most recent investigation, such as the winner of half the Nobel Prize in Physics 2021, also confirms the increase of Earth's temperature caused by the increase of CO₂ in the atmosphere. This important recognition was awarded to Syukuro Manabe and Klaus Hasselmann "for the physical modelling of Earth's climate, quantifying variability and reliably predicting global warming" In conclusion all these investigations have confirmed 3 things: See figure 1.1.

1. The Earth's temperature is increasing.
2. The temperature and CO₂ concentration of the Earth's atmosphere are intrinsically related.
3. The concentration of CO₂ has suffered a sustained increase since the beginning of the Industrial Period.

The presence of CO₂ in the Earth's atmosphere is not intrinsically harmful, in fact, without the presence of this and other gases, the temperature of the Earth's surface would be about 18°C below zero¹⁸. In order to the Earth's atmosphere to maintain an average temperature of 14°C¹⁹, gases such as CO₂ retain part of the radiation from the sun. This phenomenon is known as the "Greenhouse effect", and it is easy to explain; the atmosphere is a layer

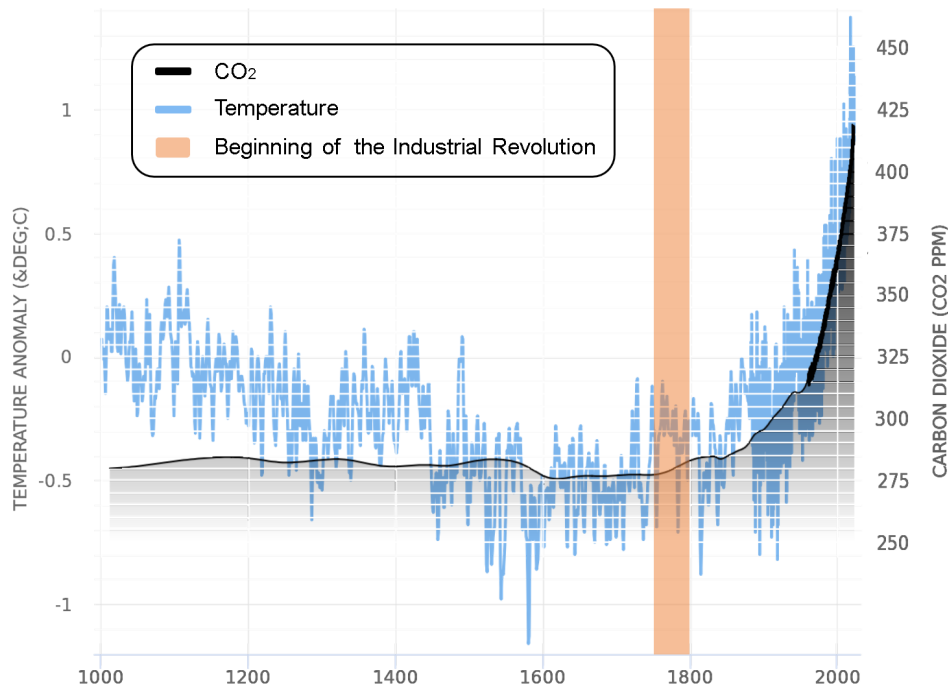


Figure 1.1: Correlation between global temperature and CO₂ levels during the last millennium. Adapted figure from¹.

surrounding the surface of the Earth that contains a large number of gases such as oxygen and nitrogen, but also others in lesser amounts such as ozone, noble gases, water vapor, methane, and CO₂. This latter gas allows visible radiation from the sun to pass so that it reaches the Earth's surface and heats up. This heating, in turn, causes infrared emission that in principle is sent back to the space. However, CO₂ is not transparent to these wavelengths of and it blocks it from leaving. As a consequence, this radiation is trapped in the Earth in form of heat.

The problem is that from the beginning of the industrial period, humans have been emitting large amounts of CO₂ into the atmosphere by burning fossil fuels in order to satisfy their energetic needs. This has caused that the concentration of CO₂ in the atmosphere exceeds the normal levels, in this way, a heating of the atmosphere is produced and if that is not reversed urgently, it will bring drastic changes for all life on Earth. In other words, humans are responsible for global warming and its consequences. Therefore and in an attempt to contribute to humanity's energy transition, this work presents a successful and viable alternative that helps reduce CO₂ emissions the overheat the Earth's surface.

To face this challenge in an intelligent way, first, it would be convenient to identify which is the main source of CO₂ emission, within this, coal is by far the main one, with 14.68 billion tons emitted into the atmosphere only in 2018². See figure 1.2. Then, it would be important to know which are the main energy sectors that demand coal and its purpose. Worldwide, the most energy-demanding sectors are the transport and industrial sectors³, being the latter

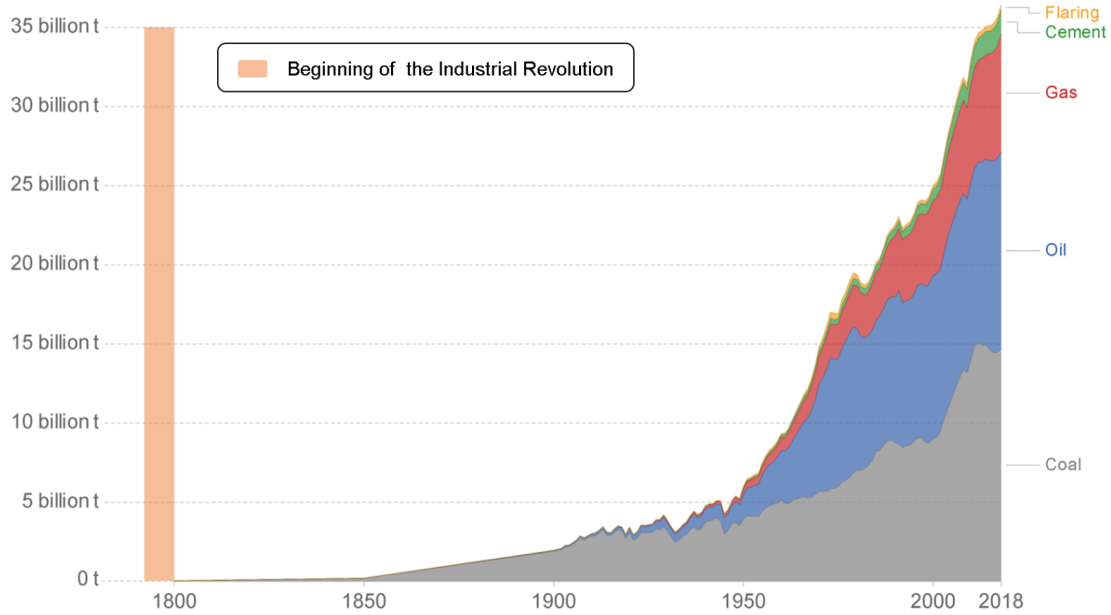


Figure 1.2: Global CO₂ emissions (in tons) by fuel type, from the beginning of Industrial Revolution to 2018. Adapted figure from².

the first one with 32% of world demand. Within this sector, 74% of the energy is used in the form of heat, which comes from different sources, but mainly from coal with 45% of the total supply. All these sources are reflected in figure 1.3.

In conclusion, it can be said that global warming is a consequence of high concentrations of CO₂ in the atmosphere. The responsibility for this is humanity, which has emitted enormous amounts of CO₂ to the atmosphere since the beginning of the Industrial Period, as a byproduct of its energy needs. In other words, the records derived from ice measurements show that the average global CO₂ concentration in the atmosphere for the pre-industrial period (1750 to 1800) was around 278 ppm. Now, in March 2021, levels have reached around 417 ppm, which means a increase of about 50% over the 1750-1800 average²⁰. Furthermore, one of the main sources of the sudden increase of the CO₂ concentration is the huge use of coal, by the Industrial Sector, for the generation of heat. Taking this into account, it is clear that humanity, for its own well-being, needs to generate and consume energy from cleaner sources for the environment. These are sources that emit small to no amounts of CO₂, including both production (making materials for the technology) and implementing (using the technology) stages of the energy conversion mechanism. In addition to this, this work strongly recommends to those who want to have a greater impact on the global transition to more sustainable energies, to focus on the most demanded sectors and forms of energy, such as the industrial sector and energy in the form of heat that these sectors require.

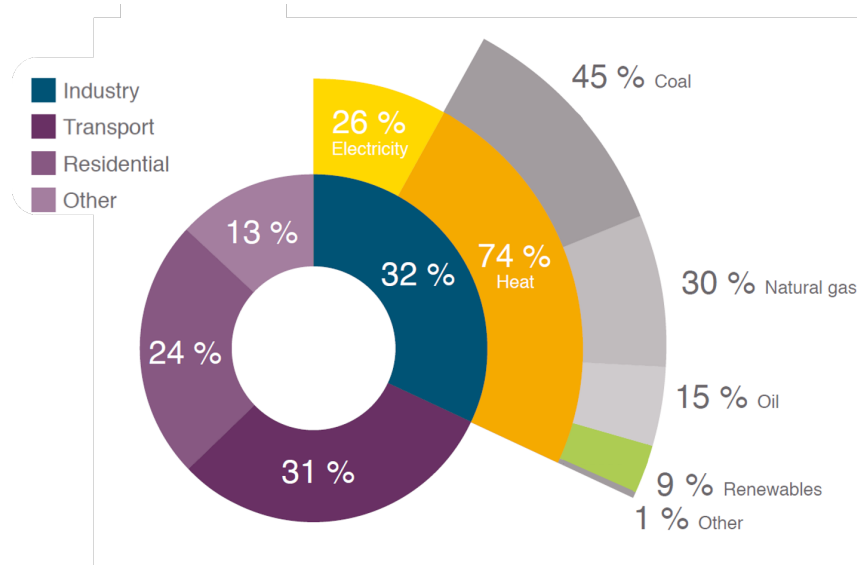


Figure 1.3: World energy consumption in 2014. The data used to perform this graph was taken from the International Energy Agency (IEA). Adapted figure from³.

1.2 Sun as a source of heat energy

"The United Nations Development Programme in its 2000 World Energy Assessment found that the annual potential of solar energy was 1,575–49,837 Exajoules (EJ). This is several times larger than the total world energy consumption, which was 559.8 EJ in 2012"²¹. This is a huge amount of energy, in fact theoretically, the sun, in an hour and a half, gives us more energy (480 EJ) than the world energy consumption in 2001 (430 EJ)²², and it will continue to do so for the next 5 billion years. Therefore, it can be said that the sun is an almost inexhaustible source of energy that humans can use to satisfy their needs. How to harness this energy nevertheless is non-trivial because of efficiencies of conversion, use of Earth's surface for energy capture, and variability of the incoming radiation due to atmospheric conditions.

In order to transform solar radiation into other forms of energy, like electricity or heat, different technologies have been developed during the last century. Within these technologies, the main ones are photovoltaic, which transforms the sun's energy into electricity, and solar-thermal, which transforms the sun's energy into heat. For the purpose of this work, solar-thermal has special importance, in fact, this report talks about how to convert solar radiation into usable heat. The aim is that the sun's energy in form of heat can be used as an alternative to the conventional sources of energy in the industrial sector.

1.3 Heat capture technologies

Currently, in the industrial sector, the main technology used in order to transform solar radiation into usable heat are solar collectors. Solar collectors are systems that concentrate solar radiation into a specific substance with the aim to increase its temperature. Following, this substance transfers the heat energy to the system of interest. The efficiency at the time to absorb solar energy depends on the type of solar collector, in this sense, these devices can be divided into two types; stationary and tracking, see figure 1.4. In stationary ones are the flat plate collectors, vacuum tube collectors with and without compound parabolic concentrators (CPC). On the other hand, in the tracking ones are parabolic, linear Fresnel, and concentrating dish collectors. The main difference between these two types is the temperature, while the stationary ones are made for low and medium temperatures, which means lower than 150 [°C], the tracking ones are made for high temperatures, which means from 150 to 400 [°C] or more. Furthermore, each type of solar collector is designed to absorb the shorter wavelengths of solar radiation (0.3 - 2 μm) and to prevent heat loss in form of infrared radiation²³.

Although this kind of technology has been developed since the 1760s, today, almost all solar collectors use the same kind of materials and the same operation principle used many years before. Possibly this is due to the resistance in the industrial sector for investing in new technologies because of the large investment and risk involved. In consequence, common and old technologies are still used and the transition to cleaner and sustainable energies is slow. Therefore, in this work, another type of material is proposed in order to improve the absorption of solar radiation and its subsequent conversion into heat.

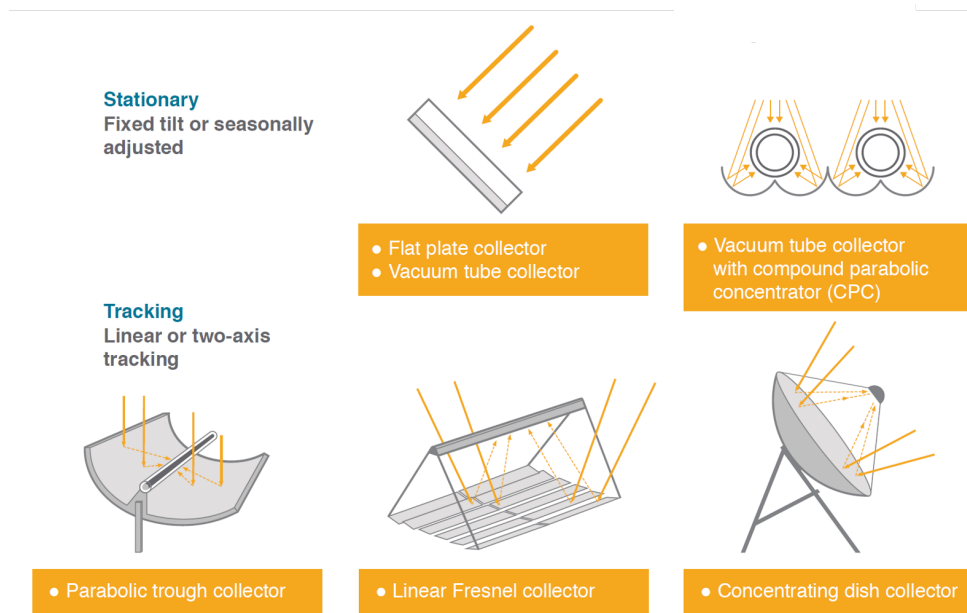


Figure 1.4: Solar collector types; stationary and tracking³.

A material whose physical and chemical properties make an excellent candidate for this kind of application are Carbon Nanotubes (CNTs) over surface activated (textured) aluminum or CNTs/sa-Al.

1.4 Problem statement

Global warming is possibly the biggest and the most critical challenge of our time. In fact, according to The Intergovernmental Panel on Climate Change (IPCC) of the UN, humanity only has until 2030 to take action and avoid an irreversible climate catastrophe²⁴. Although many sectors contribute to increasing the temperature of the Earth, such as agriculture, transport, and industrial, they all have something in common: the need for energy. This means that humanity needs a quick transition that allows using cleaner and safer sources of energy. With this in mind, renewable energies offer an attractive and convenient solution to achieve this aim because it is free, abundant, and clean. In this work, we will focus on a specific mechanism for converting solar radiation into heat to contribute to this global call. This work proposes to use a carbon-metal device designed to harness the largest range of the spectral emission of the sun and the spectral windows of the atmosphere to absorb the most significant amount of solar radiation. Chemical vapor deposition (CVD) to synthesize carbon nanotubes and a surface-activated process will be used to build the device. A thermodynamic analysis will be performed to assess the device's capacity for producing work (exergy) on the basis of the temperature contrast achieved with the environment.

1.5 General and specific Objectives

1.5.1 General objective

Contribute to the global energy transition towards clean and renewable energy sources, using the CVD synthesis technique to build a solar absorber material that transforms solar radiation into usable heat for the industrial sector. This material will be based on carbon nanotubes over a surface-activated aluminum (CNTs/sa-Al).

1.5.2 Specific objectives

- Synthesize a solar absorber material based on carbon nanotubes over a surface-activated aluminum substrate (CNTs/sa-Al).
- Determine the structural properties of the material through the characterization techniques; Raman, Scanning Electron Microscopy (SEM) and X-ray Photoelectron Spectrometer (XPS).
- Perform a solar-thermal analysis between the device proposed in this work (CNTs/sa-Al) and other three solar absorbers; black carbon over surface-activated aluminum (bC/sa-Al), black anticorrosive paint over aluminum (bap/Al) and carbon nanotubes black anticorrosive paint solution over surface-activated aluminum (CNTs-bap/sa-Al).
- Execute a theoretical exergy analysis to establish the efficiency of CNTs material.

Chapter 2

Theoretical/Experimental background

The first step to producing devices with optimal radiation absorbing properties is to understand what one does to emulate/approximate a black-body. An ideal black-body absorbs in all frequencies, which is convenient for absorbing radiation from the sun (a black-body to a good approximation) avoiding reflectivity. The most recent strategies for doing this is by creating a light trap, that like a cavity, lets in radiation and minimizes light reflection that leads to no heating. Trapping of light enables absorption/excitation processes some of which can re-emit or convert this excitation to heating (phonons) of the appropriate substrate. Thus this work seeks to achieve the highest possible temperature in order to obtain the highest exergy, or heat available for work. With this in mind and in order to get the best results, a device based on carbon nanotubes in form of a brush over a well textured Al substrate is built in this work. CNTs in form of a brush emulate a light trap while a textured Al substrate, allows a greater growth of CNTs over it. In this sense, this chapter was developed as follows: First, in the theoretical section, the surface activation process of Al is described, as well as, the general, thermal and solar features of CNTs. Then, the physics behind blackbody are studied. Also, the theoretical efficiency model (exergy) to analyze the device was performed. On the other hand, in experimental section, some important features about the synthesis of the devices and the characterization techniques are briefly discussed.

2.1 Theoretical background

2.1.1 Surface activation of aluminum (sa-Al)

Surface activation is a chemical process for the elimination of the alumina (passive oxide layer) and the formation of nanopyramidal structures on the Al surface, (see figure 2.1). This enables high-efficiency catalysis of well structured carbon nanotubes and the direct integration of the CNTs into the metal with flexible free-form configurations. The aforementioned proposal is a solution to the passive oxide layers on metal substrates that impose remarkable interfacial resistance for electron and phonon transport¹². Furthermore, the CNT-metal architecture facilitates a free energy carrier transport pathway and blocks the reformation of the passive oxide layer¹².

Aluminum is the third most common element found on the earth's surface, this feature makes it a cheap material and therefore, a very interesting option for the industrial sector. Notwithstanding, for the development of this work, aluminum has some pros and cons for the objective of this work summarized below:

Advantages

- Density: Aluminum has a low density of $2812 \text{ [kg/m}^3\text{]}$,
- Thermal conductivity: It is a good thermal conductor with thermal conductivity of $237 \text{ [W/m}\cdot\text{K]}$.
- Reflectance: It reflects very well the electromagnetic radiation of the visible spectra. This is an advantage because when the incident light is not absorbed, this feature gives the device a second chance to absorb reflected light.

Disadvantages

- Melting point: It has a low melting point of $660 \text{ [}^\circ\text{C]}$
- Chemical properties: It reacts with the atmosphere's oxygen forming a thin layer of alumina, which protects the material from corrosion.
- Reflectance: It reflects very well the electromagnetic radiation of the thermal spectra. This is an disadvantage because if the goal is to heat some substance under the device, the thermal radiation will not be able to reach the substance and therefore the efficiency of the device will be affected.

Aluminum is an interesting material with some advantages like low density, which enables low weight devices, also, it has a good thermal conductivity, which allows efficiently using the generated heat. Finally, its good reflectant properties in the visible spectrum make for multiple scattering scenarios that allow incoming radiation to be absorbed on less reflecting components of the assembly (see figure 2.6). In contrast, its low melting point creates difficulties at the time to synthesize CNTs over it, also the surface-activated process eliminates the alumina from its surface, making that aluminum lose its anti-corrosive property, ultimately, its reflectant properties in the thermal spectrum could increase the heat losses of the system. In conclusion, this work makes use of the advantages of aluminum and proposes some alternatives to overcome the disadvantages.

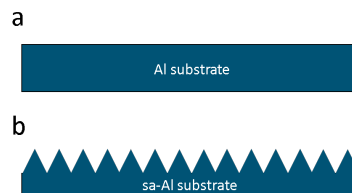


Figure 2.1: Al substrate; (a) without the treatment and (b) with the surface activated treatment.

2.1.2 Carbon nanotubes (CNTs)

Sumio Iijima, one of the principal discoverers of carbon nanotubes (CNTs) said in 2002 that; "Carbon nanotubes have drawn tremendous interest from fields ranging from condensed-matter physics to chemistry, and from both academia and industry, because of the unique properties enabled by their nanoscale structure"⁴. All these features give nanotubes extraordinary mechanical, electrical, and thermal properties. However, for this work, the latter one is analyzed in more detail. In addition, since the discoveries of Iijima, the study of CNTs has increased enormously and today it is possible to categorize their properties according to the following principal features:

- **Shape:** Single-Wall Carbon Nanotubes (SWCNTs) and Multi-Wall Carbon Nanotubes (MWCNTs). See figure 2.2.

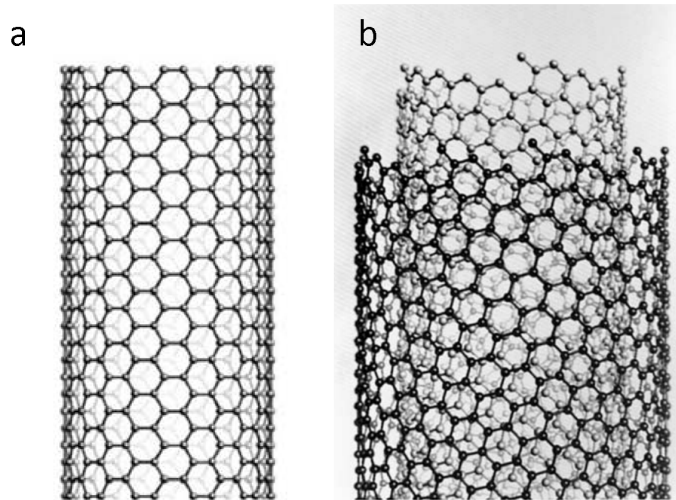


Figure 2.2: Computer-generated images of (a) SWCNTs and (b) MWCNTs. Adapted figure from⁴.

- **Structure or chirality:** A CNT is a graphene sheet that can be rolled in many different ways that satisfy periodic boundary conditions and can be described by their chiral vector $C = na_1 + ma_2$ where a_1 and a_2 are the base cell vectors of graphene while n and m are the chiral indices. See figure 2.3.
- **Diameter:** The diameter also depends on the chiral indices and follows the equation 2.1 where $a = 0.246$ [nm] while n and m are the chiral indices. Depending on the number of layers, the inner diameter of MWCNTs goes from 0.4 [nm] up to a few nanometers and the outer diameter varies characteristically from 2 [nm] up to 30 [nm]. On other hand, SWCNTs diameters differ from 0.4 to 3 [nm]¹³.

$$d = \frac{a}{\pi} \sqrt{n^2 + nm + m^2}. \quad (2.1)$$

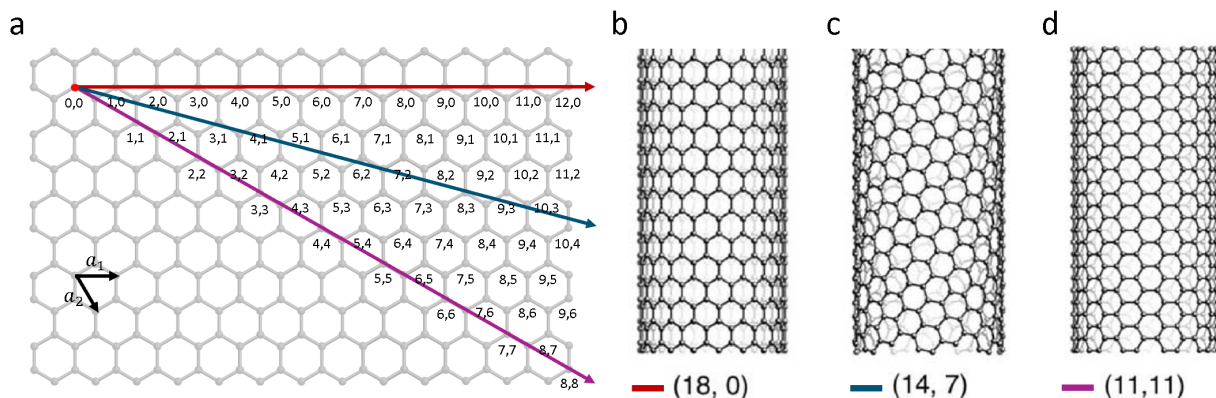


Figure 2.3: (a) 2D graphene sheet and the chiral vectors for computer-generated images of SWCNTs; (b) zig-zag type [$m = 0$], (c) helical type [$n \neq m$] and (d) armchair type [$n = m$]. The numbers in parenthesis are the chiral indices⁴. Modified graph.

- **Functionalization:** When CNTs are processed, they exhibit a bundle arrangement due to their strong intermolecular $\pi - \pi$ interactions. In consequence, covalent and non-covalent functionalizations are usually carried out for their dispersion and individualization²⁵.
- **Defects and Vacancy:** CNTs have a well-defined theoretical structure, however, when they are synthesized, some structural defects, intrinsic from the growth process, appear. Then, the defects can be divided into two main categories; the first one is known as Stone-Wales structural defects (S-W) structural defects, and it forms when four hexagons became two heptagons and two pentagons. This defect is called 5-7-7-5 defect. See figure 2.4a. Another type of S-W defect is created when an atom is removed from a pentagon structure and new bonds are formed. This defect is known as 5-8-5 structural defect. See figure 2.4b. The second one is known as Vacancy defect and it is produced when an atom is missing in the CNT structure and no new bonds are created. See figure 2.5²⁶.

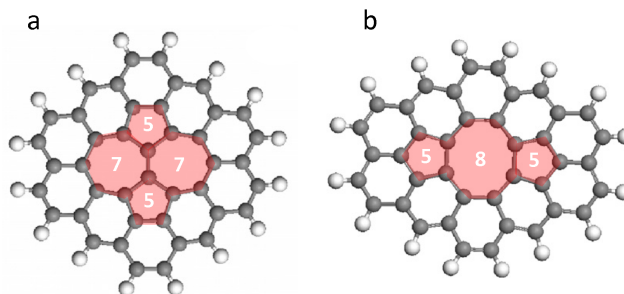


Figure 2.4: Stone-Wales defects on CNTs structure; (a) 5-7-7-5 defect and (b) 5-8-5 defect. Modified picture⁵.

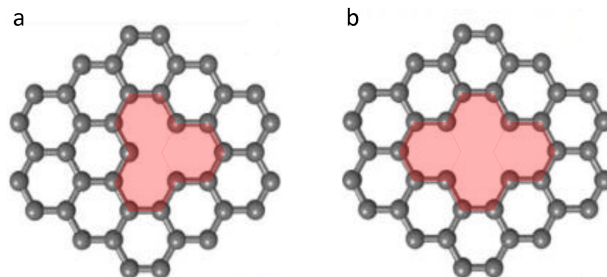


Figure 2.5: Vacancy defects in CNTs structure; (a) Mono-vacancy and (b) Di-vacancy.

- **Length:** In CNTs, the length is typically much larger than its diameter.
- **Synthesis technique:** The process of synthesis impacts the shape, number of defects in the crystalline network as well as on the contaminants present in the CNTs. Some of these synthesis techniques are Chemical Vapor Deposition (CVD), Electric arc discharge, and Laser ablation methods. See table 2.1

| Method | Arc discharge | Laser ablation | CVD |
|----------------|--|--|---|
| Yield rate | >75% | >75% | >75% |
| SWCNT MWCNT | Both | Both | Both |
| Advantage | Simple, inexpensive, high-quality nanotubes | Relatively high purity, room-temperature synthesis | Simple, low temperature, high purity, large-scale production, aligned growth possible |
| Disadvantages | High temperature, purification required, tangled nanotubes | Method limited to the lab scale, crude product purification required | Synthesized CNTs are usually MWCNTs, defects |

Table 2.1: Summary and comparison of three most common CNTs synthesis methods. Adapted table from¹³.

Multi-walled carbon nanotubes (MWCNTs)

Based on the bibliography, the expected results will be MWCNTs, therefore, in this section a deed analysis of these carbon structures in performed. Basically, multi-walled nanotubes consist of multiple graphene layers rolled. The number of nanotubes that are within a MWCNT can vary from as little as 3, to over 20. On the other hand, this structures can be described through two models, the Russian Doll model, which says that graphene sheets are arranged in concentric cylinders, while the Parchment model says that a single graphene sheet is rolled around itself, like a rolled newspaper. The Russian Doll model is more commonly observed. In addition, the internal distance in multi-walled nanotubes is close to the distance between graphene layers in graphite²⁷.

On the other hand, just like SWCNTs, MWCNTs are still classed as a 1-dimensional form of carbon and exhibit exceptional electrical, thermal, and mechanical properties. However, due to the increased number of walls, there is a higher probability of defects being present compared to single-walled nanotubes, resulting in reduced performances. These disadvantages are offset by the increased dispersability of MWCNTs, and the reduced cost in synthesis and purification of these materials²⁸.

Each MWCNT consists of some single-walled nanotubes held mostly by van der Waals forces, this is interesting because allow the individual cylinders of MWCNTs easily slide or rotate with respect to one another, forming near ideal linear and rotational nanobearings²⁹. The telescopic motion ability of inner shells and their unique mechanical properties permit to use multi-walled nanotubes in many application such as a improve the mechanical properties of a material, or to improve the electrical properties of a material. MWCNTs can be produced in high quantities and are easier to purify (in comparison to single walled and double-walled nanotubes). This makes their production costs significantly lower, and is a reason for their adoption in multiple areas of scientific research²⁸.

2.1.3 Thermal properties of CNTs

The extremely high thermal conductivity through a CNT is often considered to be dominated by the phonon conduction mechanism in the strong carbon sp^2 bond network of its walls^{14,30}. Therefore, depending on their structure, form, and method of synthesis, the thermal conductivity of CNTs varies significantly¹⁴. For example, from a theoretical thermal conductivity of 6600[W/m·k]³¹ in SWCNTs up to below 0.1[W/m·k] in MWCNTs¹⁴ (compare the last values with 237[W/m·k] and 372[W/m·k] for aluminum and copper respectively). On the other hand, the diameter and the chirality also have a great influence on its thermal properties, for example, in order to have high values of thermal conductivity, CNTs, must have metallic features. This means that the chiral indices (n,m) have to follow the following relation: $2n+m=3l$, where n, m, l are integers. Furthermore, a big diameter makes CNTs behave like a graphene sheet³² and in consequence, they have excellent thermal properties. Also the length of CNTs have an important role, in fact, the thermal conductivity increases with length up to the mean free path of phonons, which is about 500 [nm] for MWCNTs and longer for SWCNTs¹⁴. On the other hand, defects and vacancies in CNTs dictate the better structure (SWCNTs or MWCNTs) to transmit heat in the best way. For example, defects or vacancies in SWCNTs structures have a much stronger impact on conductive properties than in MWCNTs. This results from the fact that in MWCNTs, the increase in diameter of nanotubes and their neighboring shells create more optical phonon modes and channels, which contribute to thermal conductivity¹⁴. Finally, in order to have high-quality CNTs, the synthesis method is fundamental, therefore, among various analyzed methods, the CVD method clearly emerges as the best one for the production of MWCNTs¹⁶. Defects and vacancies have special importance in the synthesis of CNTs because once they have been characterized, the goal is to find a way to implement them in real-life applications, like in the solar-thermal sector. However, when it comes to implementing this amazing material, a multidimensional problem of manufacturing arises. In summary, it can be dived into two:

1. There is no device capable of producing perfect CNTs, in other words, CNTs always have morphological defects like vacancies. This decreases the mean free path of phonons¹⁴.

| Type of CNT | Method of synthesis | Method of measurement | Additional information | K(W/m K) |
|----------------------------|---------------------|-----------------------|------------------------|----------|
| CNT film | CVD methane | PTC method | In-plane 300 K | 110 |
| | C:Fe 1900 | | | |
| | CVD toluene | | | 67 |
| | C:Fe 400 | | | |
| | CVD n-butanol | | | 30 |
| | C:Fe 800 | | | |
| | CVD n-butanol | | | 7 |
| SWCNT | CVD | Steady state | Isolated | 4500 |
| Individual MWCNT | pCVD | LFA | 275 K | 600 |
| Bundled MWCNT | | | 255 K | 150 |
| Hybrid films SWCNT + MWCNT | CVD | | | 8.3 |

Table 2.2: Thermal conductivity of different CNTs structures, calculated by physical simulations. Adapted table from¹⁴.

2. CNTs always have some kind of contamination. This can be other forms of carbon, residual catalyst, etc.¹⁴. Unfortunately, the actual methods used to remove these unwanted pollutants also affect the structure of CNTs.

Due to all these difficulties, some researchers have conducted their investigations through computational simulations which help to analyze theoretically the results of CNTs with different configurations in an easier way. Table 2.2 shows the thermal conductivity values of many mathematical simulations performed in different conditions.

In conclusion, CNTs is one of the best thermal material that the scientific community has discovered in the last decades and it can replace the common material used in the solar-thermal industry. In addition, the thermal properties of CNTs depend on their general features (shape, diameter, length, functionalization, chirality, defects, etc.). Therefore, for the purpose of this work, the best CNTs are MWCNTs and the ones that have metallic characteristics. Furthermore, a CVD method is the best synthesis technique in order to achieve these features in CNTs.

2.1.4 Solar absorption properties of CNTs

"Solar energy has a great potential to meet the global energy demand while reducing the carbon emission footprint"³³. In this way, an appealing material for solar absorbers, which is still not fully explored, is CNTs. This material not only has unique optical, electrical, and mechanical properties but also is considered as one of the best light-absorbing materials among other important properties; like high physical and chemical stability³⁴.

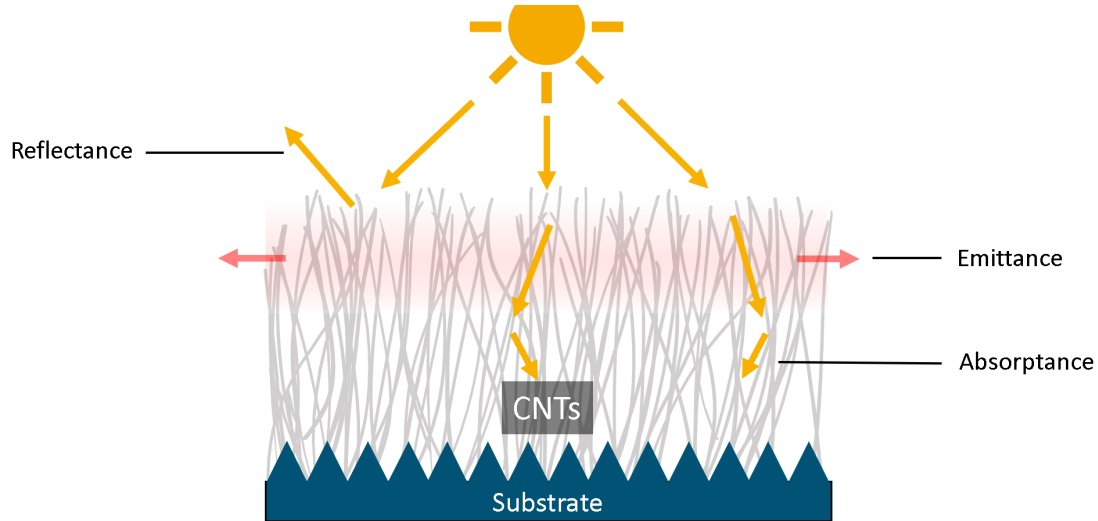


Figure 2.6: Solar radiation is absorbed and reflected by CNTs, besides its emittance generated when the system heats up.

On the other hand, CNTs have high absorbance in a broad spectrum (0.25-200 [μm]) which is attributed to the interband and $\pi - \pi^*$ transitions, while at the same time they have very low reflectance resulting from their porous structure³³. Another important characteristic of a solar absorber is the amount of energy delivered to the environment in the form of heat once the system heats up. As a CNT absorbs almost all the incident radiation, it behaves like a blackbody, an interesting object that is described in the next section. These last features are better defined by the next concepts and are also represented in figure 2.6:

- **Emissivity or Emittance (ϵ):** It is the proportion of thermal radiation emitted by a surface due to its temperature or in other words; it is the ratio between the radiant emittance of the heat of a surface and the radiant emittance of the heat of a blackbody.³⁵ To be more specific it also can be called thermal emittance.
- **Absorptance (α):** It is the amount of incident radiation absorbed by the surface or in other words; it is the ratio between the absorbed radiant power and the incident radiant power over a surface³⁵. It also can be called solar absorptance.
- **Reflectance or Reflectivity (ρ):** It is the amount of incident radiation that is not absorbed by a surface or in other words; it is the fraction of incident radiation reflected by a surface³⁵.

In conclusion, the combination of these properties makes CNTs an ideal material for realizing a super black solar absorber, or in other words, when the solar radiation reaches CNTs it is reflected and absorbed multiple times until the incident radiation is almost completely absorbed. Thus is how CNTs behave like a blackbody.

2.1.5 Blackbody (BB) physics

Just to remember the specific definition, a blackbody is a theoretical object that absorbs all incident electromagnetic radiation, no matter the frequency or the angle of the incident radiation. This makes the object look black and heat up, after that, it begins to emit the absorbed energy in form of radiation and this is known as blackbody radiation. In 1900, the German physicist Max Planck proposed for the first time the mathematical model that describes how a blackbody emits that radiation as a function of the body's temperature. Thereafter, many materials and applications have been developed in order to take advantage of these interesting characteristics of BB matter. For example, CNTs material and solar absorption applications.

Furthermore, anyone can see the physical phenomena of blackbody radiation in a stove. For example, when the burner of an electric stove is heated, it first turns dull red and progressively becomes redder as the temperature increases, it means that if the temperature of a body continuously increases then, it is possible to see that there is a continual shift of the color of the heated body from red through white to blue as the body is heated to higher temperatures. This is what happens in a blackbody when it absorbs a large amount of incident radiation³⁶.

This physical phenomenon can be explained in the following way. If the temperature of the blackbody increases, not only the emitted energy but also the frequency of the outgoing radiation increases, i.e. the radiation wavelength decreases. Recall that red is in a lower frequency range of the spectrum while blue higher relative frequency. Furthermore, another important aspect of the spectrum is that the emitted radiation does not have the same intensity at all frequencies, instead, it follows Planck's Law

- **Planck's Law**

$$I_{BB}(T, \lambda) = \frac{2hc^2}{\lambda^5 e^{hc/\lambda kT} - 1}, \quad (2.2)$$

where h is Planck's constant, $6.626 \times 10^{-34} [J \cdot s^{-1}]$, k is the Boltzmann constant, $1.3806 \times 10^{-23} [J \cdot K^{-1}]$, c is the speed of light in a vacuum, $3 \times 10^8 [m \cdot s^{-1}]$, λ is the wavelength in [m] and T is the absolute temperature in [K]. Another important aspect of blackbody objects was postulated in 1859 by Gustav Kirchhoff, who through arguments based on thermodynamics proved that for any body in thermal equilibrium with radiation, the emitted power is proportional to the power absorbed according to

- **Kirchhoff's Law**

$$e_f = J(f, T)A_f, \quad (2.3)$$

where e_f is the power emitted per unit area per unit frequency by a particular heated object, A_f is the absorption power and $J(f, T)$ is a universal function (the same for all bodies) that depends only on f , the light frequency, and T , the absolute temperature of the body. The fundamental aspect here is that a blackbody absorbs all incident radiation falling on it and therefore $A_f = 1$.

2.1.6 BB-CNTs; emission spectrum and thermal losses

BB-CNTs denote an approximation to a blackbody made from CNTs. The first person to offer a successful explanation of blackbody radiation was the German physicist Max Planck. He made the revolutionary assumption that the energy of emitted radiation of a blackbody cannot take continuous values, instead of that, the energy takes discrete values and it had to be proportional to an integral multiple of the frequency³⁶. After this discovery, it was possible to perform a plot that describes the experimental data with precision. Figure 2.7 shows the spectral emission of a blackbody and at the same time shows the spectral emission of Vertically Aligned Carbon Nanotubes (VA-CNTs) sample from $T=450[K]-600[K]$. Note that the spectra emission of the CNTs and the blackbody source are nearly identical for all tested temperatures and wavelengths. This indicates that CNTs sample behaves close to a perfect blackbody, or in other words, by Kirchoff's, a perfect absorber implies perfect emitter of radiation that follows Planck's Law⁶.

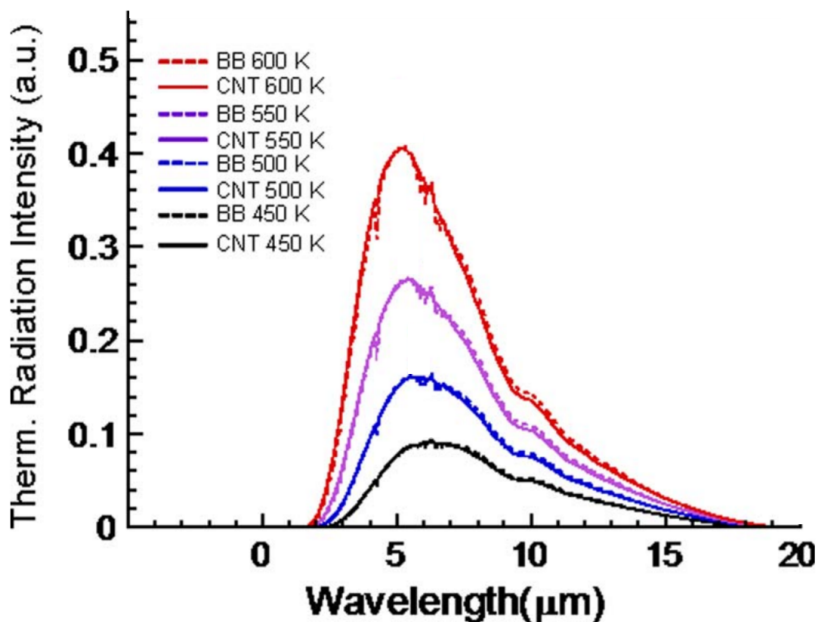


Figure 2.7: Blackbody (BB) radiation spectra (dashed lines) and near-perfect blackbody radiation from VA-CNTs sample (solid curves) as a function of the wavelength for several temperatures. Modified graphic taken from⁶.

Once the energy has been absorbed, the aim is to keep that energy in order to use it in form of heat, otherwise, the energy will be lost and the efficiency of the material to transform radiation into heat will be reduced. To overcome the blackbody emission problem, especially the infrared emission, there are some special mirrors that current solar collectors use to block infrared wavelengths. As consequence, it reduces radiation losses and convection to the atmosphere²³.

2.1.7 Theoretical exergy analysis

In this work, one of the most important aspects is how much of the absorber energy by the device can be used in order to perform work. Consequently, the first important thing in this section is to be clear about the concepts of energy and exergy. While the first law of thermodynamics defines energy as a conserved quantity, the second law shows that for some energy forms (heat) only part of the energy is convertible to work. Table 2.3 summarizes the main differences between energy and exergy. The exergy quantifies this fraction in terms, in our case, of the temperature contrasts with the environment. Thus, exergy is a very useful tool in engineering¹⁵. The exergy of a system follows the relation (the Euler relation of thermodynamics) 2.4 and its unit of measurement is in joules (J).

$$E = U + P_0V - T_0S - \sum_i \mu_{i0}n_i, \quad (2.4)$$

where U, V, S and n_i denote extensive parameters of the system A , and P_0, T_0 and μ_{i0} are intensive parameters of the environment A_0 . The extensive quantities are directly proportional to the size of the system, while on the other hand, the intensive quantities are actual measures of contrast¹⁵ to the environment. These quantities are not affected by the size but by only the level of contrast. This situation is described in table 2.4.

This expression is composed of four different terms. First, the internal energy U which is the energy carried within the system. Second, the external energy P_0V which is the work as a volume V that occupies a space of the environment at pressure P_0 . Third, the energy as ambient temperature T_0S which is the disordered part of the energy U and fourth, energy as ambient substances $\mu_{i0}n_i$, another part of U . In summary, Eq. 2.4 is the expression of the available work from system A when it is brought to equilibrium with the environment A_0 . This means that all contrasts have been reversibly transformed into work. On the other hand, work and heat are concepts related to a time-dependent process, therefore, when it is said that work and heat are stored in a body, what is stored is exergy as some form of time-dependent contrast¹⁵.

| Energy | Exergy |
|--|---|
| The first law of thermodynamics | The second law of thermodynamics |
| Nothing disappears | Everything disperses |
| Energy is motion or ability to produce motion | Exergy is work (i.e., ordered of motion) or ability to produce work |
| Everything is energy | Contrast is exergy |
| Energy is always conserved (i.e., in balance); it can neither be produced nor consumed | Exergy is only conserved in a reversible process but partly consumed in a irreversible process, (i.e., real process). Thus, exergy is never in balance for real process |
| Energy is a measure of quantity | Exergy is a measure of quantity and quality |

Table 2.3: Energy and Exergy differences. Adapted table from¹⁵.

| Intensive quantities | Extensive quantities |
|---|---|
| $T_O = \text{temperature}$ | $U = \text{internal energy}$ |
| $P_O = \text{pressure}$ | $V_O = \text{volume}$ |
| $u_{iO} = \text{chemical potential for substance } i$ | $S_O = \text{entropy}$ |
| | $n_{iO} = \text{number of moles of substance } i$ |

Table 2.4: System A surrounded by the environment A_0 that is assumed to be much larger than the system. Adapted table from¹⁵.

Then, by using the Gibbs relation,

$$U = ST - VP + \sum_i n_i \mu_i. \quad (2.5)$$

The following expression is derived from Eq. 2.4:

$$E = S(T - T_0) - V(P - P_0) + \sum_i n_i (\mu_i - \mu_{i,0}), \quad (2.6)$$

from which is seen that in the case of this work $P = P_0$, $\mu_i = \mu_{i,0}$. Therefore, the exergy of the devices analyzed in this work is written as:

$$E = S(T - T_0), \quad (2.7)$$

or,

$$dE = dS(T - T_0). \quad (2.8)$$

Then, by using thermodynamic relations $dQ = cdT$ and $dQ = TdS$:

$$\int dE = \int (T - T_0) \frac{cdT}{T}, \quad (2.9)$$

$$E = c \int_T^{T_0} (1 - T_0/T) dT. \quad (2.10)$$

Finally, the exergy expression as a function of T and T_0 is obtained:

$$E = \left| c(T - T_0) \left[1 - \frac{T_0}{T - T_0} \ln \left(\frac{T}{T_0} \right) \right] \right|, \quad (2.11)$$

where c represents the heat capacity of the medium. Here the absolute value is placed in order to fix exergy as a positive quantity.

2.2 Experimental background

2.2.1 Making BB-CNTs; the CVD technique

Chemical vapor deposition or CVD is a furnace in which the carbon filaments are formed from the catalytic decomposition of carbon-containing gas (reactant gases) with the aid of supported transition metal catalyst placed over a metal surface (substrate). This means that the general growth of CNTs involves the saturation of carbon atoms on metal nanoparticles (catalysts), (see figure 2.8). This "deposition" of carbon atoms leads to the formation of tubular carbon structure in an sp^2 hybridization. Normally, the reaction is carried out in a gas flow furnace at atmospheric pressure, then, the substrate with the catalyst is placed in a ceramic or quartz boat which is put into the furnace in a quartz tube. The reactant gases are a mixture of hydrocarbon and inert gas that goes in and out of the furnace (quartz tube) at temperatures ranging from 500 °C to 1100 °C. After the reaction, the system is cooled down to room temperature.

The features of CNTs produced by the CVD method depend on the working conditions such as; temperature, pressure, the concentration of hydrocarbon, metallic catalyst, and reaction time. For example, the length of the CNTs depends on the reaction time, however, care must be taken because using the CVD method other carbon structures are formed, such as amorphous carbon, and the reaction time plays a fundamental role in the formation of different structures. Table 2.5 shows a summary of different working conditions.

In conclusion, using CVD technique, it is possible to build a blackbody made of CNTs that allows transforming the solar radiation into heat. This can be achieved through the configuration of the right conditions in temperature, pressure, the concentration of hydrocarbon, metallic catalyst, and reaction time.

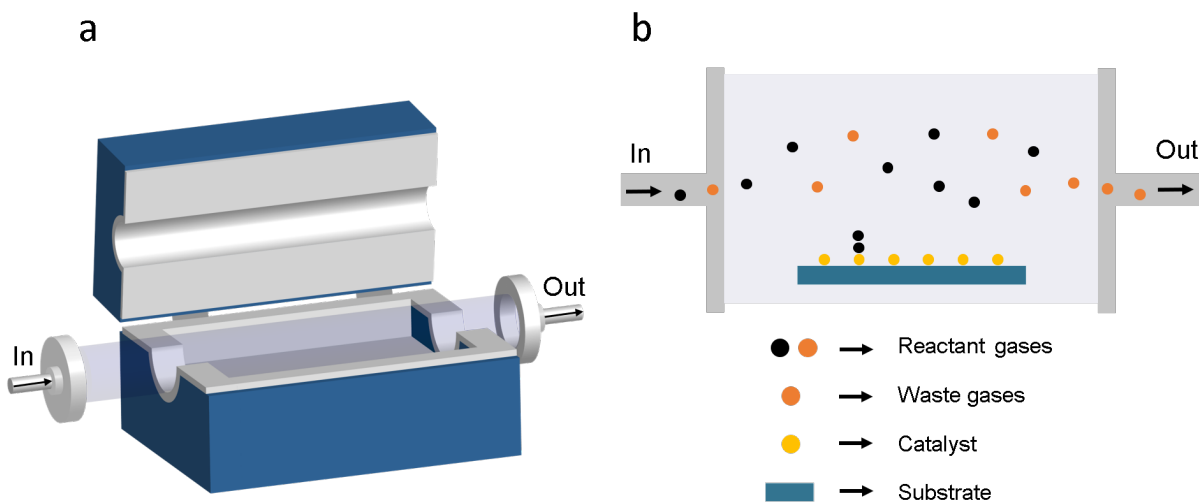


Figure 2.8: CVD technique; (a) external scheme and (b) internal mechanism.

| Method | Product | C source, catalyst |
|--------|--|--|
| CVD | Filled CNTs, Fe ₃ C nanowires | Acetylene, titanate modified palygorskite |
| | SWNTs | Fe-Mo/Si substrate, methane |
| | MWCNTs | K-doped Co and Co-Fe/zeolite and CaCO ₃ |
| | CNTs | Different metals and rare-earth promoters |
| | Aligned CNTs | Single-crystal of sapphire or quartz |

Table 2.5: Summary of the articles reporting CVD production of carbon nanoarchitectures. Adapted table from¹⁶.

2.2.2 BB-CNTs; benefits and problems for practical applications

Nowadays, there are many surfaces that come close to the definition of a blackbody, one of them is CNTs (BB-CNTs). To produce this material chemical vapor deposition or CVD is the technique that seems to offer the best chance to obtain a controllable process to produce CNTs with predefined properties, like very high absorptance, >95%, a prerequisite for solar thermal coatings. Inside these practical applications there are some important benefits of CNTs:

Benefits

- Structure: CNTs have a very adaptable and stable structure that can be chosen in order to have the desired properties. Furthermore, it has a very low weight, which makes CNTs an interesting option for the industrial sector. See section 2.1.2.
- Thermal conductivity: CNTs have an incredible thermal conductivity that overlaps that of common materials like aluminum and copper. See section 2.1.3.
- Absorptance: CNTs surface absorb almost all the incident radiation, which means a high efficiency at the time to absorb solar energy. See section 2.1.4.

The question that could arise at this point is; if CNTs are so good material for solar-thermal applications, why are they still not widely used by the industrial sector? and the answers could be

Problems

- Emittance: The emission rate of CNTs is the same as the absorption rate. This means that a blackbody cannot retain any energy by itself. See section 2.1.6.
- Synthesis: CVD is the best technique to produce BB-CNTs and is suitable only for small-scale devices and needs costly equipment³⁴. See section 2.2.1.

In conclusion, with the right setup, after the absorption, the energy can be used in many different processes like in solar absorption applications. Furthermore, despite the drawbacks, the writer of this work, in agreement with³⁷, believes that in a few years, ongoing investigations will decrease the manufacturing cost of CNTs, making possible a new generation of materials that can be used in the renewable energies field.

2.2.3 Characterization techniques

The characterization techniques used in this work were: X-ray Photoelectron Spectrometer (XPS), Raman Spectroscopy and Scanning Electron Microscopy (SEM) and are described in the next subsection.

X-ray Photoelectron Spectrometer (XPS)

X-ray photoelectron spectroscopy is an important and key technique for surface characterization and analysis. This technique provides a total element analysis of the top 10-200 Å of any solid surface. The basic principle of XPS is the photoelectric effect, figure 2.9 part (a) represents schematically the interaction of a photon with an electron placed in an atomic orbital. Since the photon energy is greater than the binding energy of the electron, it is ejected from the atom with kinetic energy approximately equal to the difference between the incident photon energy and the electron binding energy³⁸. Therefore, the basic equation for XPS is 2.12.

$$E_b \simeq h\nu - E_k \quad (2.12)$$

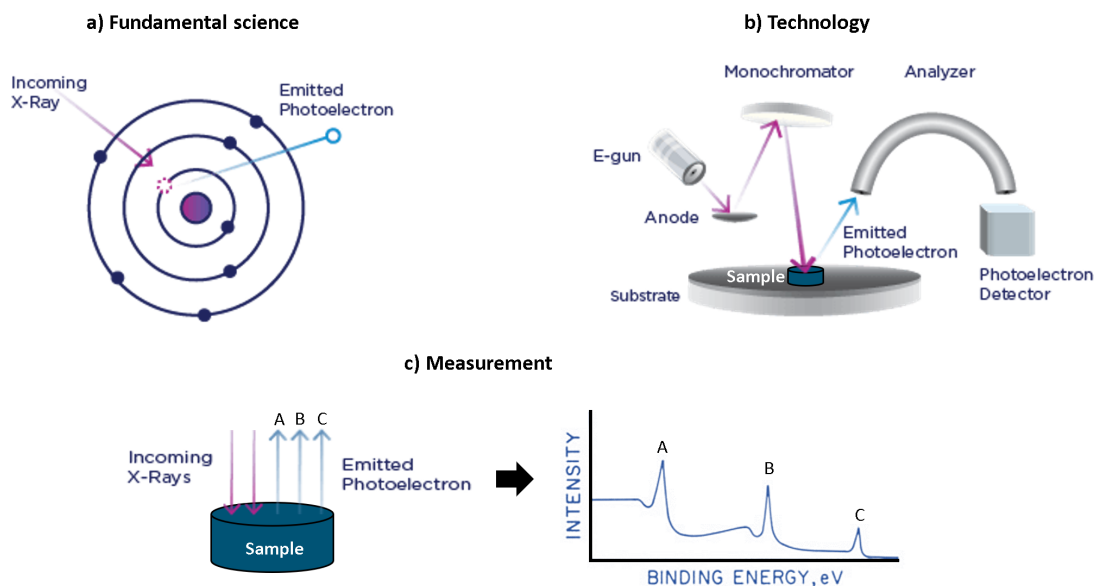


Figure 2.9: Schematic view of XPS characterization technique.

Where E_b is the electron binding energy, E_k is the electron kinetic energy and $h\nu$ is the photon energy (h is the Planck's constant and ν is the X-ray frequency). On the other hand, XPS analysis starts with mounting the sample over the substrate and then placing it in a high-vacuum environment. An X-ray source emitting monochromatic X-ray photons towards the sample. The X-ray photons statistically interact with the electrons of the sample. This process creates photoelectrons and some fraction it is directed up to the analyzer. The analyzer basically measures the number of electrons of different kinetic energies, see figure 2.9 part (b). On the other hand, measuring the kinetic energy allows to calculate the binding energy, and in consequence, identify the atoms present in the sample. The information is processed by a computer to produce a spectrum of photoelectron intensity as a function of binding energy. The binding energy position is like a fingerprint for each chemical element, in this way, elemental identification is made³⁸. See figure 2.9 part (c). All energies are usually expressed in electron volts [eV].

Raman Spectroscopy

Raman spectroscopy is a technique used to study low-frequency modes as vibrational, rotational, etc. This technique is based on the effects of the inelastic scattering of light by a molecule, or Raman effects. In other words, when a photon of visible light, too low in energy in order to excite an electronic transition, interacts with the matter, it can be scattered in one of three ways, see figure 2.11, one elastic and two inelastic;

- **Rayleigh scattering:** This is the elastic one. The incident photons are recovered (no energy gains or losses).
- **Stokes Raman scattering:** Incident photons give energy up to the molecule (it lose energy).
- **Anti-Stokes Raman scattering:** Incident photons removing energy from the molecule (it gain energy).

On the other hand, due to the Raman effect is very weak compared to another optical interaction process, the Raman spectrometer uses a high light intensity to generate a signal from the sample. In general, a Raman spectrometer consists of the light source (diode laser), a sample, a dispersive element of light, and a detector. In summary, the laser light source hits the sample and the light interacts with the molecule scattering the three different ways previously mentioned, after that, the light is redirected to the filter in which the Rayleigh scattered light is blocked while the inelastically scattered light (Stokes and Anti-Stokes) goes to the dispersive element in which it is separated into different wavelengths. Finally, then the light of different wavelengths and intensities are analyzed by the detector and converted into the final spectrum³⁹.

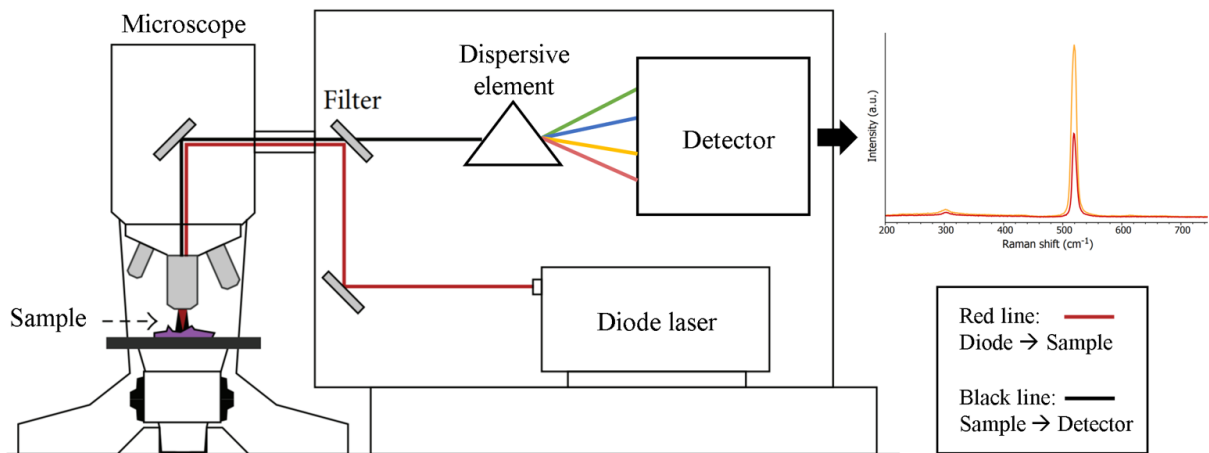


Figure 2.10: Typical setup for Raman spectrometer with a laser attached to a microscope⁷. Modified graph.

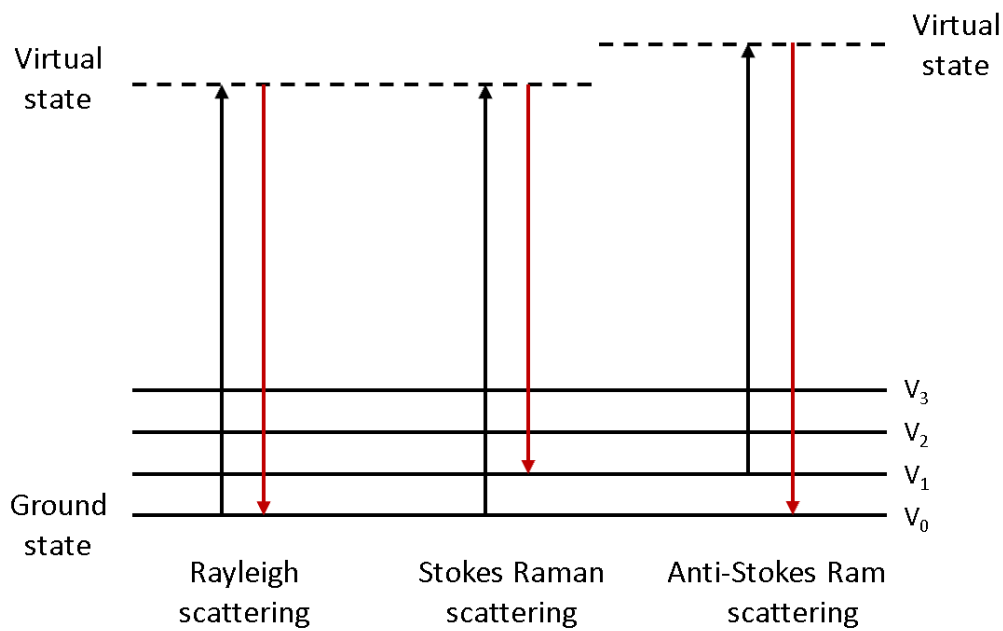


Figure 2.11: The three energy level diagram of Raman scattering⁸

Scanning Electron Microscopy (SEM)

Scanning electron microscopy is a worldwide characterization technique used in the scientific and technological community⁴⁰. SEM is a type of electron microscope capable of producing images of the order of tens of Angstrom. Furthermore, it can be used in the analysis of organic and inorganic molecules. Basically, an SEM is composed of an electron gun, anode, magnetic lenses, sample, and one or more detectors⁹.

In principle, the electron is produced in the electron gun by, either heating a filament or by applying a strong electric field to it. Then, the electron is accelerated by the anode, which is negatively charged and therefore, pushes the electron in a specific direction. After that, the electron is focused onto the sample by magnetic lenses, which creates a very narrow electron beam. The sample scatters the incident electrons as a function of many sample factors, like; height, chemistry, and crystal structure⁹. Furthermore, the electron fired to the sample are called primary electrons, and when they touch the surface sample, a wide range of useful interactions can occur⁴¹, see figure 2.12 part (b). Finally, the detector receives the outgoing interactions traveling in a different direction and with different energies, in this way, an SEM machine produces information about the morphology and composition of the sample, see figure 2.12 part (c).

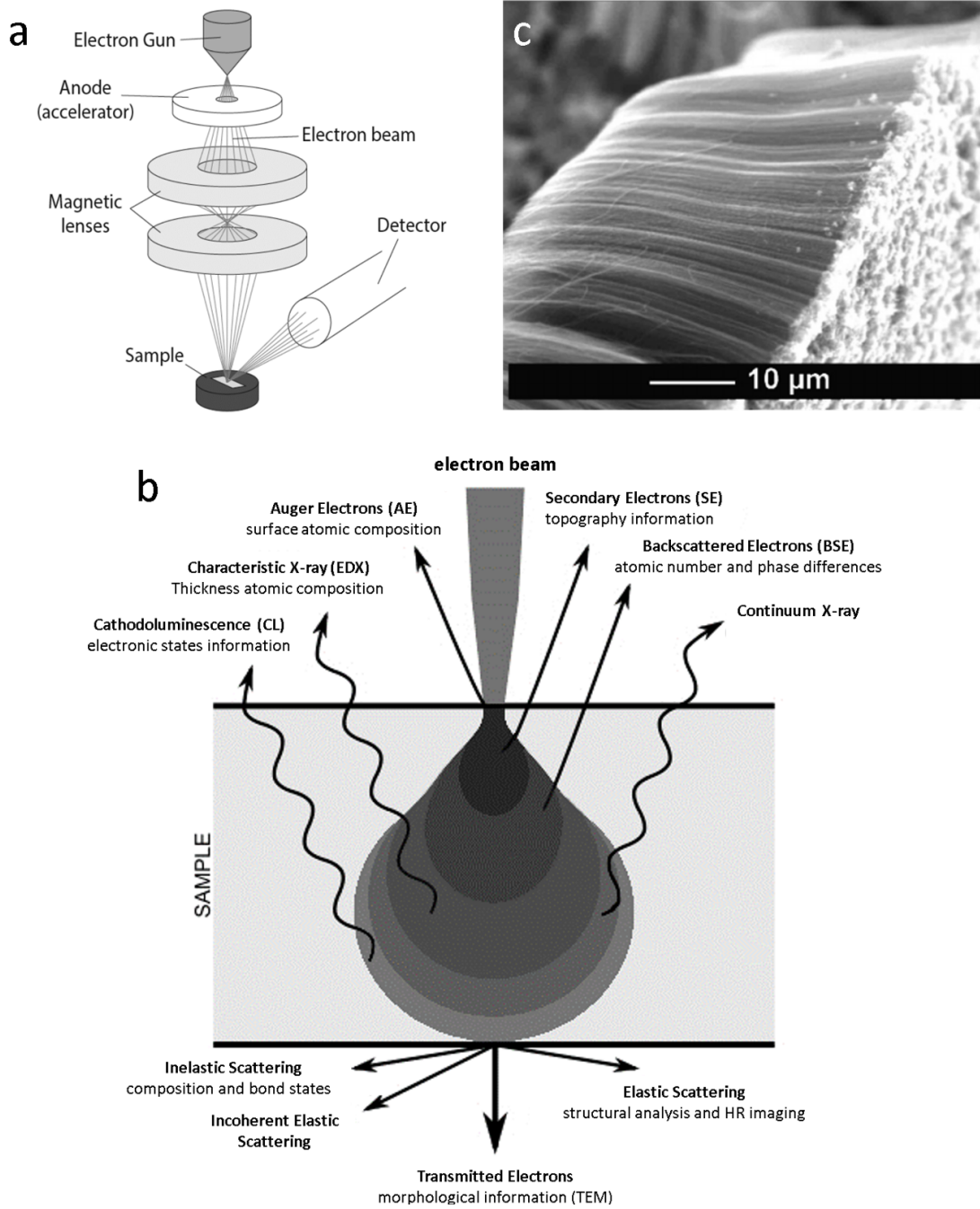


Figure 2.12: Scanning Electron Microscope (SEM); (a) scheme of the instrumentation⁹, (b) signals generated on the sample by the primary electrons¹⁰ and (c) SEM images of CNTs film¹¹. Modified graph.

Chapter 3

Methodology

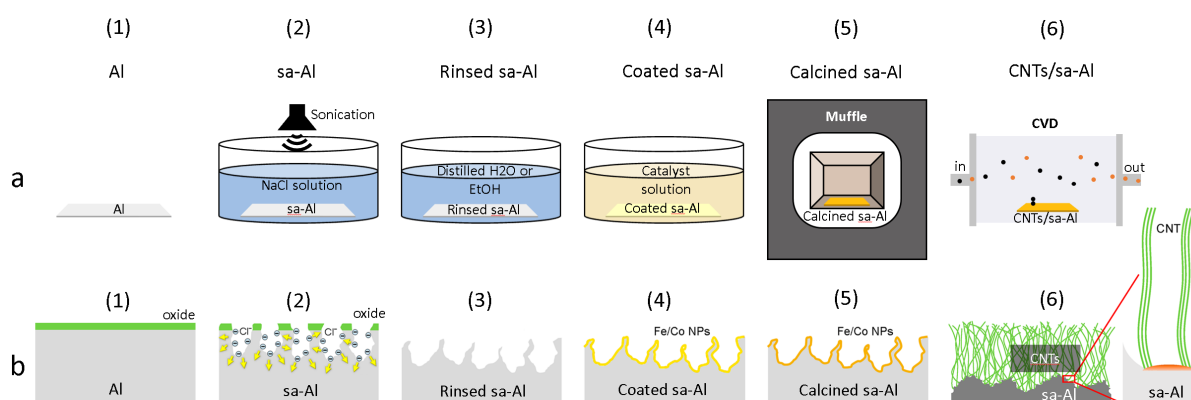


Figure 3.1: Surface structural evolution of the Al substrate; (a) process flow diagram and (b) schematics¹². (1) Preparation of Al sheet, (2) surface activation of Al, (3) rinsed of sa-Al, (4) catalyst deposition of Fe/Co NPs, (5) calcination process and (6) CNTs synthesis. Modified graph.

First, a brief summary of the methodology process is shown in figure 3.1; a flow diagram in part (a) and a schematic in part (b), while the details of each process are specified in the next sections.

3.1 Aluminum substrate evolution

3.1.1 Preparation of aluminum substrate

In this work, Al sheets with a thickness of 25.4 μm (All-Foils trademark) were used. The first step was to cut 12 Al sheets of 2x3 [cm], see figure 3.2.

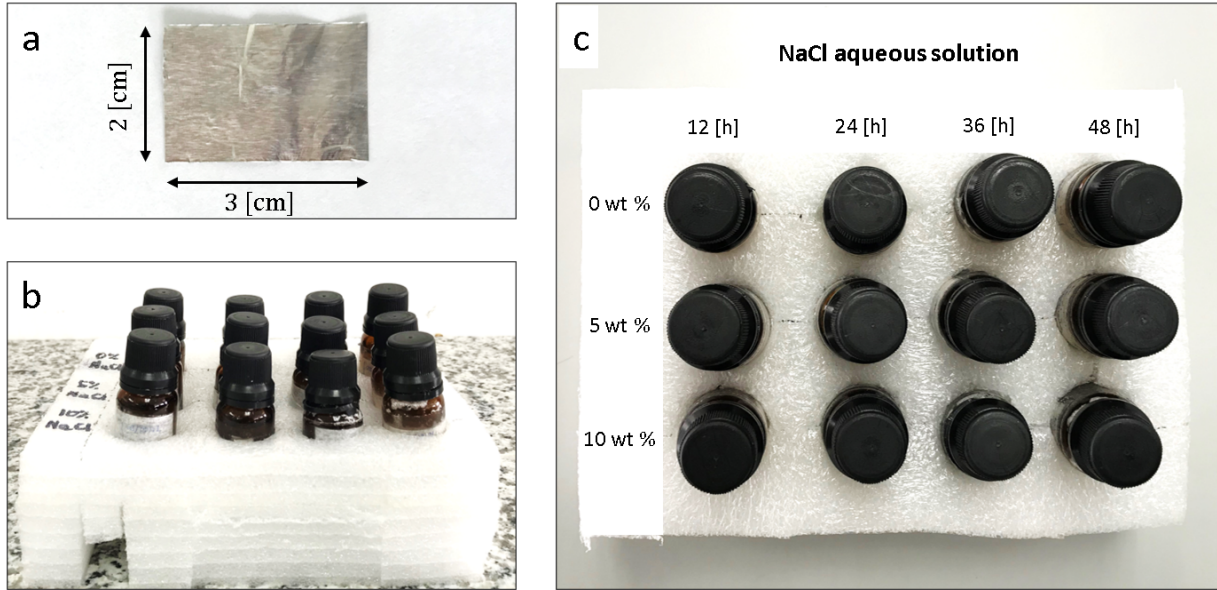


Figure 3.2: Surface activation process (part 1); (a) Al sheet, (b) side view, and (c) top view of the system.

3.1.2 Surface activation of aluminum (sa-Al)

Surface activation can be defined as a method used to alter the morphology of a surface. This can be accomplished by exposing the surface to chemical groups. Furthermore, in order to improve the penetrations of the chemical groups, a sonication process can be performed. The aim of this treatment is, through the generation of nanopyramidal structure on the substrate surface, to increase the Al superficial area in which CNTs will grow.

Al substrate exposed to NaCl aqueous solution without (part 1) and with (part 2) sonication process

- Part 1:** Twelve Al sheets were immersed in the 0 wt %, 5 wt % and 10 wt % NaCl aqueous solution for 12, 24, 36, and 48 [h] at each concentration respectively, see figure 3.2. This process was performed in order to see the NaCl concentration and exposition time that produces the best nanopyramidal surface morphology. The substance used is shown in figure 3.5.
- Part 2:** Four Al sheets of 2x10 [cm] were introduced in a 10 wt % NaCl aqueous solution. Then, two Al sheets were subjected to a sonication process of 5 [min] and the other two, at 10 [min]. The objective of this process was to see the penetration of Cl ions and activate the Al substrate at two different times, see figure 4.2. After seeing the results of the sonication process, the Al sheets subjected to 5 [min] sonication were cut into four pieces and each one was soaked in the same 10 wt % NaCl solution for 1.5, 3, 6, and 12 [h] respectively. Part 2 was carried out with the aim to get the desired nanostructured surface morphology but reducing the time exposition of the Al substrate to the aqueous solution.

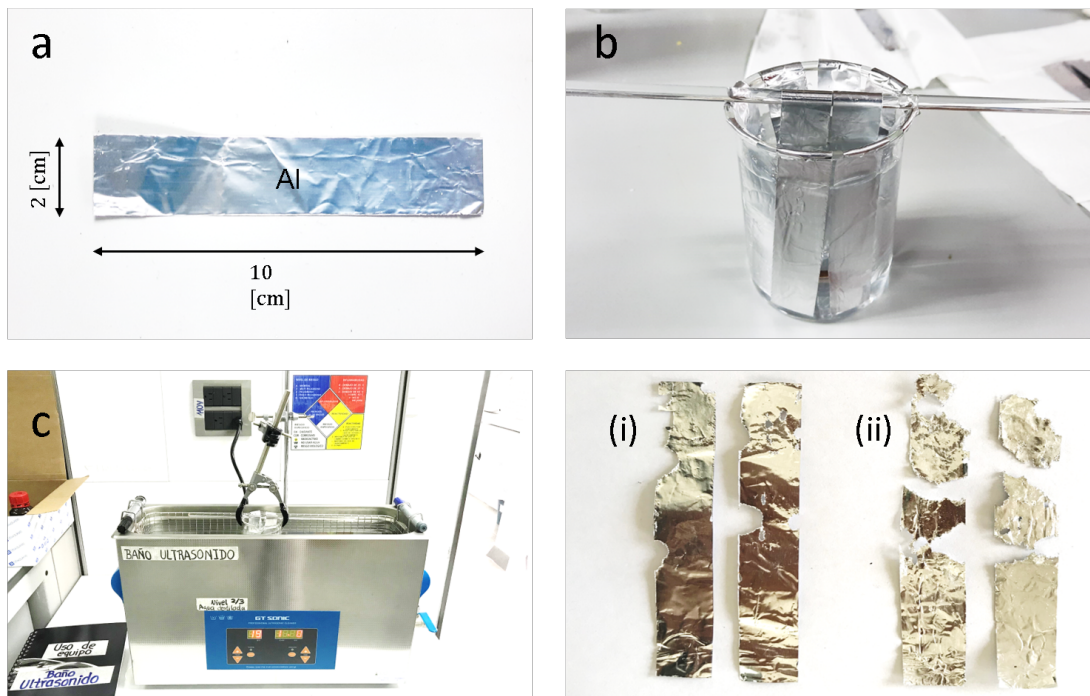


Figure 3.3: Surface activation process (part 2); Al sheet (a) size, (b) immersed in the 10% NaCl aqueous solution, (c) during the bath sonication treatment, (i) after 5 [min] and (ii) after 10 [min] of sonication process.

In conclusion, after comparing the results obtained in part 1 with part 2, ten Al sheets of 2x10 [cm] were sonicated in 10 wt % NaCl aqueous solution for 5 [min] and then soaked in the same solution, one Al sheet during 3[h] and the other 9, and 12 [h]. One Al sheet has a different treatment because it was used to corroborate that more surface-activated Al substrates offer higher performance in the growth of CNTs, this Al sheet was labeled as; Al-3[h]NaCl.

3.1.3 Rinsed of sa-Al

From this point, the Al sheets used in the next steps of the methodology process were the ones mentioned in the conclusions part. Then, in order to remove the aqueous solution from the Al substrates, they were rinsed with distilled water and ethanol, for 10 [min] in each substance, (see figure 3.4).

3.1.4 Catalyst deposition

Subsequently, the Al sheets were immersed in the catalyst solution during 18 [h], (see figure 3.4). The catalyst solution contains 0.1 M iron (III) and 0.1 M cobalt (II) nitrate in ethanol. The substances used are shown in figure

3.5. This type of catalyst has already been used in previous investigations offering favorable results in the growth of CNTs⁴².

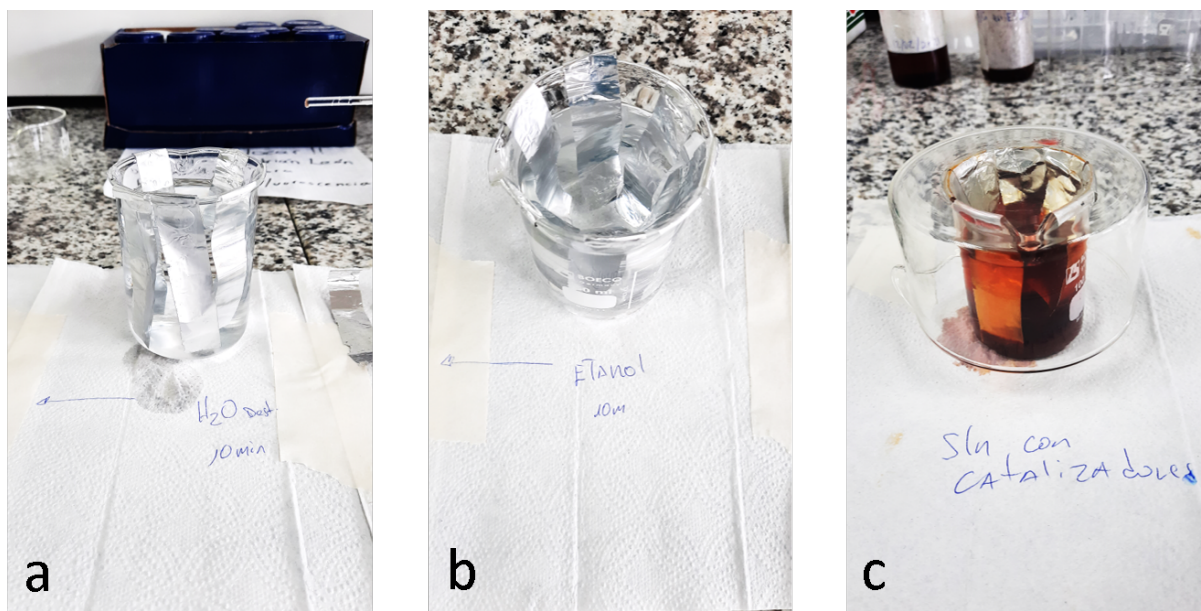


Figure 3.4: Rinsed and catalyst deposition process; sa-Al immersed in (a) deionized water (b) ethanol and (c) catalyst solution.

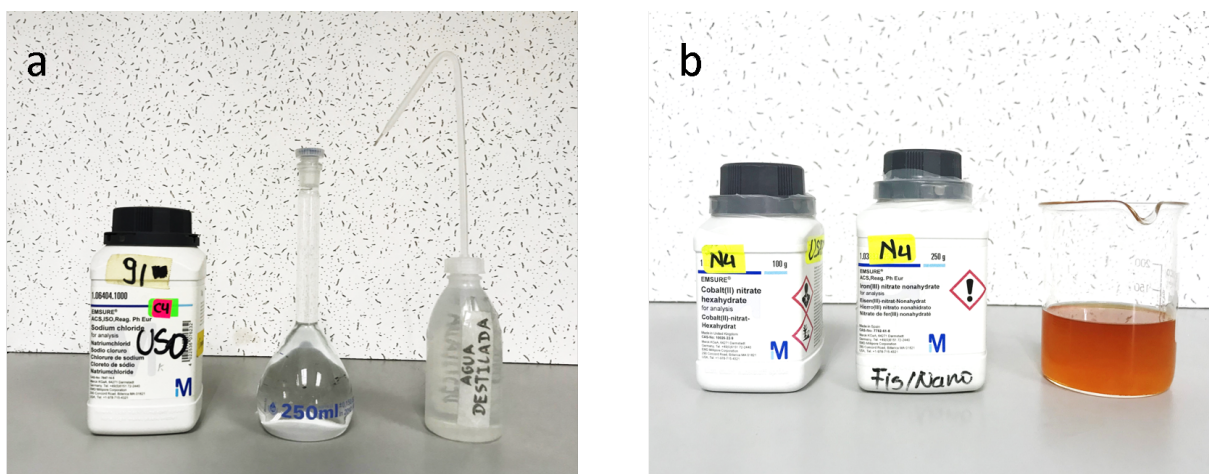


Figure 3.5: Substances used in this work; (a) for the 10% NaCl aqueous solution and (b) for the catalytic solution.



Figure 3.6: Calcination process of the sa-Al substrates loaded with the catalyst solution; (a) inside melting pots, (b) melting pots with sa-Al inside the muffle furnace, and sa-Al substrate (i) before and (ii) after the calcination.

3.1.5 Calcination process

After the surface activation of Al and catalyst deposition, the substrates were subjected to the calcination treatment. The Al substrates were placed inside the muffle furnace and heated up to 600 [°C] for 6 [h], (see figure 3.6). It has been reported in previous investigations that after a calcination process the growth of CNTs improves considerably⁴³. In order to corroborate this assumption, one sa-Al substrate was not calcined, among the remaining 9 sa-Al substrates we include the "Al-3[h]NaCl", described in the conclusion paragraph of subsection 3.1.2. On the other hand, the uncalcinated Al sheets were labeled as; Al-12[h]NaCl-UC.

3.1.6 Low-temperature CNTs synthesis

In this work, CNT structures were synthesized by using a CVD technique. CVD has been widely used for the large-scale synthesis of high-quality CNTs due to its controllability and relatively low process temperature. On the other hand, in this work, different reaction conditions were carried out in order to synthesize CNTs over the sa-Al substrate. These conditions can be seen in table 4.1. The one that allowed the growth of CNTs were the "D" conditions, described below.

After Al substrate preparation process, the sa-Al sheets were loaded in a quartz tube with 450 [ml/min] Ar flow. The substrate then was heated to 650 [°C] and kept in those conditions for 15 [min] under 50 [ml/min] C₂H₂ flow. After the reaction, the sample was cooled to room temperature under 450 [ml/min] Ar flow. In conclusion, CNTs were grown using 50 [ml/min] 10% C₂H₂ diluted in 450 [ml/min] Ar flow. Furthermore, the Al substrates; "Al-3[h]NaCl" and "Al-12[h]NaCl-UC" were not used until the right initial conditions were found.

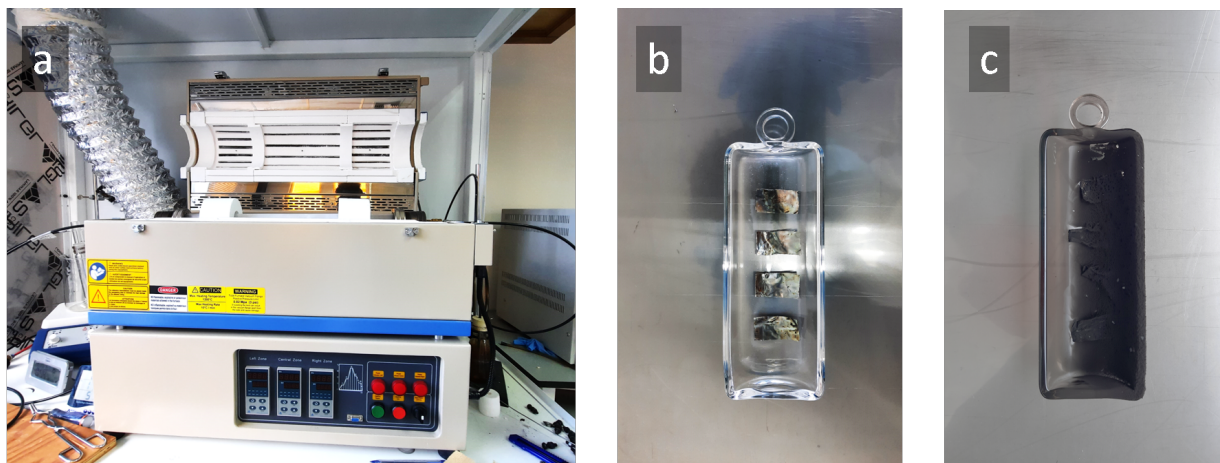


Figure 3.7: CNTs synthesis; (a) CVD machine, (b) Al substrate before, and (c) after the synthesis.

3.2 CNTs characterization

The morphologies of the Al substrate and CNTs were observed by Phenon ProX Desktop Scanning Electron Microscopy (SEM). The surface chemical analysis of activated Al and catalysts were carried out using PHI VersaProbe III X-ray Photoelectron Spectrometer (XPS). The Raman spectra of CNTs were performed by Horiba LabRAM HR Evolution, using 532 [nm] laser excitation, see figure 3.8.

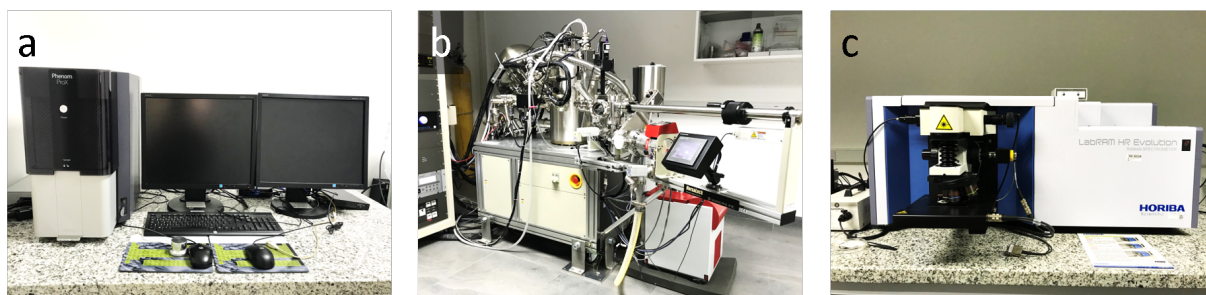


Figure 3.8: Characterization equipment; (a) Phenon ProX Desktop SEM, (b) PHI VersaProbe III XPS, and (c) Horiba brand Raman spectra.

3.3 Measuring heating of different BB reference materials

This section describes the system developed in order to test the hypothesis of this work. That is if the device performed during this investigation (CNTs/sa-Al) heats up more than materials already used in solar-thermal applications. Therefore, in addition to CNTs/sa-Al, the efficiency of the other 3 solar absorbers, at transforming solar radiation into heat, was analyzed and compared. Because in the market there are many solar absorbers, the first material used in this comparison was black anticorrosive paint over an Al surface, the most common one⁴⁴. Furthermore, with the aim of seeing the effect of CNTs at the time to absorb solar radiation, the second material is a residue of the CNTs synthesis process, which does not have CNTs in its structure, while the third material is a solution of the common material and CNTs. The detailed description of each material are below:

1. **Black anticorrosive paint over aluminum (bap/Al):** On the other hand, in the solar industrial sector, after cooper, aluminum is the best readily available conductor, and therefore, it is a convenient material used in solar thermal applications. Normally this material is covered by a selective absorber that increases the absorption of solar radiation and the most common is black anticorrosive paint (bap). Therefore, an Al sheet painted with *bap* is used in this work in order to make a contrast of efficiencies between the common materials already used and CNTs/sa-Al, see figure 3.9 part (a).
2. **Black carbon over surface-activated aluminum (bC/sa-Al):** During the search for the adequate conditions to produce CNTs, a series of irregular carbon-based structures were found. In this work, these structures have been named as black Carbon (bC). Furthermore, because these structures were synthesized over the surface-activated aluminum, their key name was bC/sa-Al, see figure 3.9 part (d).
3. **Carbon nanotube black anticorrosive paint solution over surface-activated aluminum (CNTs-bap/sa-Al):** The last solar absorber material is a solution of the proposed material of this work and black anticorrosive painting. Furthermore, this solution is placed over the surface-activated aluminum and therefore his name is CNTs-bap/sa-Al. In addition, CNTs were dispersed in *bap* in two different concentrations, 1 wt % CNTs *bap* solution and 5 wt % CNTs *bap* solution, see figure 3.9 part (c). The aim was to see if a higher concentration of CNTs would increase solar absorption.

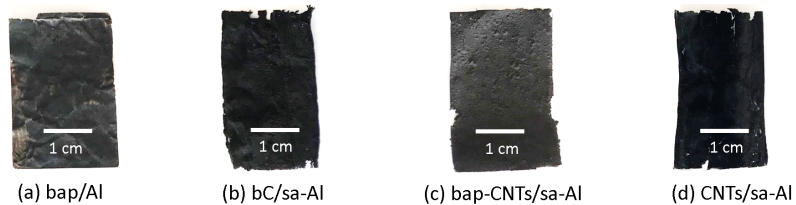


Figure 3.9: The 4 solar absorber devices compared in this work; (a) black anticorrosive paint [bap], (b) black carbon [bC], (c) CNTs-bap solution and (d) carbon nanotubes [CNTs]. (b, c and d) are over a surface-activated Al [sa-Al] while (a) is over an Al sheet without treatment.

3.3.1 Temperature system setup

A thermal insulating box was built in order to analyze how, the BB model device, proposed in this work and the other 3 solar absorber materials, transforming absorbed solar radiation into heat. Because wood and expanded polystyrene are materials with a low thermal conductivity index and are easy to acquire, we used them in our setup. Furthermore, because the box was placed outdoors, an aluminum layer was used to cover it and in this way avoid overheating caused by solar radiation, as aluminum has a high reflectivity index. The structural scheme of the box is shown in figure 3.10.

On the other hand, to record the variations in the temperature of the samples, five temperature sensors were located inside the box, 4 for each sample and 1 to register the temperature of the box. The temperature sensors were connected to an Arduino board, which allowed to visualize a temporal register of the variations in temperature in a PC, see appendix A. The general scheme of the system is shown in figure 3.11. Furthermore, in order to have a good thermal transfer between the temperature sensors and the samples, a thermal paste was used in the connection. The actual system is shown in Fig.3.12.

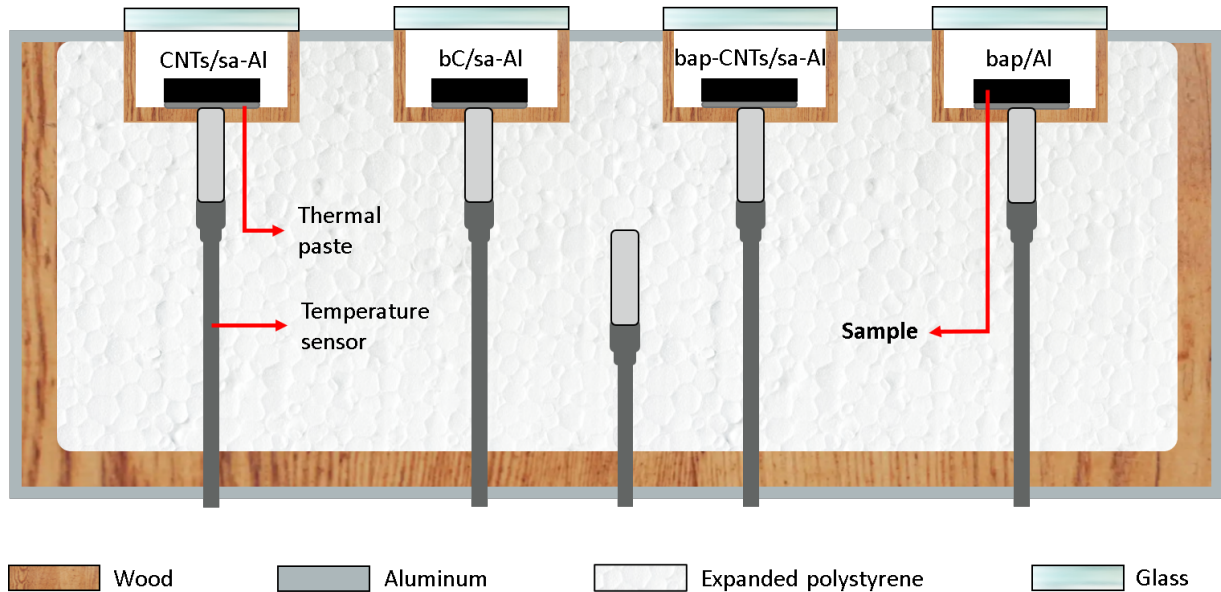


Figure 3.10: Schematic representation of the materials used in the construction of the thermal insulating box.

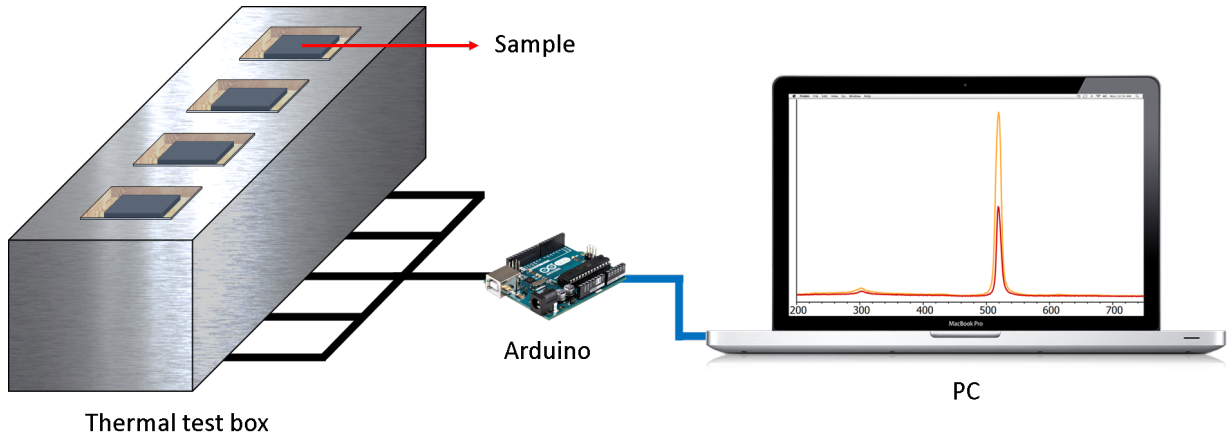


Figure 3.11: The general scheme of the system used to perform the thermal analysis of the material proposed in this work (CNTs/sa-Al) and other 3 solar absorber devices.

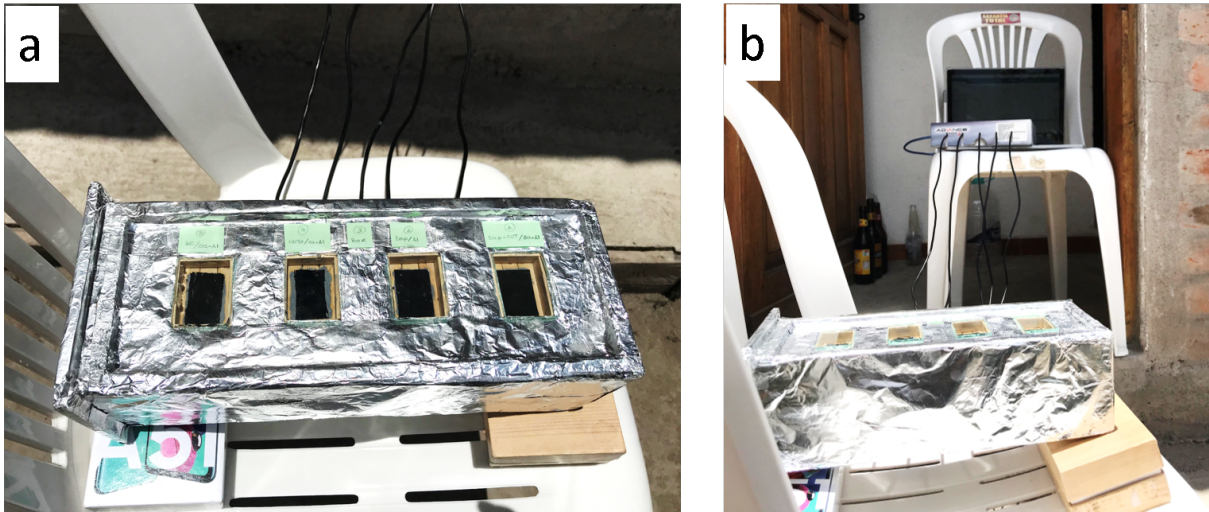


Figure 3.12: Real thermal analysis system; (a) thermal insulating box and (b) general system.

3.3.2 Sensors temperature calibration

Due to many physical and electronic factors, the temperature sensors are noisy (exhibit fluctuating readings), as well as, slightly different temperature values with respect to each other. An example is presented in figure 3.13 which represent temperature measurements of boiling water, using the 5 temperature sensors during 4 [min], also see appendix B. In order to overcome this issue and calibrate the system, the following process was performed.

First, the temperature sensors were calibrated using three temperature references; frozen water, water at room temperature, and boiling water. The process was to record the 5 temperature sensor for 4 [min] at each temperature reference and register the data obtained. After this, the average value of each sensor temperature at each temperature reference was calculated, see table 3.1 part (a).

The next step was to choose one of the five sensors as a reference, in this case, it was sensor four (S4) which offers the most exact values at the frozen water temperature reference, that is, the closest value to 0 [°C], In well know that the ions present in the water can reduce the freezing point, however, the water used was taken off out the tap, therefore, according to⁴⁵ the of ions present in the water is not enough to alter the freezing point. After this, the difference between the average value of S4 with the average value of the other sensors were found, this for each temperature reference. Then, for each sensor, the average value of the 3 differences, one for each temperature reference, was found. Therefore, 5 values are obtained, one for each sensor, see table 3.1 part (b). These values were the calibration factors (CF) that were added to temperature data obtained in the thermal analysis process. An example is presented in table 3.1 part (c) which shows the temperature values of part (a) but with the calibration factors added.

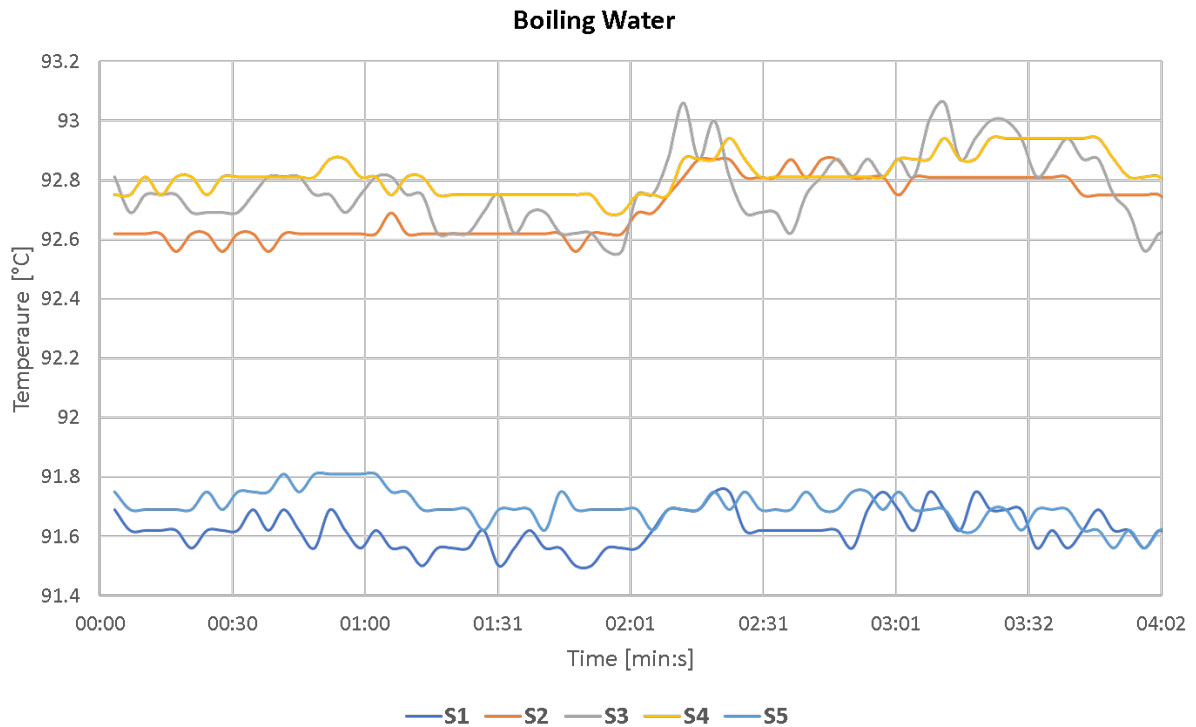


Figure 3.13: Temperature measurements of boiling water, using the 5 temperature sensors during 4 [min].

| (a) Average values of sensors temperature - Miscalibrated | | | | | |
|--|---------|---------|---------|---------|---------|
| Temperature references | S1 [°C] | S2 [°C] | S3 [°C] | S4 [°C] | S5 [°C] |
| Frozen water | -0.952 | -0.208 | -0.547 | -0.106 | -1.144 |
| Ambient water | 19.448 | 20.541 | 20.294 | 20.485 | 19.652 |
| Boiling water | 91.620 | 92.708 | 92.769 | 92.818 | 91.698 |

| (b) Calibration factor [CF] | | | | | |
|------------------------------------|-------------|-------------|-------------|-------------|-------------|
| Temperature references | S4-S1 [°C] | S4-S2 [°C] | S4-S3 [°C] | S4-S4 [°C] | S4-S5 [°C] |
| Frozen water | 0.846 | 0.102 | 0.441 | 0.000 | 1.038 |
| Ambient water | 1.037 | 0.057 | 0.191 | 0.000 | 0.833 |
| Boiling water | 1.198 | 0.110 | 0.049 | 0.000 | 1.120 |
| Average | 1.027 (CF1) | 0.090 (CF2) | 0.227 (CF3) | 0.000 (CF4) | 0.997 (CF5) |

| (c) Average values of sensors temperature - Calibrated | | | | | |
|---|---------------|---------------|---------------|---------------|---------------|
| Temperature references | S1 + CF1 [°C] | S2 + CF2 [°C] | S3 + CF3 [°C] | S4 + CF4 [°C] | S5 + CF5 [°C] |
| Frozen water | 0.075 | -0.118 | -0.32 | -0.106 | -0.147 |
| Ambient water | 20.475 | 20.631 | 20.521 | 20.485 | 20.649 |
| Boiling water | 92.647 | 92.798 | 92.996 | 92.818 | 92.695 |

Table 3.1: Calibration factor process; at three temperature references the (a) average value of the 5 sensors temperature measures during 4 [min], (b) difference between the temperature sensor reference (S4) and the other temperature sensor, in the end, the average values are presented, these values were the calibration factors, and (c) the values of part (a) but with the calibration factors added.

Chapter 4

Results & Discussion

4.1 Carbon nanotubes over surface-activated aluminum (CNT/sa-Al)

First, a brief summary of the obtained results is shown in figure 4.1. This figure shows the surface structural evolution of the Al substrate, from the Al sheet without any treatment until the Al substrate with CNTs over it. The results are detailed in the next subsections.

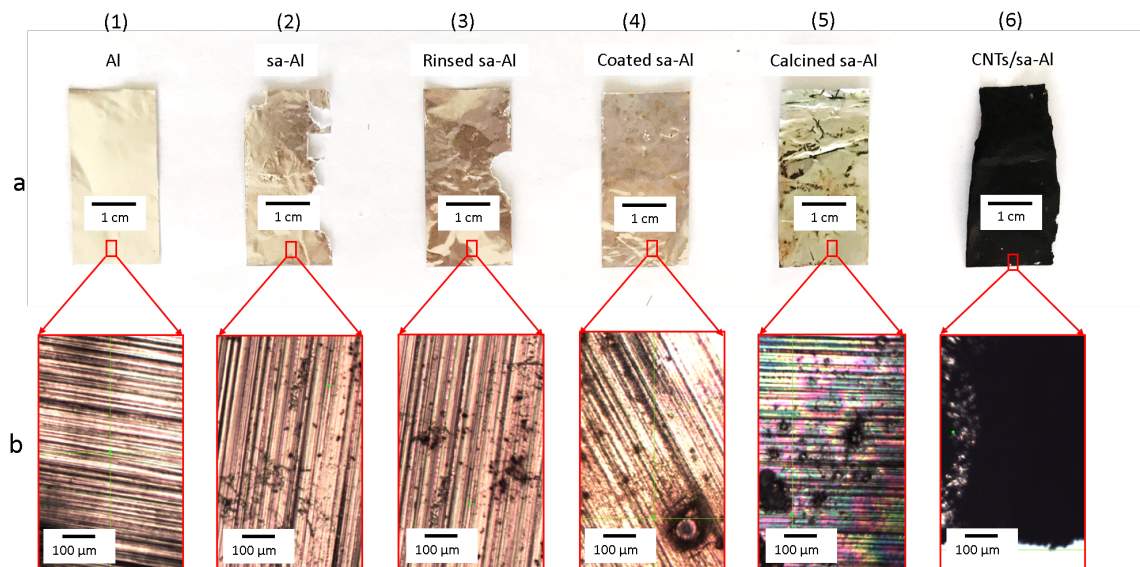


Figure 4.1: Surface structural evolution of the Al substrate in (a) and (b); (1) preparation of Al sheets, (2) surface activation of Al, (3) rinsed of sa-Al, (4) catalyst deposition of Fe/Co NPs, (5) calcination process and (6) CNTs synthesis.

4.1.1 Surface activation of aluminum (sa-Al)

Al substrate exposed to NaCl aqueous solution without (part 1) and with (part 2) sonication process

The contact with an aqueous solution induces the penetration of chloride ions in the oxide layer and in the metallic Al bulk. This caused the breakdown of the oxide layer, as well as, the dissolution of the Al bulk to later, create the nanopyramidal structure morphology¹². The aim of this process is to increase the superficial area in which CNTs will grow.

- **Part 1**

The previous procedure was to see how the chemical group activated the Al substrate at different concentrations and times. The Al sheets were exposed to 0 wt %, 5 wt %, and 10 wt % NaCl aqueous solution, during 12, 24, 36, 48 [h] in each concentration respectively. The results of this process are shown in figure 4.3.

In figure 4.3 part 1 the first row represents the control group, that is, 0 wt % NaCl aqueous solution, where it is possible to see that the Al sheets did not suffer any morphology alteration on their surface. Furthermore, it confirms that aluminum has an oxide layer on it that avoids the corrosion of the material. The second row represents the Al sheets at 5 wt % NaCl aqueous solution. At this concentration, the substrate started to show morphological alteration on its surface, or in other words, the second row shows how black holes start to appear after 24 [h] of Al sheet exposition to the solution and how the density of these black holes increases as well with the exposition time. These holes have a diameter of a few microns. Finally, the third row shows the results of the Al sheets exposition to 10 wt % NaCl. The effects on the Al substrate morphology were more evident, the black holes started to appear after 12 [h] of Al sheets exposure, and after 48 [h] the Al sheet has a high hole density.

- **Part 2**

In order to improve the penetration of Cl ions in the Al sheet surface, a sonication process was performed. The aim of this procedure was to reduce the exposure time of the Al sheet to the NaCl aqueous solution, and in this way, optimize the process of surface activation. In this part, Al sheets were immersed in a 10 wt % NaCl aqueous solution and subjected to a sonication process of 5 and 10 [min].

The results of this treatment are shown in figure 4.2, which shows how destructive this process can be to Al sheets with a thickness of 25.4 μm . As in part 1, black holes appeared on the Al surface morphology, and as it was expected, the effects of the 10 [min] sonication process were more intense than 5 [min]. The penetration of Cl ions at 10 [min] was so strong that it fully penetrated the Al structure, cutting them in many parts. On the other hand, the Al sheets subjected to 5 [min] of sonication process also suffered visible structural damage, but not so intense, in fact, the Al sheet stayed in one piece. Therefore, the Al sheets subjected to 5 [min] of sonication were chosen to continue with the surface activation process. Then, the chosen Al substrates were immersed in 10 wt % NaCl aqueous solution during 1.5, 3, 6, and 12 [h]. Figure 4.3 part 2 shows the evolution of the Al substrate morphology during this time and as it was expected, after a sonication process the desired Al substrate morphology was obtained after only 12 [h] of exposure to NaCl aqueous solution.

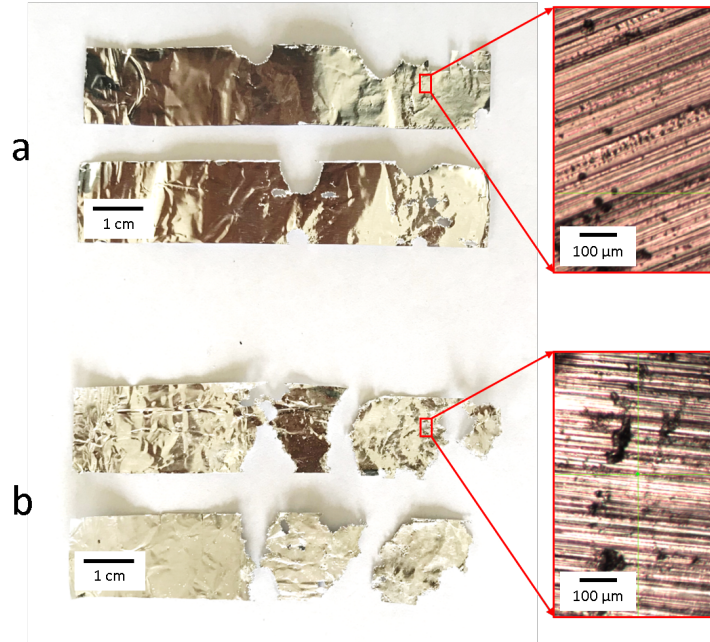


Figure 4.2: Sonication process results; (a) after 5 [min] and (b) after 10 [min] of sonication time.

Finally, figure 4.4 shows the best result of part 1 (figure 4.3 picture 12), the best result of part 2 (figure 4.3 picture 16), and an Al substrate without any treatment. Then, if the surface-activated Al substrate (a or b) are compared with the Al sheet without any treatment (c), it can be seen that the surface-activated process changes the morphology of the substrate creating holes in its surface. Furthermore, while in (a) the morphology shows black holes with a diameter of few microns, (b) shows black holes with a diameter of tens of microns. This is important because, it is right in the middle of the black holes where the Cl ions have penetrated the Al surface and therefore, it is in these areas in which the desired nanopyramidal morphology appears. In this way, the Al substrate was activated.

In conclusion, due to a shorter activation time and a larger diameter of the holes created in the substrates surface the sonication treatment remarkably improves the surface activation Al process. In fact, sonication process reduces the processing time to just a quarter of the time spent in the Al substrate without sonication process, in other words, the surface activation process went from lasting 48 [h] to just 12 [h]. On the other hand, in order to have an Al substrate with a full nanopyramidal morphology surface, the black holes should be present across the entire surface. In this work, this was not possible to achieve because the structural integrity of the Al substrate would be compromised due to its small thickness. Therefore, in future work, it is recommended to use thicker Al substrates in order to increase the time of the surface activation process without affecting the structural integrity of the material.

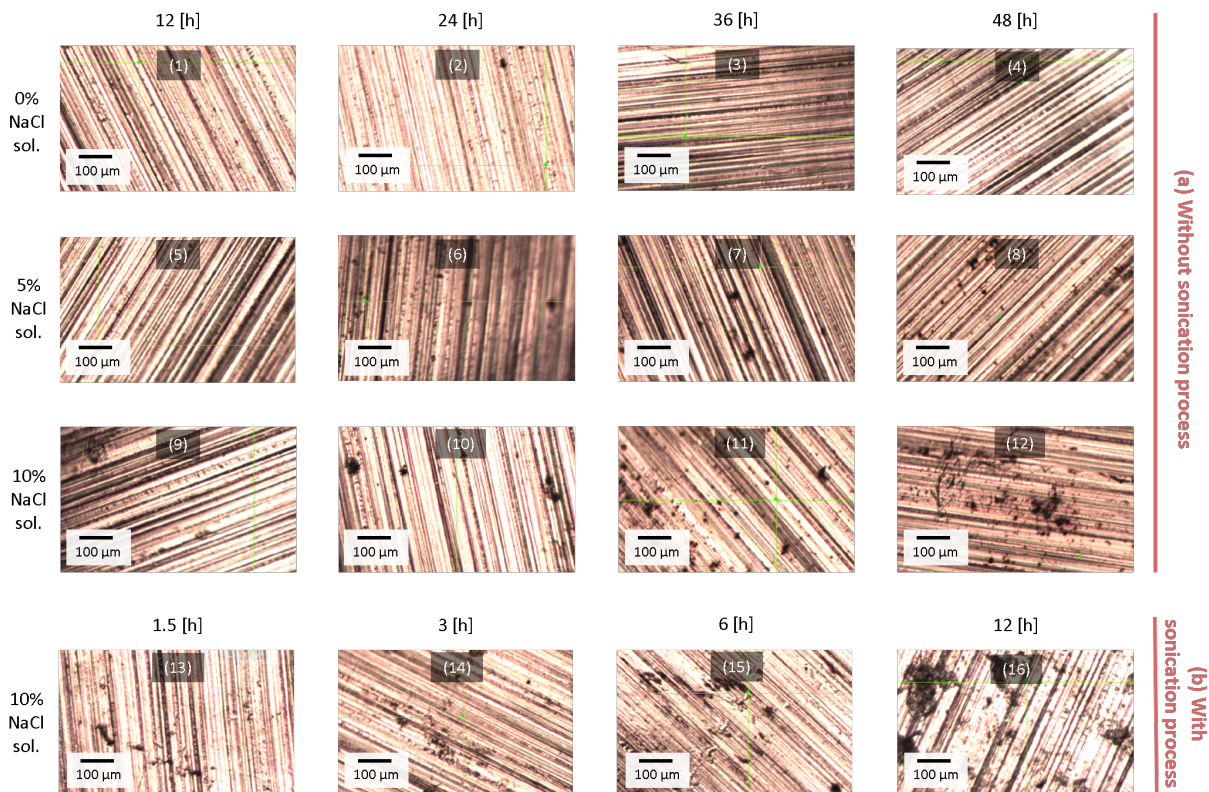


Figure 4.3: Surface activation process. Part 1: Morphology of Al substrate subjected to 0 wt %, 5 wt % and 10 wt % NaCl aqueous solution, during 12, 24, 36, 48 [h] in each concentration respectively. Part 2: Morphology of Al substrate subjected to a 5 [min] of sonication process in 10 wt % NaCl aqueous solution and then soaked in the same solution during 1.5, 3, 6, and 12 [h].

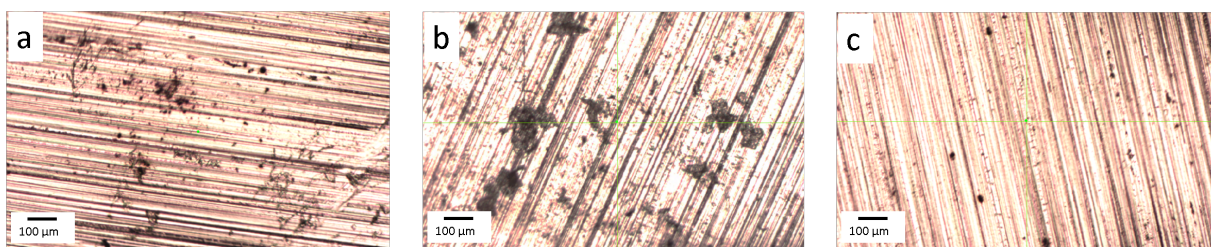


Figure 4.4: Comparison between: (a) Al substrate exposed to 10 wt % NaCl aqueous solution during 48 [h] without sonication treatment, (b) Al substrate subjected to a 5 [min] of sonication process in 10 wt % NaCl aqueous solution and then soaked in the same solution during 12 [h] and (c) Al substrate without any treatment.

4.1.2 Rinsed of sa-Al and Catalyst deposition of Fe/Co nanoparticles

In order to remove the Cl ions and to avoid the over activation of the Al substrate, it was thoroughly rinsed using deionized water and ethanol. In this way, the nanopyramidal surface structure of Al substrate enables excellent wettability for both water and ethanol, causing an uniform liquid film coating during the rinsing process, which prevents the exposure of sa-Al to the ambient¹².

The catalytic deposition process was carried out in a beaker where the sa-Al substrates were placed vertically, (see figure 4.5). After 18 [h], the catalytic solution had risen to the top, even spilling out of the beaker, this suggests that "the nanoporous structure of sa-Al could significantly improve the catalyst loading and distribution uniformity through a capillary effect"¹².

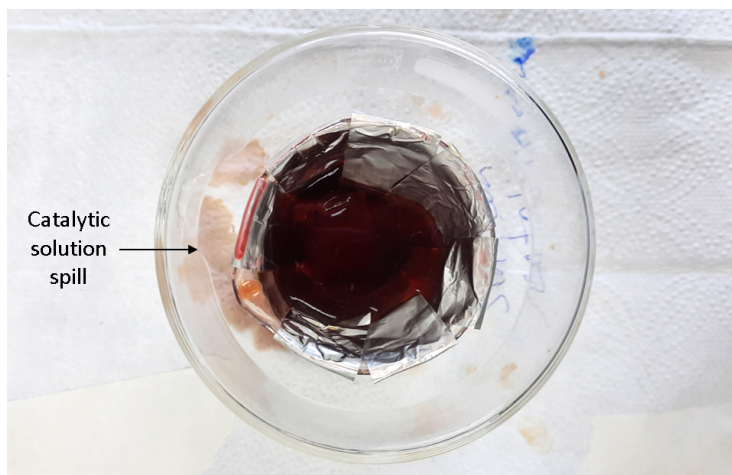


Figure 4.5: Catalytic solution spilling out of the beaker due to the capillary effect of the surface-activated Al substrate.

4.1.3 Low-temperature CNTs synthesis

Producing CNTs at 650 [°C] was a big change. In order to get CNTs, different reaction conditions were carried out, see table 4.1. Two reactions were performed with the same conditions in order to corroborate the results. These conditions are detailed and discussed below.

- **Reaction condition "A"**

Based on the literature, in our first attempt to synthesize CNTs a 15 [min] reaction time was used. For partial flows of Ar = 280 [ml/min] and C₂H₂ = 120 [ml/min] were used (total flow = 400 [ml/min]). On the other hand, due to the low melting point of Al (660 [°C]) the temperature of the reaction was fixed at 650 [°C]. With these conditions, it was not possible to synthesize CNTs. Instead, abundant undefined carbon-based structures were formed. Possibly this result was caused by the high C₂H₂ flow and by the low-temperature synthesis reaction.

| Parameter | A | B | C | D |
|---|-----|-----|-----|-----|
| Ar flow [ml/min] | 280 | 140 | 450 | 450 |
| C ₂ H ₂ flow [ml/min] | 120 | 60 | 50 | 50 |
| Total flow [ml/min] | 400 | 200 | 500 | 500 |
| Temperature [°C] | 650 | 700 | 650 | 650 |
| Time reacción [min] | 15 | 15 | 30 | 15 |

Table 4.1: Reaction conditions used to produce CNTs in the CVD machine.

- **Reaction condition "B"**

Based on the experience of "A", in this reaction, the total flow was reduced while the temperature of synthesis was increased. In other words, the new partial flows were; Ar = 140 [ml/min] and C₂H₂ = 60 [ml/min] (total flow = 200 [ml/min]). Furthermore, the temperature was increased to 700 [°C] while the time reaction was kept. The aim of these new partial flows was to try to reduce the creation of undefined carbon-based structures. The temperature increase was meant as an attempt to separate, in a better way, the carbon atoms from the acetylene gas. Also, it was a test in order to measure the resistance of Al substrate to temperatures higher than its melting point. The results were not good, after the synthesis, the structure of the Al substrate was very damaged, furthermore, despite that, an abundant carbon structure was not formed, a low quantity of undefined carbon-based structure remained. Therefore, with these conditions was not possible to synthesize CNTs.

- **Reaction condition "C"**

Based on the experience of "B", in this reaction the total partial flow of C₂H₂ was further reduced to 50 [ml/min] while the Ar flow was increased to 450 [ml/min] (total flow). On the other hand, the temperature of synthesis was restored to 650 [°C] but, in this case, the time of reaction was increased to 30 [min]. These new conditions aimed to avoid the formation of undefined carbon-based structures, diluting C₂H₂ in a higher Ar flow. Furthermore, due to the C₂H₂ concentration was reduced significantly, the time of reaction was increased and finally, the temperature was decreased in order to take care of Al substrate. However due to the increase in the reaction time, again, an abundant carbon structure was formed.

- **Reaction condition "D"**

Based on the experience of "C" in this reaction the only parameter changed was the reaction time, all other conditions of "C" were maintained. The result was a mix of CNTs with undefined carbon-based structures. Although

we expected better results, the small number of CNTs present in the sa-Al was enough to corroborate the hypothesis of this work; CNTs are better than conventional materials at the time to generate heat from solar radiation.

Note: The characterization of these results are presented in the next sections.

Calcinated vs uncalcinated substrate synthesis results

Definitely, the calcination process notably improves the growth of CNTs over Al substrates. Figure 4.6 part 1 shows how the uncalcinated Al substrate (a) has a small number of carbon structures on its surface while the calcinated Al substrate (b) is full of carbon structures. The reason for this improvement is due to the removal of nitrogen atoms from the substrate. The nitrogen atoms were added to the substrate during the catalysis deposition process but due to their high volatility, they are removed during the calcination process.

3 [h] vs 12 [h] of surface activated substrate synthesis results

Figure 4.6 part 2, shows how the surface activation process improves performance CNT synthesis, while (c) shows an Al substrate with a surface full of carbon structures, (d) shows an Al substrate with some white spots on its surface. The difference between (c) and (d) is the time exposition to the 10 wt % NaCl aqueous solution, while (c) was exposed during 12 [h], (d) was only exposed during 3 [h]. This result is because (c) had a higher superficial area than (d) due to the formation of nanopyramidal morphology more pronounced on its surface. This allowed the formation of more carbon structures in (c).

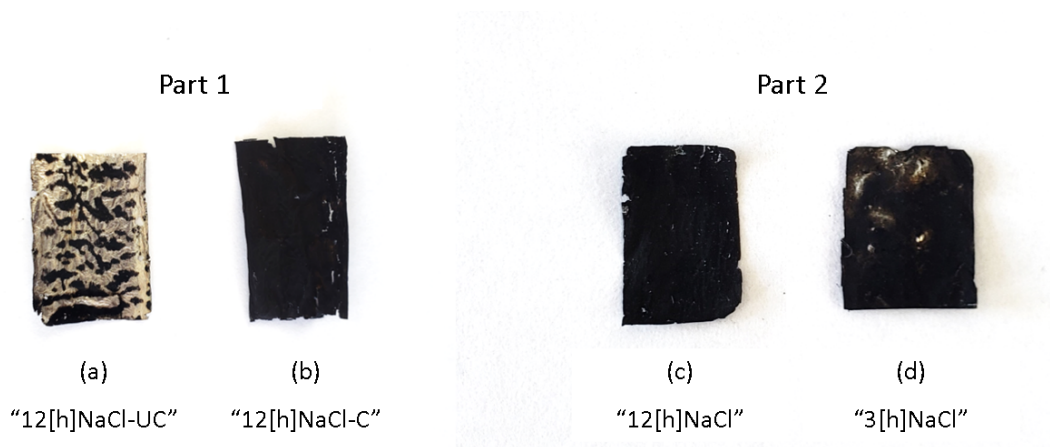


Figure 4.6: Part 1: Al substrates subjected to 5 [min] of sonication treatment with 12 [h] of time exposition to NaCl 10 wt % NaCl aqueous solution (a) uncalcinated and (b) calcinated. Part 2: Al substrate subjected to calcination process after 5 [min] of sonication treatment with a time exposure to 10 wt % NaCl aqueous solution of (c) 12 [h] and (d) 3 [h].

4.1.4 Raman Spectroscopy characterization

Raman analysis represents the most important results of this investigation. The information provided by this technique allows to identify if there are or are not CNTs in the sample, the shape and the quality of their structures, among other features that for the purpose of this investigation are not of vital importance. In this sense, the Raman results of this analysis are shown in figure 4.7, which display the spectra of the four reactions (RX) conditions carried out during this research and explained in section 4.1.3. Furthermore, the Rayleigh peak was omitted in order to visualize the CNTs spectra in a better way. The spectra were taken using an excitation wavelength of 532 [nm].

According to⁴⁶, the spectra obtained in RX "D" correspond to a MWCNTs sample. In other words, the typical feature of king of structure are shown, that is, the first ordered D, G and 2D band peaks located at 1346, 1582 and 2692 [cm⁻¹] respectively. The position of the peaks was found using Lorentzian-curve fitting plotted in the "Peak-o-Math" software, see figure 4.8 and appendix C.

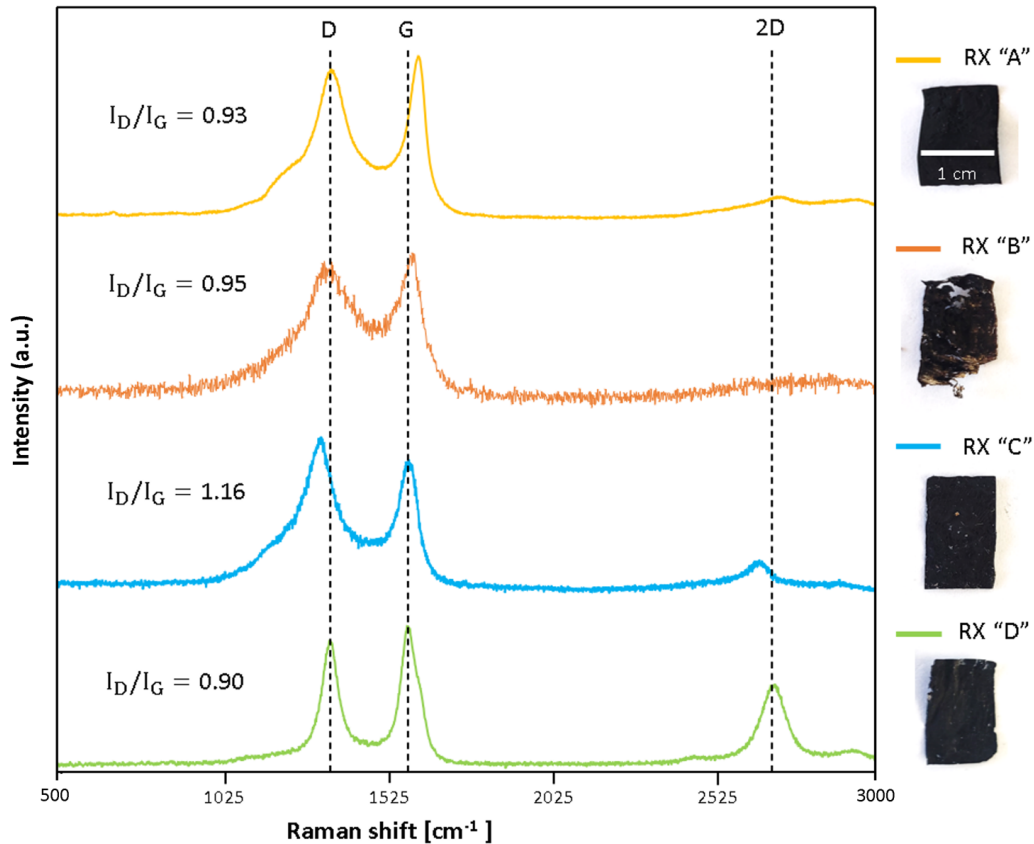


Figure 4.7: (RX "A", "B" and "C") Raman spectra of undefined carbon structure. RX "D" Raman spectrum of MWCNTs.

On the other hand, according to⁴⁶, the position of D and G band peaks, for a reference MWCNTs material with 100% purity, are 1350 and 1582 [cm^{-1}] respectively. That is, the position of G-band peak, obtained in this research, match with the value of reference MWCNTs material, while the position of D-band peak differs. This may be because, according to⁴⁶, the position and intensity of the D-band peak are varied with the excitation wavelength of the laser to a greater extend.

In addition, D-band peaks are found when the disorder is introduced into the CNTs structure, while G-band peak is assigned to "in-plane" displacement of the carbons strongly coupled in the hexagonal sheets⁴⁶. For this reason, the intensity ratio of D-band to G-band (I_D/I_G) has been used to determine the crystallinity of CNTs structure. in this way, the conditions of RX "D" reflects the higher crystallinity obtained in this research (0.9). In conclusion, Raman results allows to confirm was possible to synthesize multi-walls carbon nanotubes with the conditions of reaction (RX) "D", furthermore, these conditions offer the structure with higher crystallinity, which means, $I_D/I_G=0.9$.

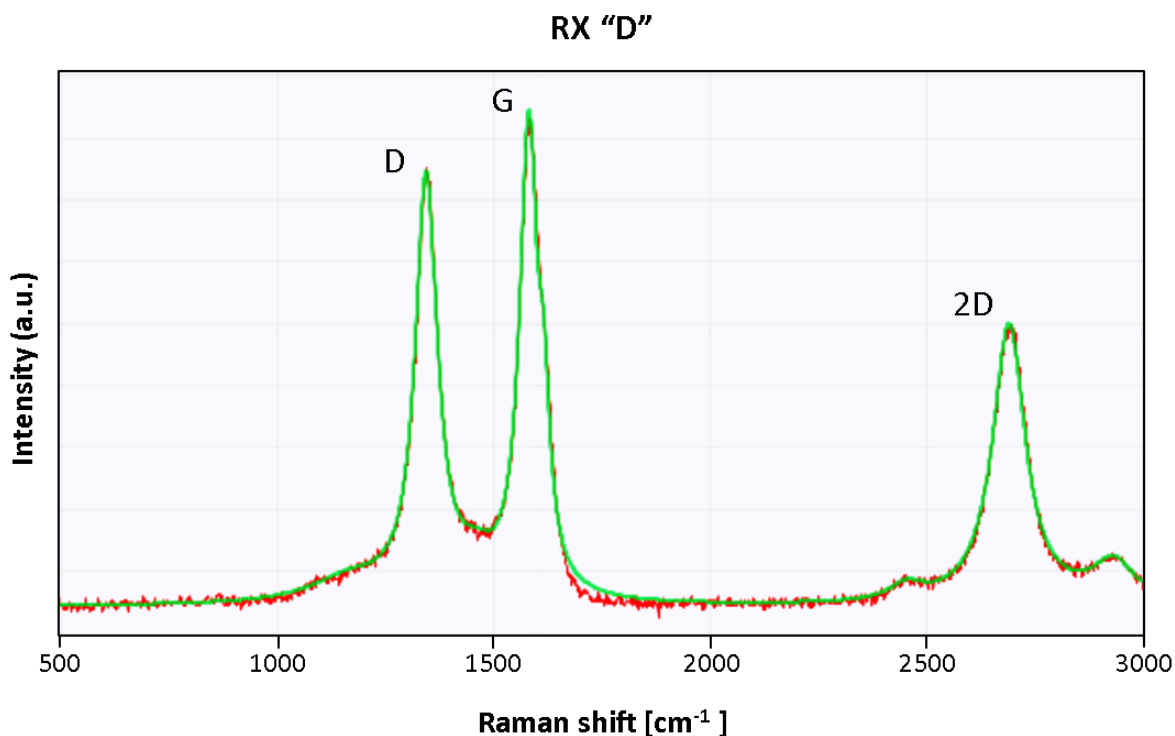


Figure 4.8: Lorentzian-curve fitting of RX "D"

4.1.5 Scanning Electron Microscopy (SEM) characterization

One of the best ways to analyze the CNTs synthesis results is to use the SEM test. In this way, figure 4.9 shows that the morphology of Al substrate and the CNTs. In this way, in part (a) it is possible to see how the surface of Al substrate had been activated, or in other words, how the Al surface had been altered in such way that a random network of Al nanopyramids have been formed. "The changes in the roughness is reflected by the structural color change of the substrate"¹². Furthermore, due to the small thickness of the substrate, there are some black areas in which the Al structure had been completely fractured.

However, it is precisely in these areas where it is most likely to observe the CNTs structures, see parts (b and c). These parts shows longitudinal structures forming a randomly networked mat, due to the nanostructured surface of the sa-Al substrate. Comparing these structures with those found in the literature¹², it can be assumed that the randomly networked mat are CNTs. Furthermore, in part (d), with some resolution difficulties, it is possible to see that they have a diameter of 60 [nm] approximately, according to the literature¹³, it means that the CNTs synthesized in this work were MWCNTs. On the other hand, due to the random structure of the CNTs, their length cannot be determined. Finally, some important properties like chirality were not possible to observe due to the resolution of the SEM equipment used, and its analysis remains open to future works. These photos were taken at a voltage of 15 kV.

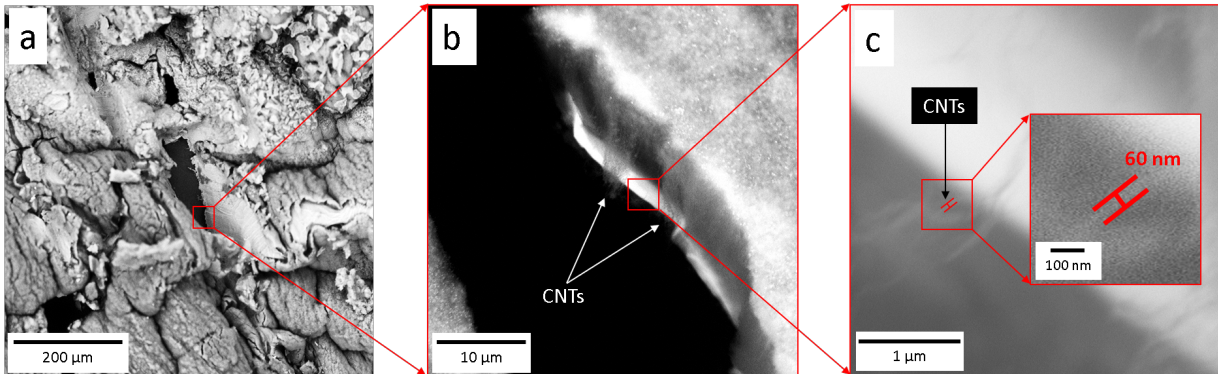


Figure 4.9: SEM images of (a) surface-activated Al and of (b, c) CNTs.

4.1.6 X-ray Photoelectron Spectrometer (XPS) characterization

The chemical status of the Al substrate was probed by XPS to investigate the changes in its chemical composition during the fabrication process. Each analysis was performed in a spot of 100 μm in diameter and 5 to 7 [nm] deep. In this way, figure 4.10 shows the XPS the spectra of Al substrate evolution, and in the next section each spectrum is described in detail.

Chemical composition of Al substrate before (spectrum a) and after (spectrum b) of the surface activation process

In spectrum (a) there is an intensive C1s peak indicating carbon contamination from manual handling. The C1s peak for contamination typically has C-C, O-C=O, and C-O-C components placed in 284.8, 286, and 288.5 [eV] respectively. However, for carbon on native oxide of aluminum, the C1s appears at 286 [eV]. Most samples that have been exposed to the atmosphere will have a detectable quantity of carbon contamination, in order to remove it, an argon sputtering could be used⁴⁷. On the other hand, the O1s is another strong peak present in (a). It reflects the presence of oxygen atoms, that always will be present in samples exposed to the atmosphere, either due to contamination, oxidation, or water. The interpretation of O1s spectra is not straightforward, because the O1s binding energy of many compounds and species falls within a very narrow range, however, in this case, it can be assumed that the O1s peak is due to the presence of alumina in the surface of the sample. In such case, the O1s peak is at 531.1 [eV]⁴⁸. Also, the Al2p peak is present in (a). Although an Al sample was analysed, there were many pollutants on the Al surface and therefore, the intensity of the Al2p peak was reduced. Furthermore, aluminum is a highly reactive metal, so it always has a oxide layer on its surface. This is important because the Al2p peak position, as well as its intensity, may vary or split depending on the thickness of the oxide film. In a common state, the Al2p peak of an Al oxide on Al foil is placed at 75.6 [eV]⁴⁹. Furthermore, in part (a) there are some other contaminants present in a small amount such as; Ca2p peak, referring to calcium as well as S2p peaks, referring to sulfur.

In spectrum (b), the pollutants peaks of (a), are not present or were reduced. This corroborated that the surface activation process removes atoms from the Al surface, altering its morphology and in this case, eliminating unwanted impurities. For example, the atomic % of the C1s peak went from 56.6% in (a) to 33.6% in (b), while the Ca2p and S2p peaks, present in (a), disappeared in (b). However, in (b) the N1s peak appears, it refers to nitrogen atoms and could be consider as a contaminant. On the other hand, due to the increase in the surface area of the Al substrate, caused by the surface activation process, the atomic % of O1s and Al2p increased. The atomic % of O1s and Al2p went from 33.8 % and 7 % in (a) to 52.3 % and 13.3 % in (b) respectively. Finally, due to exposure of Al substrate to the NaCl aqueous solution, the Na1s peak, referring to sodium, appears in (b), specifically at 1071-1071.05 [eV] accompanied by a strong Auger peak at 497 [eV] and at 536 [eV], the last one overlaps with O1s peak⁵⁰.

Chemical composition of Al substrate covered with the catalytic solution before (spectrum c) and after (spectrum d) of calcination process

In spectrum (c) the O1s, C1s, Al2p, and N1s peaks, present in (b), were maintained but with some variation in their atomic %. For example, the atomic % of the O1s peak went from 52.3% in (b) to 46.2% in (c), this is because the sample of the spectrum (b) is not the same as the spectrum (c). The sample of the spectrum (c) was immersed in the catalytic solution immediately after the rinsed process, therefore, the catalytic solution fills the Al substrate surface, before the it reacts with the atmosphere creating an oxide film over it. This is also corroborated by the Al2p peak, which went from 13.3 % in (b) to 3.5 % in (c). Also, the Cs1 peak went from 33.6 % in (b) to 39.2 % in (c), this reflects the carbon contamination from manual handling. On the other hand, in (c) the Co2p3 and Fe2p3 peaks appear. These peaks correspond to the cobalt (II) and iron (III) nitrate salts used in the catalyst deposition process.

In the case of Co2p3, the peak for Co (II) is placed at 786 [eV]⁵¹ while for Fe (III) was not possible identify the position of the peak, because a high-resolution XPS analysis is needed.

Then, after the calcination process, the principal difference between the spectra (c) and (d) is the elimination of the N1s peak. This is because the nitrogen atoms a very volatile, therefore, after subjecting the Al substrate to 600 [°C] during 6 [h], the N1s peak placed at 397 [eV]⁵² was removed. Furthermore, the carbon contamination was reduced after the calcination process, in other words, the C1s atomic % went from 39,2 in (c) to 23,5 [eV] in (d). On the other hand, there were also changes in the atomic % of the Co2p3 and Fe2p3, it means, they went from 6.1 % and 1.5 % in (c) to 6.2 % and 11.6 % in (d) respectively. These increases may be due to the elimination of the nitrogen atoms and the reduction of carbon contamination. These two factors could improve the detection of the cobalt and iron atoms. In addition, due to the oxidation of the salts caused by the calcination process, the O1s peak also increased, it went from 46.2 % in (c) to 55 % in (d). Finally, the atomic % of Al2p was reduced in (d), maybe due to the increase of the other peaks, it went from 3,5 % in (c) to 2.4 % in (d).

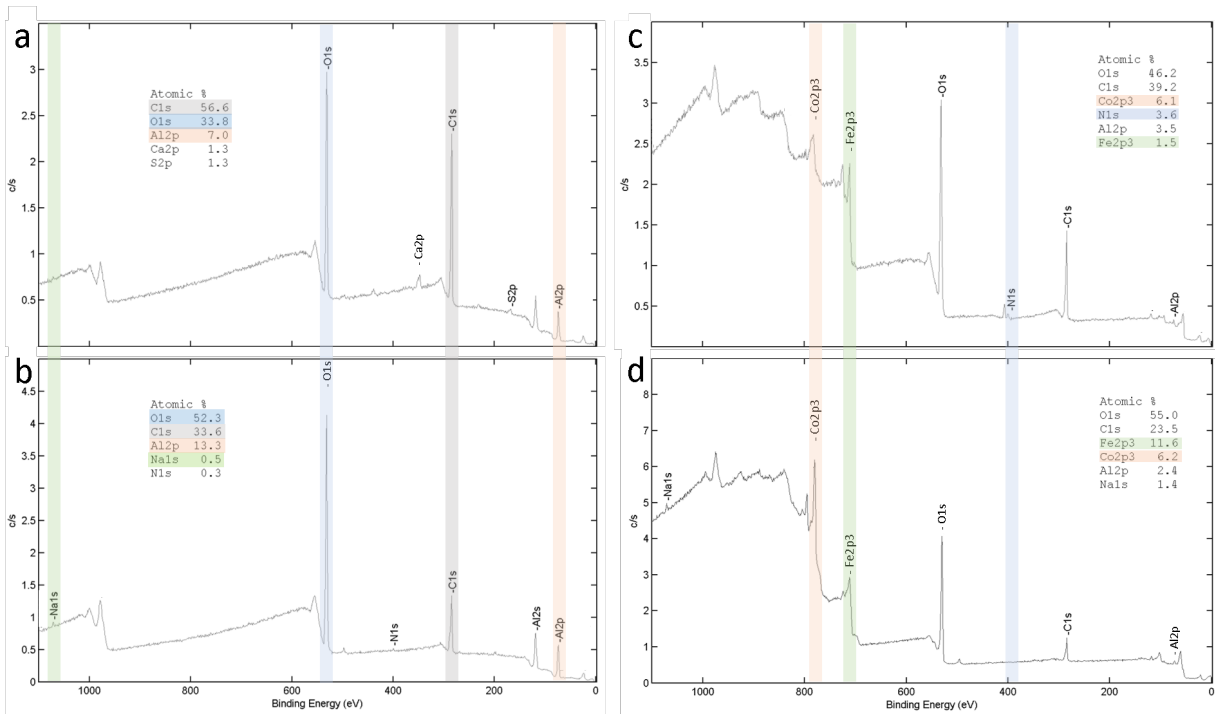


Figure 4.10: (a,b) XPS spectra of the Al substrate without (a) and with (b) surface activation. (c, d) XPS spectra of surface-activated Al impregnated with the catalytic solution without (c) and with (d) calcination process.

Finally, the high resolution XPS of the C1s feature is shown in figure 4.11. The peaks related to C-C at 284.5 eV and C=C at 285.4 [eV] binding energies represent the sp² and sp³ carbon hybridisation, related with the synthesis of multi-walled carbon nanotubes^{53,54}. The other peaks are related with the formation of byproducts that includes

amorphous carbon. The fitting analysis comes from the fact that the nanotubes were synthesized in a non-oxidative environment therefore having oxide functional groups attached to them. Voigt function was used for XPS peak deconvolution of the C1s of analysed sample. Table 4.2 shows the binding energy of the bonds. This data was compared with those reported in the literature⁵⁵⁻⁵⁸

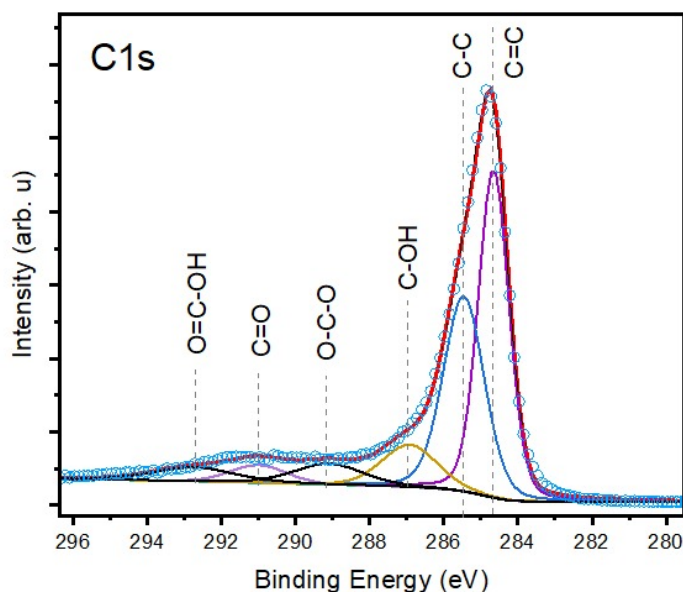


Figure 4.11: High resolution XPS C1s core level presenting the main binding energies

| | |
|--------|--------------------|
| C=C | 284.38–284.53 [eV] |
| C-C | 285.11–285.5 [eV] |
| C-O | 286.21–287.53 [eV] |
| C-OH | 286–288.5 [eV] |
| O-C-O | 286.45–287.92 [eV] |
| C=O | 288.39–289.54 [eV] |
| O=C-OH | 289–291.6 [eV] |

Table 4.2: XPS analysis data.

4.2 Radiation heating results

In this section are displayed the solar-thermal analysis results of the 4 solar absorber devices that were compared in this investigation. That is, the material proposed in this research (CNTs/sa-Al) and of other 3 solar absorber materials (bC/sa-Al, CNTs-bap/sa-Al and bap/Al) described in section 3.3. The aim of this part was to measure the efficiency of these 4 devices at the time to transform solar radiation into heat. The equipment used and all the process performed to record the temperature data of the materials are described in the section 3. Furthermore, once the data was obtained, they were transferred to an Excel document where all the graphs were made. Finally, all studies were performed in the city "San Miguel de Urququí - Ecuador", specifically in the coordinates: 0.41209922855835335, -78.19097501534286. In this sense, the solar-thermal analysis was performed as follows.

4.2.1 Part 1: "(5%)CNTs-bap/sa-Al" vs "(1%)CNTs-bap/sa-Al"

First, in section 3.3 point 3, two devices were prepared, the first one was a surface-activated Al substrate cover with at 1 wt % CNTs bap solution [(1%)CNTs-bap/sa-Al] and the other one was a surface-activated Al substrate cover with at 5 wt % CNTs bap solution [(5%)CNTs-bap/sa-Al]. These two devices were tested in this part, for this, the temperature data collection system (thermal insulating box) was placed outdoors, for 3 days and from 12 [pm] to 2 [pm] in each day. Once the data temperature of the aforementioned devices was analysed, it was possible to identify which one reaches higher temperatures, and therefore, use it in the next test (part 2). The results of this part are presented in the next subsection.

The idea of these devices was to prove if a mixture of the common material with the carbon structure proposed in this work, will improve the absorption of solar radiation. Also, if the concentration of CNTs will affect this process, and therefore, the efficiency of the device at the time to transform solar radiation into heat. In this subsection, the values of the temperature data collection of these two devices are presented in figure 4.12 while in figure 4.13 part (a) a zoom of the temperature differences can be visualized.

After analyzing the obtained results some important observations can be made. First, in figure 4.12 some mountains and valleys can be viewed, this corresponds to the variations of the solar intensity due to the movement of the clouds. Second, the shaded zone corresponds to the interval of values taken in order to make an average of the device temperature differences for each day, then, a new average of the previous values were performed, see figure 4.14, this value is 1.08 [°C] and represents the average of the devices temperature differences during the 3 days. Third, day 1 was a very cloudy day, see appendix D part (a), therefore temperature reached by the devices were not too high compared with day 2 and 3, which were cloud-free at the beginning, see appendix D part (b), therefore the maximum temperature reached was 74.76 and 72.12 [°C] for (5%)CNTs-bap/sa-Al and (1%)CNTs-bap/sa-Al respectively on day 3. These are interesting values taking in count that the tested samples have an area of 2x3[cm].

In conclusion, the (5%)CNTs-bap/sa-Al device heats, on average, 1.08 [°C] more than (1%)CNTs-bap/sa-Al device, this result allows inferring that a higher concentration of CNTs allows absorbing a greater amount of solar radiation or photons that create a series of vibrations in the carbon structures or phonons. This allows the material to heat up and therefore, a higher temperature is reached. Finally, after this analysis, the (5%)CNTs-bap/sa-Al device was chosen to be tested in part 2.

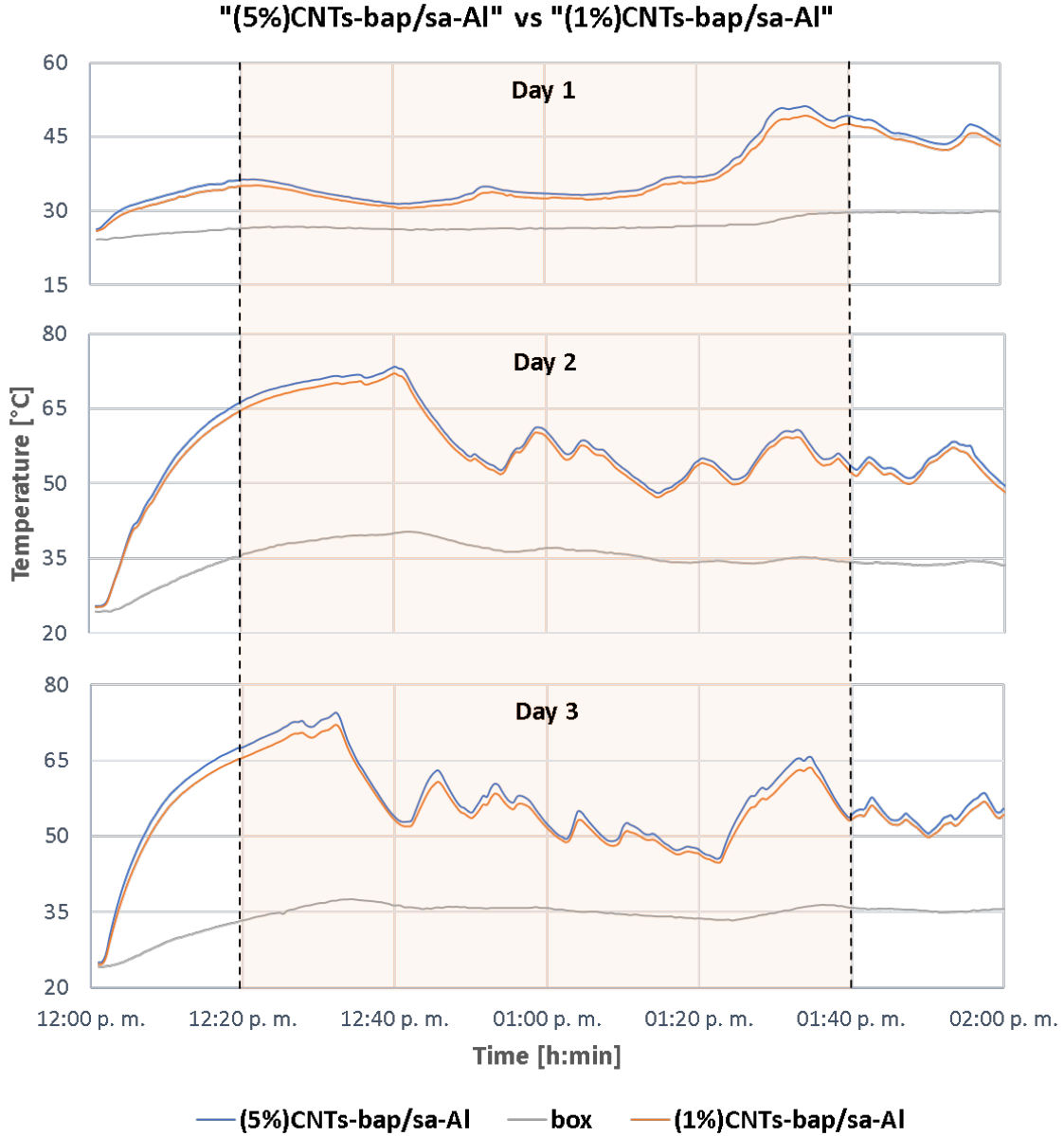


Figure 4.12: Thermal analysis of surface-activated Al substrates covered with; 1 wt % CNTs vs 5 wt % CNTs black anticorrosive paint (bap) solutions. The shadow zone represents the data section used to find the average temperature differences between these two devices.

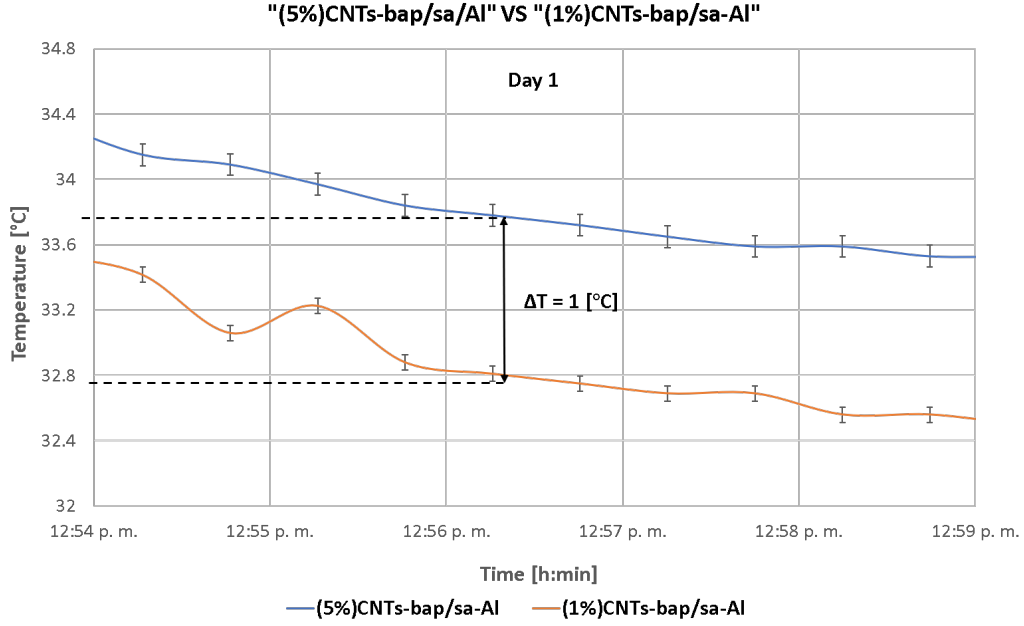


Figure 4.13: (a) Thermal analysis zoom of surface-activated Al substrates covered with; 1 wt % CNTs vs 5 wt % CNTs black anticorrosive paint (bap) solutions

Temperature differences average

| Day | A – B [°C] |
|---------|------------|
| 1 | 0.97 |
| 2 | 0.98 |
| 3 | 1.30 |
| Average | 1.08 |

A → (5%)CNTs-bap/sa-Al

B → (1%)CNTs-bap/sa-Al

Figure 4.14: Average of temperature differences between surface-activated Al substrates covered with; 1 wt % CNTs and 5 wt % CNTs black anticorrosive paint (bap), for each day.

4.2.2 Part 2: "CNTs-bap/sa-Al", "bap/Al", "CNTs/sa-Al" and "bC/sa-Al"

This part shows the solar-thermal analysis of the material proposed in this research (CNTs/sa-Al), and of other 3 solar absorber materials (CNTs-bap/sa-Al, bap/Al and bC/sa-Al) described in section 3.3. In sense, the test in this part was performed in a similar way as in part 1. That is, the temperature data collection system was placed outdoors, for 3 days and from 12 [pm] to 2 [pm] in each day. However, the time interval used to find the average temperature differences between the devices, was from 12:20 to 1:40 [pm] or 80 [min]. The results are presented in figures 4.15, 4.16 and 4.17 which represent the temperature data collection of day 1, day 2 and, day 3 respectively. The analysis of each day is performed below.

Day 1

First, the peaks and valley shown in figure 4.15 correspond to variation in solar radiation caused by the presence of clouds during the solar-thermal analysis. Second, the bap/Al and CNTs-bap/sa-Al devices show similar temperature behavior during all data collection with some intersection among them, in other words, that CNTs-bap/sa-Al device heats, on average, 0.33 [°C] more than bap/Al device during 51 [min] in a solar-thermal analysis of 80 [min]. On the other hand, the bC/Al and CNTs/sa-Al also had similar behavior at the beginning but after 40 [min] the temperature value of CNTs/sa-Al start to increase more than bC/Al temperature values. However, neither of the two aforementioned devices did not heat more than bap/Al device. Conversely, bap/Al device heats, on average, 1.24 and 1.77 [°C] more than CNTs/sa-Al and bC/Al devices respectively. See the summary of this analysis in table 4.3 - day 1. Finally, the higher temperature reached on day 1, was of 66.09 [°C] belonging to bap/Al device.

In conclusion, CNTs-bap/sa-Al device shows a little improvement over bap/Al devices, at the time to transform solar radiation into heat. While, CNTs/sa-Al and bC/sa-Al did not show any improvement. These results can be attributed to the structural damage of the devices caused during the CNTs synthesis process. In other words, the structural fractures of CNTs/sa-Al and bC/sa-Al would be reducing the thermal conductivity of the devices.

Day 2

In this analysis was performed on an almost free-cloud day, therefore, the present of valley and peak in figure 4.16 is minimal. On the other hand, in this graph, a well-defined temperature trajectories can be viewed, it means, there are no intersections in the devices temperature values. As in the day 1 analysis, only CNTs-bap/sa-Al devices heats up more than bap/Al device, with an average value of 3.44 [°C] during all the solar-thermal analysis. Furthermore, this difference can be reached during the first minutes of the analysis. This is a big improvement with respect to day 1 and it can be attributed to the solar intensity stability, which allows a quick heating of the CNTs-bap/sa-Al. On the other hand, bap/Al device overlaps to CNTs/sa-Al and bC/sa-Al with an average value of 1.35 and 7.18 [°C] respectively. See the summary of this analysis in table 4.3 - day 2. Finally, the higher temperature reached in day 2, was of 61.21 [°C] belonging to CNTs-bap/sa-Al device.

In conclusion, the temperature differences between CNTs-bap/sa-Al and bap/Al devices, could be higher on free-cloud days. This may be because, according to⁵⁹, clouds absorb infrared radiation from the sun, therefore, on a sunny day, a higher intensity of this radiation can reach the CNTs structures, which shows better absorption properties,

in the infrared range, than only black anticorrosive paint. On the other hand, again this results of CNTs/sa-Al and bC/sa-Al devices can be attributed to their structural damages, which do not allow the phonon transfer, reducing thermal conductivity.

Day 3

As can be visualized in figure 4.17, the solar-thermal analysis 3 was performed in a day with variable solar intensity, but very sunny at the beginning. Therefore, in the first minutes it is possible to see a behavior similar to day 2, that is, a quick temperature increase of CNT-bap/sa-Al over the bap/Al device, while, after 20 [min] of solar-thermal analysis some clouds start to appear in the shy causing a behavior more similar to day 1, that it, interceptions in the devices temperature values. This idea gets stronger when 2.02 [°C], the average temperature difference between CNTs-bap/sa-Al and bap/Al devices in day 3, is compared with 1.88 [°C], the average of 0.33 and 3.44 [°C], which are the temperature differences between CNTs-bap/sa-Al and bap/Al devices of day 1 and 2 respectively. On the other hand, other interesting aspect is that both CNTs/sa-Al device and bC/sa-Al device reached, on average, 0.86 and 0.25 [°C] more than bap/Al, respectively. This increase in the temperature values of CNTs/sa-Al and bC/sa-Al devices, it may be because due to poor structural quality of the devices, they were changed by new devices, while the CNTs-bap/sa-Al and bap/Al were maintained. Due to there are small-time interval in which the temperature of bap/Al is higher than CNTs/sa-Al and bC/sa-Al devices, the previous results correspond to the average performed during 70 and 66 [min] severally. See the summary of this analysis in table 4.3 - day 3. Finally, the higher temperature reached in day 3, was of 69.87 [°C] belonging to CNTs-bap/sa-Al device.

In conclusion, the presence of clouds take a crucial role in solar-thermal applications, in this particular case, it has been observed that CNTs-bap/sa-Al device heats, on average, 3.44 [°C] more than bap/Al device on a free-cloud day, 0.33 [°C] more, on a cloudy day, and 2.02 [°C] more, on a partly cloudy day. On the other hand, due to the structural damage of CNTS/sa-Al and bC/sa-Al devices, it is not possible make a precise conclusion. Therefore, in futures works the use of a thicker Al is recommended. Finally, due to day 2 offers the most convenient data, it was used in the theoretical exergy analysis.

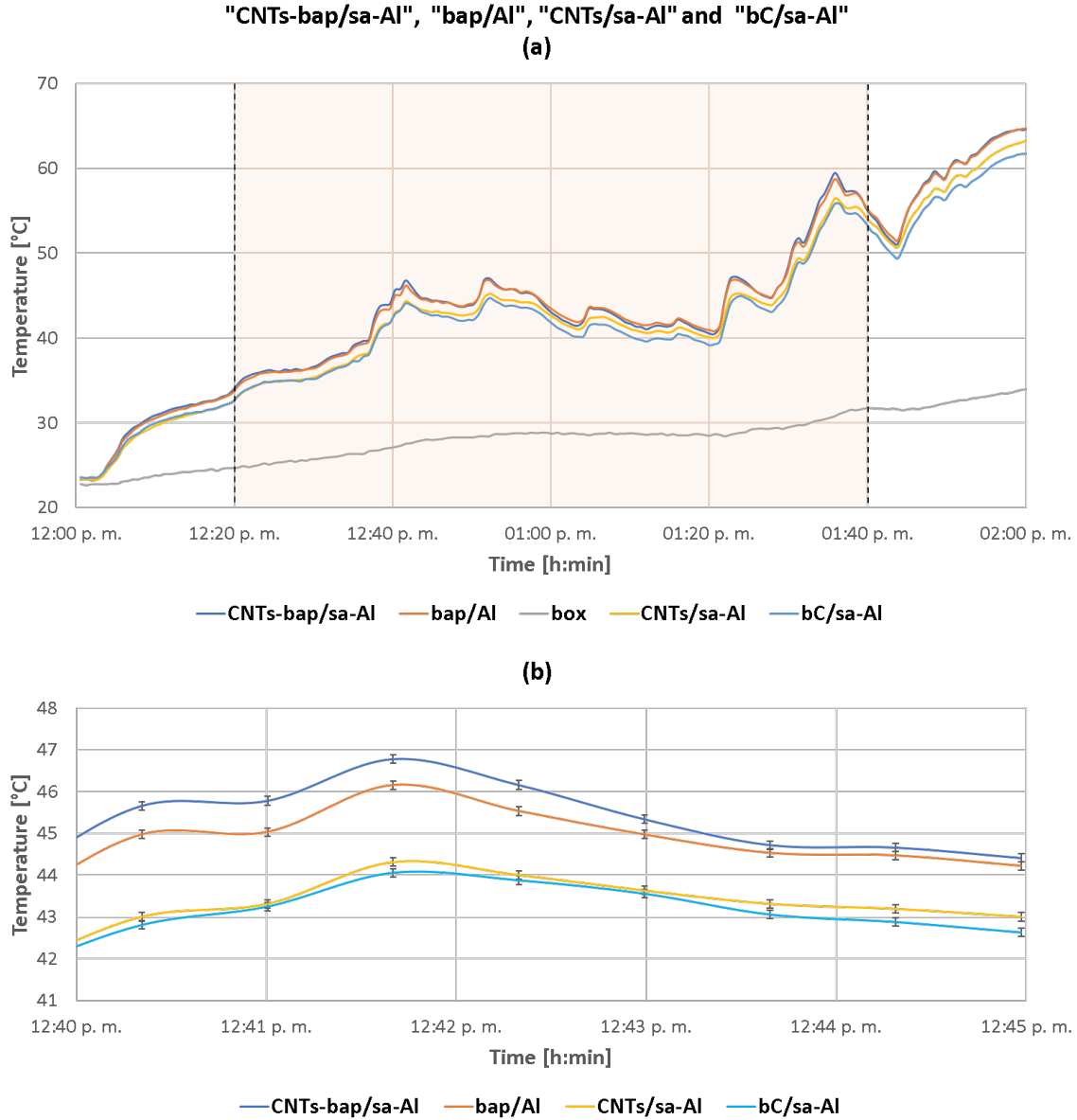


Figure 4.15: Day 1: (a) thermal analysis of the 4 BB references used compared in this research, as well as, thermal analysis reference system (box). (b) represent a zoom of (a). The shadow zone represents the data section used to find the average temperature differences between the devices.

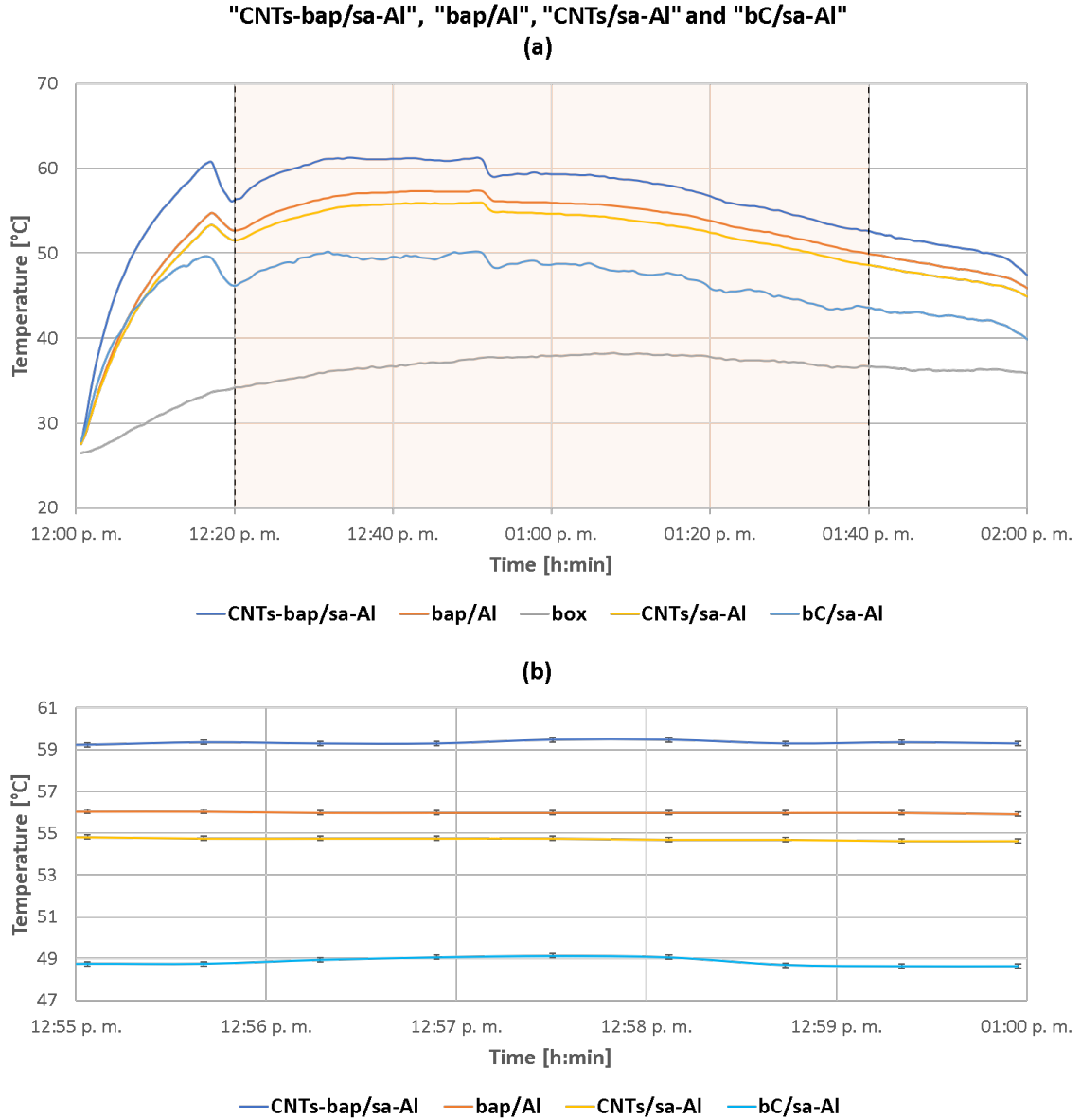


Figure 4.16: Day 2: (a) thermal analysis of the 4 BB references used compared in this research, as well as, thermal analysis reference system (box). (b) represent a zoom of (a). The shadow zone represents the data section used to find the average temperature differences between the devices.

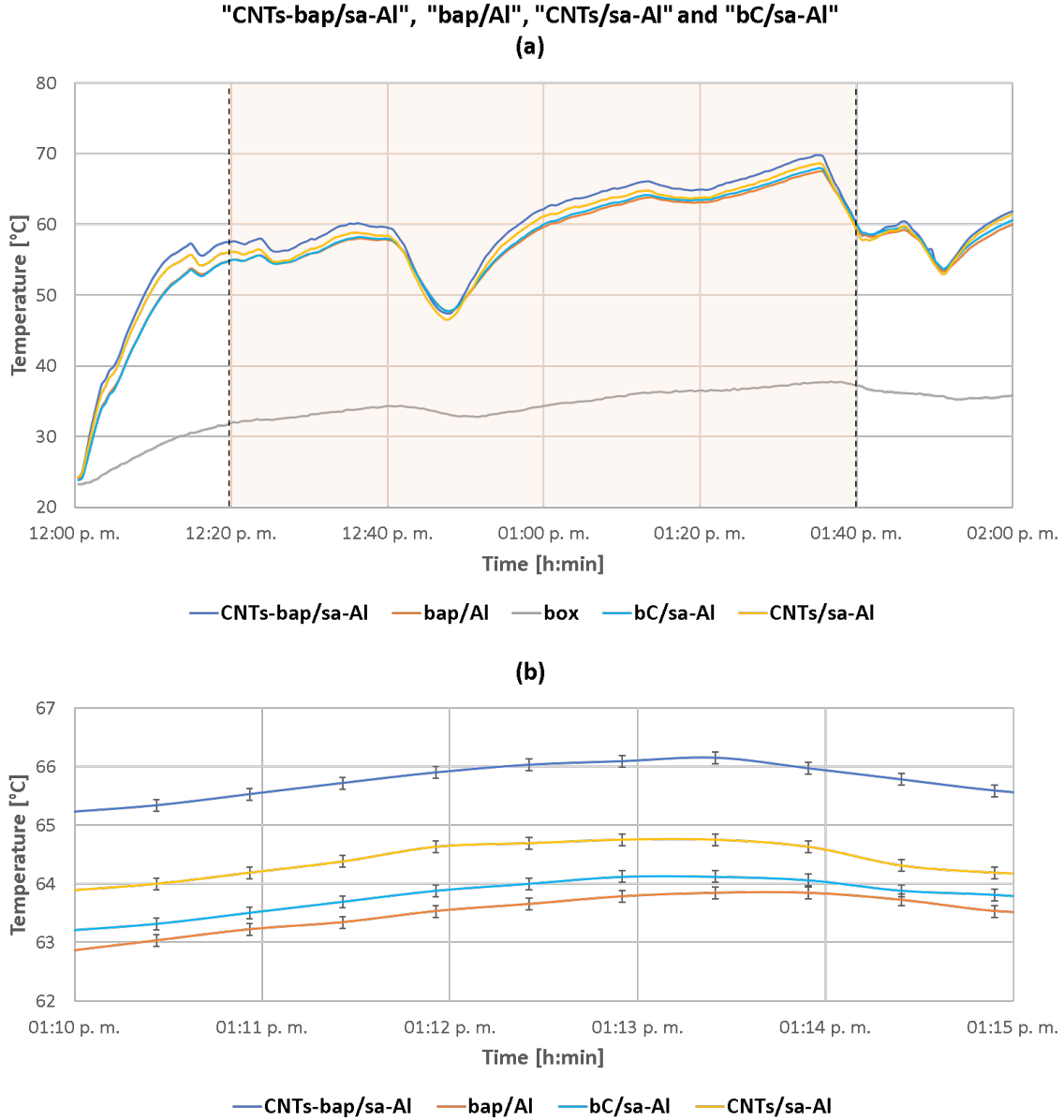


Figure 4.17: Day 3: (a) thermal analysis of the 4 BB references used compared in this research, as well as, thermal analysis reference system (box). (b) represent a zoom of (a). The shadow zone represents the data section used to find the average temperature differences between the devices.

| Sensor analysis | Day 1 | | Day 2 | | Day 3 | |
|---------------------|--------------------------|------------|--------------------------|------------|--------------------------|------------|
| | Average temperature [°C] | Time [min] | Average temperature [°C] | Time [min] | Average temperature [°C] | Time [min] |
| S1>S2 | 0.33 | 51 | 3.44 | 80 | 2.02 | 76 |
| S2>S1 | 0.21 | 29 | 0.00 | 00 | 0.38 | 04 |
| Total analysis time | | 80 | | 80 | | 80 |
| S4>S2 | 0.00 | 00 | 0.00 | 00 | 0.25 | 66 |
| S2>S4 | 1.24 | 80 | 1.35 | 80 | 0.06 | 14 |
| Total analysis time | | 80 | | 80 | | 80 |
| S5>S2 | 0.00 | 00 | 0.00 | 00 | 0.86 | 70 |
| S2>S5 | 1.77 | 80 | 7.18 | 80 | 0.75 | 10 |
| Total analysis time | | 80 | | 80 | | 80 |

S1 → CNTs-bap/sa-Al S2 → bap/Al S4 → CNTs/sa-Al S5 → bC/sa-Al

Table 4.3: Summary of the thermal analyses performed during 3 day on CNTs-bap/sa-Al, bap/Al, CNTs/sa-Al and bC/sa-Al devices.

4.3 Theoretical exergy analysis

Exergy is the amount of energy from a specific system that can be used in form of work. In principle, it is possible to have exergy when there is a time-dependent contrast between a system A and the environment A_0 that can be assumed like a much larger system (reservoir), in this case, the exergy comes from the contrast in temperature between the analyzed materials in this work and the environment. On the other hand, in this section the theoretical exergy analysis of CNTs-bap/sa-Al vs bap/Al devices, is performed. CNTs-bap/sa-Al device was chosen to do this analysis because it shows the greater temperature contrast over the bap/Al, the reference material. Using equation 2.11, in figure 4.18 one can gauge the importance of gaining a few degrees difference in heating at a particular reservoir temperature. We can see from the plot that we can produce an extra 0.023 W/cm^2 (at time 1000 [s]) by improving the temperature increase by around four degrees. This means an additional 230 Watts per square meter. This is consistent with what is expected from the impact of global warming calculations in terms of the loss of exergy of the planet (Goran Wall), except in that case the reservoir is heating up. According to⁶⁰ the heat capacity of Al is $0.9 \text{ [J/g } ^\circ\text{C]}$, or $0.05 \text{ [J/cm}^2 \text{ } ^\circ\text{C]}$ because $1 \text{ [g]} = 18 \text{ [cm}^2\text{]}$ of the Al substrate used in this research. Therefore, exergy was expressed in $[\text{W/cm}^2]$.

On the other hand, in figure 4.19 it is shows the exergy plot, in Watts/cm^2 , available as a function of the temperature T (of the sample) in relation with the fixed temperature $T_0=25 \text{ C}$ (of the box). This figure is interesting because show the faster than linear increase of exergy with T , for example, an increase of 5 [K] in the sample temperature, around 320 K , can produce an increase in exergy of 50-60%. In other words, improvements in the temperature maximum seems very promising.

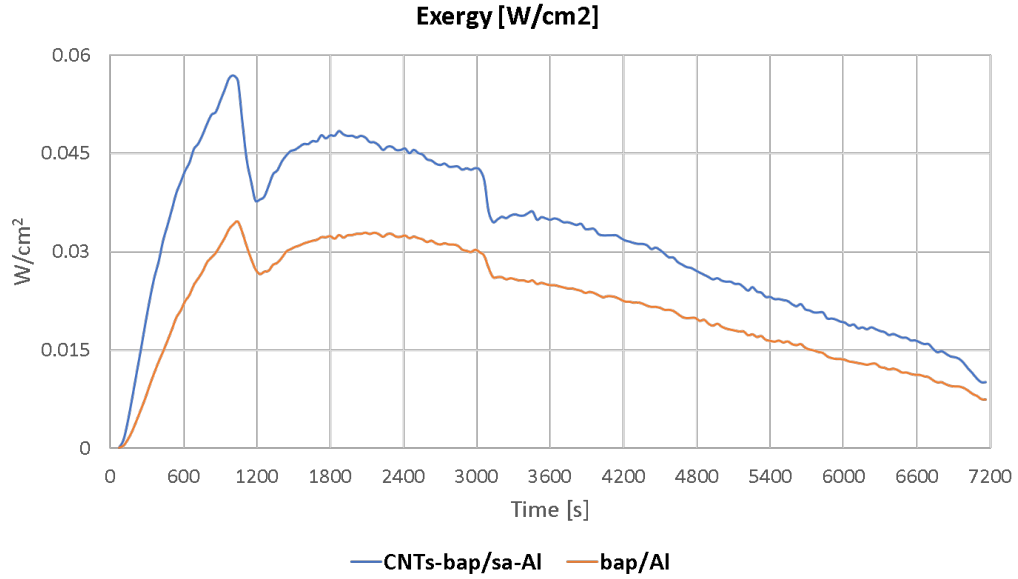


Figure 4.18: The exergy available due to the temperature difference between the two best BB coatings. Note that there can be up to 0.023 Watts per cm² extra due to the temperature achieved by the best coating.

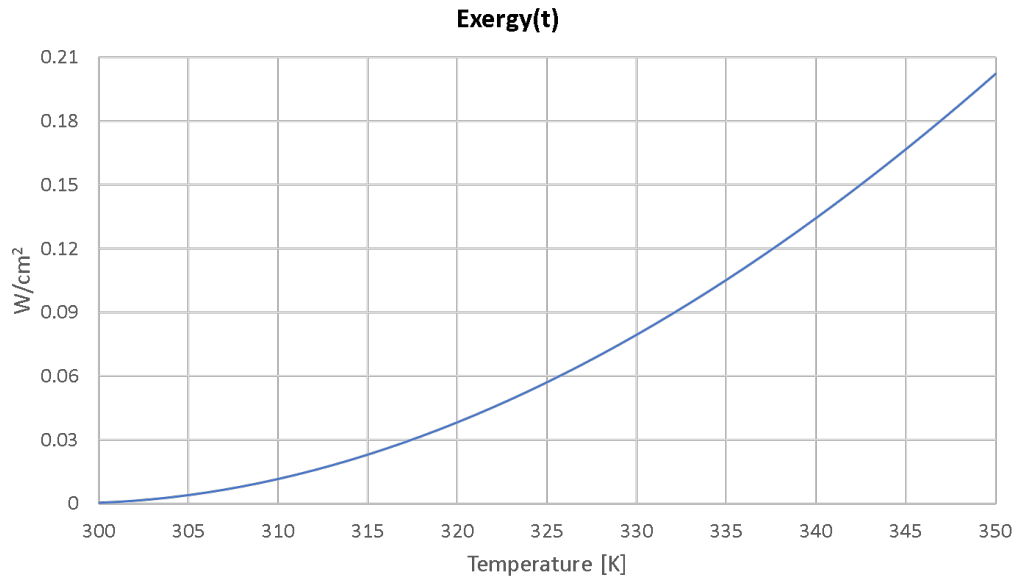


Figure 4.19: Exergy as a function of the temperature T in relation with the fixed temperature of $T_0=25$ C.

Chapter 5

Conclusions & Outlook

In conclusion, the material developed during the present research contributes to the global energy transition toward clean and renewable energy sources. In other words, through the chemical vapor deposition (CVD) synthesis technique, a solar absorber material that transforms solar radiation into usable heat (exergy) for the industrial sector, was devised. This material is based on carbon nanotubes over a surface-activated aluminum (CNTs/sa-Al). In this sense, the process performed during this research can be summarized as follows:

5.1 Synthesis of solar absorber material or CNTs/sa-Al

1. Aluminum sheets of 25.4 μm thick were used as substrate, over them, a surface-activation treatment was performed.
2. The surface activation process created a nanopyramidal surface structure that improved the growth yield of CNTs because of three reasons: (1) it reduced the oxide film and impurities, this favored the growth of CNTs, (2) the nanopyramidal structure improved the loading and dispersion of catalytic solution through capillary effect and (3) the increase in superficial area allowed the synthesis of a random network of CNTs that secured high internal reflections to maximize radiation absorption. The surface activation process was divided into two parts, after which it can be concluded that the sonication process allows reducing to 1/4 the exposition time of Al substrate to the NaCl solution.
3. After the surface activation process, Al substrates were rinsed in water and ethanol for 10 [min] in each one. This prevented direct contact between the Al substrate and the oxygen present in the air, thus, the reformation of the oxide film in the Al substrate surface was reduced.
4. Immediately after rinsing, the Al substrate was submerged in the catalytic solution for 18 [h]. The catalyst solution contained 0.1 M iron (III) and 0.1 M cobalt (II) nitrate in ethanol.

5. In order to eliminate nitrogen contamination present in the catalytic solution, Al substrates were submitted to a calcination process, that is, they were heated up to 600 [°C] for 6 [h]. This process improved considerably the CNTs synthesis.
6. Finally, the Al substrate was introduced in a CVD furnace and submitted to 650 [°C] during 15 [min] under a partial flow of 50 [ml/s] C₂H₂ and of 450 [ml/s] Ar. This process allowed to synthesize CNTs over a surface-activated Al. See the details of the process in section 3.1 and the details of the results in section 4.1.

5.2 Characterization process

The structural properties of the material were characterized through the Raman, Scanning Electron Microscopy (SEM), and X-ray Photoelectron Spectrometer (XPS) technique. Raman showed the spectrum of MWCNTs, that is, the D, G, and 2D peaks located at 1346, 1582 and 2692 [cm⁻¹] respectively. Furthermore, the I_D/I_G ratio showed a crystallinity factor of 0.9, (see the details in section 4.1.4). On the other hand, SEM technique allowed to identify the nanopyrimal surface structure of the Al substrate, as well as, the random network of CNTs formed on it. Furthermore, CNTs with an approximate diameter of 60 [nm] were possible to observe, (see the details in section 4.1.5). Finally, the XPS results showed the chemical evolution of the Al substrate throughout the entire process, that is, how the changes in the chemical composition of Al substrate came about before and after the surface activation process, before and after catalyst deposition and before and after calcination process, (see the details in section 4.1.6). Finally, the description of the characterization equipment is presented in 3.2.

5.3 Solar-thermal analysis

In this work, two solar-thermal analyses were performed.

Part 1: We performed a solar-thermal comparison between two devices (1%)CNTs-bap/sa-Al and (5%)CNTs-bap/sa-Al. The first one was a surface-activated Al substrate covered with at 1 wt % CNTs bap solution while the second one was a surface-activated Al substrate covered with at 5 wt % CNTs bap solution. After 3 days of analysis, it was possible to conclude that (5%)CNTs-bap/sa-Al device heats, on average, 1.08 [°C] more than (1%)CNTs-bap/sa-Al device. Therefore, the (5%)CNTs-bap/sa-Al device was chosen to be tested in part 2.

Part 2: We performed a solar-thermal analysis between the device proposed in this work (CNTs/sa-Al) and other three solar absorbers; black carbon over surface-activated aluminum (bC/sa-Al), black anticorrosive paint over aluminum (bap/Al) and carbon nanotubes black anticorrosive paint solution over surface-activated aluminum (CNTs-bap/sa-Al), the last one is the same device that was chosen in part 1. After 3 days of analysis, it was possible to conclude that CNTs-bap/sa-Al device heats, on average, 3.44 [°C] more than bap/Al device in a cloud-free day situation, 0.33 [°C] more, on cloudy periods, and 2.02 [°C] more, on a partly cloudy periods. On the other hand, due to structural damages of CNTs/sa-Al and bC/sa-Al devices, caused by the CNTs synthesis process, it is not possible to make precise conclusions about their ability to transform solar radiation into heat. Therefore, it is recommended the use of thicker Al substrates in future investigations.

The results of part 1 and 2 allows inferring that CNTs are responsible for CNTs-bap/sa-Al device reaching higher temperatures than bap/Al device. This is because CNTs allow absorbing a greater amount of solar radiation, due to multiple internal reflections and the radiation absorbing power of CNT's. This allows the material to heat up and therefore reach higher temperatures. Furthermore, in part 2 it can be concluded that the presence of clouds plays a very important role in this solar-thermal application, that is, on a cloudy day CNTs structures do not show significant improvements over conventional material, however in free-cloud days, the improvements shown by CNTs, over the conventional material, are evident This is because according to⁵⁹ clouds absorb infrared radiation from sun. An average improvement of 3.44 [°C] over the conventional material, is a very interesting number taking into account that the analyzed samples had a surface of 2x3[cm], see the details of this analysis in section 4.2 and in exergy analysis 4.3.

5.4 Theoretical exergy analysis

The theoretical exergy analysis of CNTs-bap/sa-Al vs bap/Al devices, is performed. CNTs-bap/sa-Al device was chosen to do this analysis because it shows the greater temperature contrast over the bap/Al, the reference material. This analysis allows identifying that CNTs-bap/sa-Al can produce an extra 0.023 W/cm² (on cloud-free periods) by improving the temperature increase by around four degrees. This means an additional 230 Watts per square meter of usable energy (convertible to work), see the details of this analysis in section 4.3. We can see that technological improvements to raise the temperature by one degree can result in industrially interesting power boosts for this application. Improvements can also be achieved by changing the heat capacity per unit area of the base material so that the exergy can be increased at a fixed temperature in contrast to the environment.

5.5 Outlook

We believe there is a very interesting prospect for capturing solar energy through artificial BB models. The goals for a close-knit carbon nanotubes network have only been achieved partially in this project and the results are very promising. Based on the exergy analysis we can improve on both increasing the radiation capture capacity by better growing the CNTs network on an activated substrate and we can also improve on the heat capacity of the substrate. Although the scaling to larger panels seems exciting, the feasibility of this project for industrial application lays in determining how to scale the process to panels of larger dimensions, from the point of view of the equipment needed and the cost of production. The pursuit for the 1.3 KW/m² ideal (average solar irradiation received from the sun) is on and we hope that this project serves to establish a new line of research and development at the Yachay Tech University.

Appendix A

Arduino code used in the temperature data collection

```
#include <OneWire.h>
#include <DallasTemperature.h>

// Data wire is plugged into digital pin 2 on the Arduino
#define ONE_WIRE_BUS 2

// Setup a oneWire instance to communicate with any OneWire device
OneWire oneWire(ONE_WIRE_BUS);

// Pass oneWire reference to DallasTemperature library
DallasTemperature sensors(&oneWire);

int deviceCount = 0;
float tempC;
```

Figure A.1: Arduino code - part 1

```
void setup(void)
{
  sensors.begin(); // Start up the library
  Serial.begin(9600);
  // Serial.println("CLEARDATA"); //aclarar los datos de proyectos anteriores
  // Serial.println("LABEL,INT_COLUMN");
  // locate devices on the bus
  Serial.print("Locating devices...");
  Serial.print("Found ");
  deviceCount = sensors.getDeviceCount();
  // Serial.print(deviceCount, DEC);
  // Serial.println(" devices.");
  Serial.println("");
}

void loop(void)
{
  // Send command to all the sensors for temperature conversion
  sensors.requestTemperatures();
  // Display temperature from each sensor
  for (int i = 0; i < deviceCount; i++)
  {
    //Serial.print("S");
    //Serial.print(i+1);
    Serial.print(" ");
    tempC = sensors.getTempCByIndex(i);
    Serial.print(tempC);
    //Serial.print((char)176); //shows degrees character
    //Serial.print("C | ");
    //Serial.print(DallasTemperature::toFahrenheit(tempC));
    //Serial.print((char)176); //shows degrees character
    //Serial.println("");
  }
  Serial.println("");
  delay(30000);
}
```

Figure A.2: Arduino code - part 2

Appendix B

Temperature references values

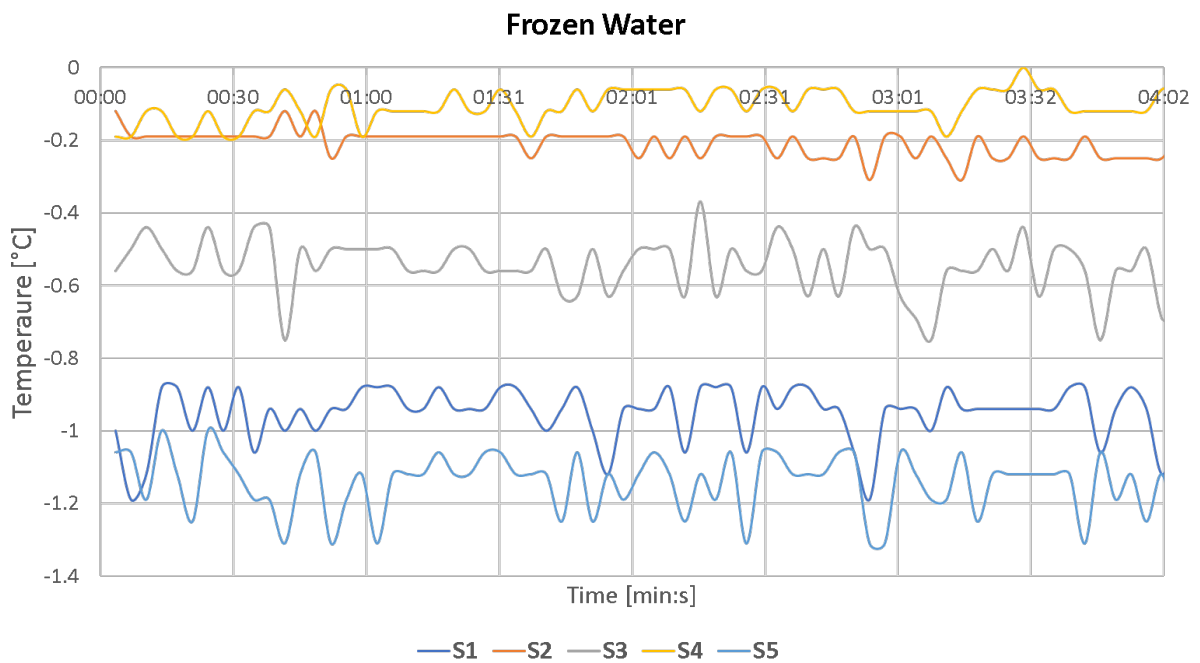


Figure B.1: Temperature measurements of frozen water. This data was used in the calibration process of the temperature sensors.

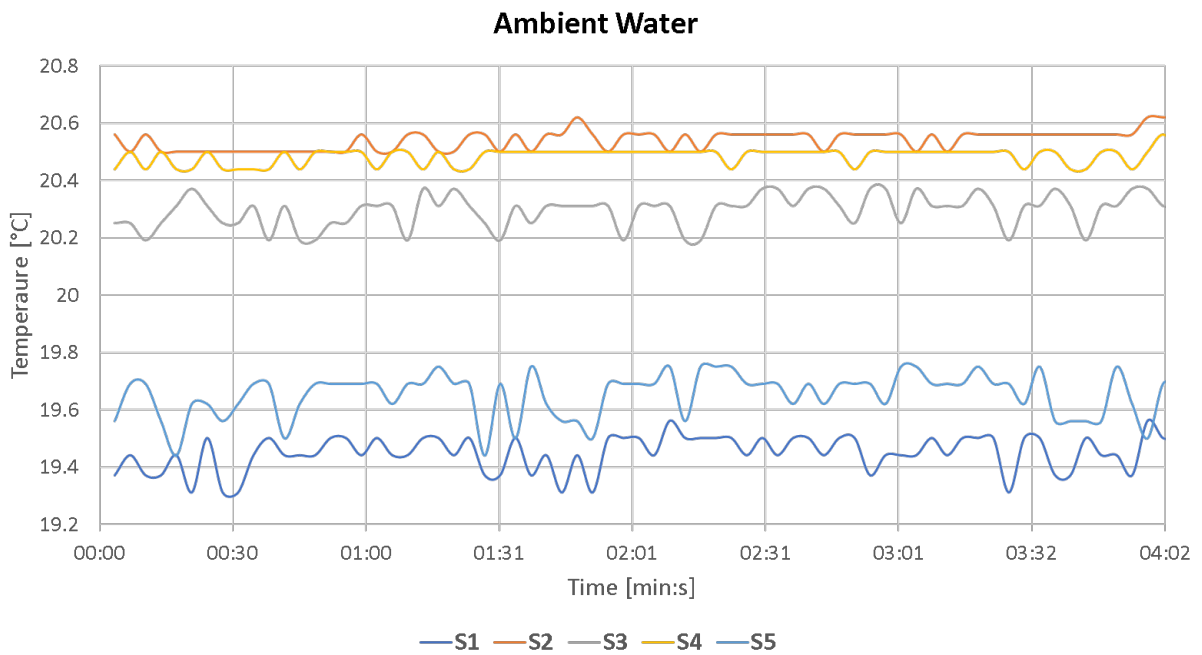


Figure B.2: Temperature measurements of water at room temperature. This data was used in the calibration process of the temperature sensors.

Appendix C

Peak-o-Math data

| par | value | error | constr. | lower | upper |
|----------|------------------|-------------------|---------|-------|-------|
| CB:const | 20.7362350933158 | 0.175450793178052 | free | nan | nan |
| LO1:amp | 18.4412563121889 | 0.564721970297096 | free | nan | nan |
| LO1:pos | 1165.86253384739 | 4.07445514970687 | free | nan | nan |
| LO1:fwhm | 219.565691096246 | 14.0717429952471 | free | nan | nan |
| LO1:area | 6191.50560259551 | | | | |
| LO2:amp | 338.849351847503 | 1.10636133380406 | free | nan | nan |
| LO2:pos | 1346.2788490046 | 0.104725419101566 | free | nan | nan |
| LO2:fwhm | 61.2713935187166 | 0.411641115183127 | free | nan | nan |
| LO2:area | 31747.2201880573 | | | | |
| LO3:amp | 22.4927821488999 | 0.84092325704249 | free | nan | nan |

Figure C.1: Positions of D, G and 2D band peak of MWCNTs synthesized under the condition of reaction (RX) "D"
- part 1

| | | | | | |
|----------|-------------------|-------------------|------|-----|-----|
| LO3:pos | 1461.71972253 | 2.18188027753056 | free | nan | nan |
| LO3:fwhm | -98.61477707313 | 9.35485030581226 | free | nan | nan |
| LO3:area | -3391.77052174554 | | | | |
| LO4:amp | 374.127103057723 | 1.84260617655307 | free | nan | nan |
| LO4:pos | 1582.28038619351 | 0.164282201757053 | free | nan | nan |
| LO4:fwhm | 50.6298267441784 | 0.499668770754477 | free | nan | nan |
| LO4:area | 28964.5575940277 | | | | |
| LO5:amp | 104.244687219652 | 2.58424811740788 | free | nan | nan |
| LO5:pos | 1618.1704360786 | 0.326573058644413 | free | nan | nan |
| LO5:fwhm | -30.8297485495231 | 1.13657909283719 | free | nan | nan |
| LO5:area | -4914.34000359718 | | | | |
| LO6:amp | 12.9777851241857 | 0.783595784782295 | free | nan | nan |
| LO6:pos | 2455.56815690064 | 2.83084170352503 | free | nan | nan |
| LO6:fwhm | 93.4011682895415 | 8.94850399299783 | free | nan | nan |
| LO6:area | 1853.54884757046 | | | | |
| LO7:amp | 226.327410369886 | 0.783418912149305 | free | nan | nan |
| LO7:pos | 2692.3526420592 | 0.160493508584223 | free | nan | nan |
| LO7:fwhm | 91.6493664653214 | 0.528224847248121 | free | nan | nan |
| LO7:area | 31718.154378219 | | | | |
| LO8:amp | 33.2067571475775 | 0.710757414186182 | free | nan | nan |
| LO8:pos | 2934.25057637261 | 1.3123060214195 | free | nan | nan |
| LO8:fwhm | 118.519121291792 | 4.81502328225314 | free | nan | nan |
| LO8:area | 6018.05532633214 | | | | |

Figure C.2: Positions of D, G and 2D band peak of MWCNTs synthesized under the condition of reaction (RX) "D"
- part 2

Appendix D

Variation of cloudiness at the test side

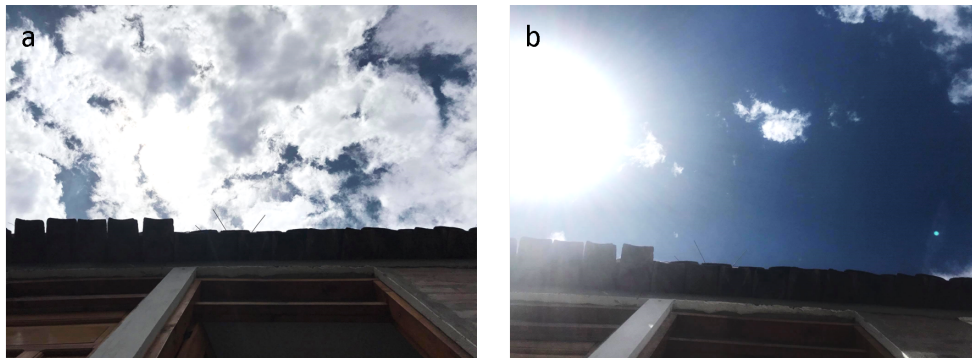


Figure D.1: Variation of cloudiness at the test side; (a) cloudy and (b) free-cloud

Bibliography

- [1] 2DegressInstitute, GLOBAL TEMPERATURE AND CO₂ LEVELS. <https://www.co2levels.org/#sources>.
- [2] CDIAC,; GCP, Annual emissions of carbon dioxide (CO) from cement, measured in tonnes. 2020; <https://ourworldindata.org/emissions-by-fuel>.
- [3] SOLAR HEAT FOR INDUTRY. 2017; <https://www.solar-payback.com/technology/>.
- [4] Iijima, S. Carbon nanotubes: past, present, and future. *Physica B: Condensed Matter* **2002**, *323*, 1–5.
- [5] Qi, X.; Guo, X.; Zheng, C. Density functional study the interaction of oxygen molecule with defect sites of graphene. *Applied Surface Science* **2012**, *259*, 195–200.
- [6] Yang, Z.-P.; Hsieh, M.-L.; Bur, J. A.; Ci, L.; Hanssen, L. M.; Wilthan, B.; Ajayan, P. M.; Lin, S.-Y. Experimental observation of extremely weak optical scattering from an interlocking carbon nanotube array. *Applied optics* **2011**, *50*, 1850–1855.
- [7] Fenn, M. B.; Xanthopoulos, P.; Pyrgiotakis, G.; Grobmyer, S. R.; Pardalos, P. M.; Hench, L. L. Raman spectroscopy for clinical oncology. *Advances in Optical Technologies* **2011**, *2011*.
- [8] Handapangoda, C. C.; Nahavandi, S.; Premaratne, M. *Nanoscale Spectroscopy with Applications*; CRC Press, 2018; pp 439–472.
- [9] of Cambridge, U. The Scanning Electron Microscope (SEM). 2021; <https://www.eng-atoms.msm.cam.ac.uk/RoyalSocDemos/SEM>.
- [10] Innovations, A. Scanning electron microscopy (SEM), what is it for? 2021; <https://www.atriainnovation.com/en/scanning-electron-microscopy-uses/>.
- [11] van de Burgt, Y. Laser-assisted growth of carbon nanotubes—A review. *Journal of Laser Applications* **2014**, *26*, 032001.
- [12] Cui, K.; Wardle, B. L. Breakdown of native oxide enables multifunctional, free-form carbon nanotube–metal hierarchical architectures. *ACS applied materials & interfaces* **2019**, *11*, 35212–35220.

- [13] Eatemadi, A.; Daraee, H.; Karimkhanloo, H.; Kouhi, M.; Zarghami, N.; Akbarzadeh, A.; Abasi, M.; Hanifehpour, Y.; Joo, S. W. Carbon nanotubes: properties, synthesis, purification, and medical applications. *Nanoscale research letters* **2014**, *9*, 1–13.
- [14] Kumanek, B.; Janas, D. Thermal conductivity of carbon nanotube networks: A review. *Journal of materials science* **2019**, *54*, 7397–7427.
- [15] Wall, G. *Encyclopedia of Energy*; Elsevier Inc., 2004; Vol. 2.
- [16] Szabó, A.; Perri, C.; Csató, A.; Giordano, G.; Vuono, D.; Nagy, J. B. Synthesis methods of carbon nanotubes and related materials. *Materials* **2010**, *3*, 3092–3140.
- [17] Arrhenius, S. XXXI. On the influence of carbonic acid in the air upon the temperature of the ground. *The London, Edinburgh, and Dublin Philosophical Magazine and Journal of Science* **1896**, *41*, 237–276.
- [18] Ballesteros, H. O. B.; Aristizabal, G. L. Información técnica sobre gases de efecto invernadero y el cambio climático. *Bogotá DC: nota técnica del IDEAM* **2007**,
- [19] Jones, P.; Harpham, C. Estimation of the absolute surface air temperature of the Earth. *Journal of Geophysical Research: Atmospheres* **2013**, *118*, 3213–3217.
- [20] Betts, R. Met Office: Atmospheric CO2 now hitting 50% higher than pre-industrial levels. 2021; MetOffice: AtmosphericCO2nowhitting50%higherthanpre-industriallevels.
- [21] Mats, I. Revolution of Solar Energy Isa Mats, Ruben Lynn and Van Jasimjn Stenden University of Applied Sciences, Netherlands.
- [22] Tsao, J.; Lewis, N.; Crabtree, G. Solar faqs. *US department of Energy* **2006**, *13*.
- [23] Alghoul, M.; Sulaiman, M.; Azmi, B.; Wahab, M. A. Review of materials for solar thermal collectors. *Anti-Corrosion methods and materials* **2005**,
- [24] Masson-Delmotte, P. Z. H.-O. P. D. R. J. S. P. S. A. P. W. M.-O. C. P. R. P. S. C. J. M. Y. C. X. Z. M. G. E. L. T. M. M. T., V.; (eds.), T. W. IPCC, 2018: Summary for Policymakers. In: Global Warming of 1.5°C. An IPCC Special Report on the impacts of global warming of 1.5°C above pre-industrial levels and related global greenhouse gas emission pathways, in the context of strengthening the global response to the threat of climate change, sustainable development, and efforts to eradicate poverty. 2021; <https://www.ipcc.ch/sr15/chapter/spm/>, World Meteorological Organization, Geneva, Switzerland, 32 pp.
- [25] Meyer, F.; Raquez, J.-M.; Coulembier, O.; De Winter, J.; Gerbaux, P.; Dubois, P. Imidazolium end-functionalized poly (L-lactide) for efficient carbon nanotube dispersion. *Chemical communications* **2010**, *46*, 5527–5529.
- [26] Rafiee, R.; Pourazizi, R. Evaluating the influence of defects on the young's modulus of carbon nanotubes using stochastic modeling. *Materials Research* **2014**, *17*, 758–766.

- [27] Das, S. A review on Carbon nano-tubes-A new era of nanotechnology. *International Journal of Emerging Technology and Advanced Engineering* **2013**, *3*, 774–783.
- [28] Ossila, Multi-Walled Carbon Nanotubes. 2021; <https://www.ossila.com/products/multi-walled-carbon-nanotubes>.
- [29] Cumings, J.; Zettl, A. Low-friction nanoscale linear bearing realized from multiwall carbon nanotubes. *science* **2000**, *289*, 602–604.
- [30] others,, *et al.* Thermal conductivity of multiwalled carbon nanotubes. *Physical Review B* **2002**, *66*, 165440.
- [31] Berber, S.; Kwon, Y.-K.; Tománek, D. Unusually high thermal conductivity of carbon nanotubes. *Physical review letters* **2000**, *84*, 4613.
- [32] Sam, A.; Hartkamp, R.; Kumar Kannam, S.; Babu, J. S.; Sathian, S. P.; Daivis, P. J.; Todd, B. Fast transport of water in carbon nanotubes: a review of current accomplishments and challenges. *Molecular Simulation* **2020**, 1–20.
- [33] Prasadam, V. P.; Gautier, N.; Bahlawane, N. CNT Nanoengineering for Thermally Stable Selective Solar Absorption. *Materials Today Communications* **2021**, 102552.
- [34] Vinetsky, Y.; Jambu, J.; Mandler, D.; Magdassi, S. Cnt-based solar thermal coatings: Absorptance vs. emittance. *Coatings* **2020**, *10*, 1101.
- [35] Chalk, S. J. The IUPAC Gold Book website. **2019**,
- [36] McQuarrie, D. A.; Simon, J. D. Physical Chemistry: A Molecular Approach. **1998**, 31.
- [37] Hoecker, C.; Smail, F.; Pick, M.; Boies, A. The influence of carbon source and catalyst nanoparticles on CVD synthesis of CNT aerogel. *Chemical Engineering Journal* **2017**, *314*, 388–395.
- [38] Andrade, J. D. *Surface and interfacial aspects of biomedical polymers*; Springer, 1985; pp 105–195.
- [39] GmbH, A. P. How can Raman spectroscopy help you? 2021; <https://wiki.anton-paar.com/be-fr/notions-de-base-de-la-spectroscopie-raman/applications-en-spectroscopie-raman/>.
- [40] Mohammed, A.; Abdullah, A. Scanning electron microscopy (SEM): A review. 2018.
- [41] Stokes, D. *Principles and practice of variable pressure/environmental scanning electron microscopy (VP-ESEM)*; John Wiley & Sons, 2008.
- [42] Hoyos-Palacio, L.; García, A.; Pérez-Robles, J.; González, J.; Martínez-Tejada, H. Catalytic effect of Fe, Ni, Co and Mo on the CNTs production. 2014.
- [43] Chai, S.-P.; Zein, S. H. S.; Mohamed, A. R. The effect of catalyst calcination temperature on the diameter of carbon nanotubes synthesized by the decomposition of methane. *Carbon* **2007**, *45*, 1535–1541.

- [44] Isravel, R. S.; Saravanan, S.; Vijayan, V. A review of material and coatings in solar collectors. *Materials Today: Proceedings* **2020**, *21*, 497–499.
- [45] Ming, F.; Chen, L.; Li, D.; Du, C. Investigation into Freezing Point Depression in Soil Caused by NaCl Solution. *Water* **2020**, *12*.
- [46] Choi, Y. C.; Min, K.-I.; Jeong, M. S. Novel method of evaluating the purity of multiwall carbon nanotubes using raman spectroscopy. *Journal of Nanomaterials* **2013**, *2013*.
- [47] XPS, T. S. Carbon. 2021; <https://www.jp.xpssimplified.com/elements/carbon.php>.
- [48] XPS, T. S. Oxygen. 2021; <https://www.jp.xpssimplified.com/elements/oxygen.php>.
- [49] XPS, T. S. Aluminum. 2021; <https://www.jp.xpssimplified.com/elements/aluminum.php>.
- [50] XPS, T. S. Sodium. 2021; <https://www.jp.xpssimplified.com/elements/sodium.php>.
- [51] XPS, T. S. Cobalt. 2021; <https://www.jp.xpssimplified.com/elements/cobalt.php#aboutthiselement>.
- [52] XPS, T. S. Nitrogen. 2021; <https://www.jp.xpssimplified.com/elements/nitrogen.php>.
- [53] Fedoseeva, Y. V.; Bulusheva, L.; Okotrub, A.; Kanygin, M.; Gorodetskiy, D.; Asanov, I.; Vyalikh, D.; Puzyr, A.; Bondar, V. Field emission luminescence of nanodiamonds deposited on the aligned carbon nanotube array. *Scientific reports* **2015**, *5*, 1–7.
- [54] Sadri, R.; Hosseini, M.; Kazi, S.; Bagheri, S.; Zubir, N.; Solangi, K.; Zaharinie, T.; Badarudin, A. A bio-based, facile approach for the preparation of covalently functionalized carbon nanotubes aqueous suspensions and their potential as heat transfer fluids. *Journal of colloid and interface science* **2017**, *504*, 115–123.
- [55] Okpalugo, T.; Papakonstantinou, P.; Murphy, H.; McLaughlin, J.; Brown, N. High resolution XPS characterization of chemical functionalised MWCNTs and SWCNTs. *Carbon* **2005**, *43*, 153–161.
- [56] Hou, P.; Bai, S.; Yang, Q.; Liu, C.; Cheng, H. Multi-step purification of carbon nanotubes. *Carbon* **2002**, *40*, 81–85.
- [57] Miller, D.; Biesinger, M.; McIntyre, N. Interactions of CO₂ and CO at fractional atmosphere pressures with iron and iron oxide surfaces: one possible mechanism for surface contamination? *Surface and Interface Analysis: An International Journal devoted to the development and application of techniques for the analysis of surfaces, interfaces and thin films* **2002**, *33*, 299–305.
- [58] Lee, J.-M.; Kim, S. J.; Kim, J. W.; Kang, P. H.; Nho, Y. C.; Lee, Y.-S. A high resolution XPS study of sidewall functionalized MWCNTs by fluorination. *Journal of Industrial and Engineering Chemistry* **2009**, *15*, 66–71.
- [59] Observatory, N. E. Clouds & Radiation. 2021; <https://earthobservatory.nasa.gov/features/Clouds>.

- [60] Dragulin, D.; R  ther, M. Specific heat capacity of alu-minium and aluminium alloys. *Heat. Process.* **2018**, *3*, 81–85.

Abbreviations

bap black anticorrosive paint 33

bap/Al black anticorrosive paint over aluminum 6, 64

bC black Carbon 33

bC/sa-Al black carbon over surface-activated aluminum 6, 64

CNTs Carbon Nanotubes 6

CNTs-bap/sa-Al carbon nanotubes black anticorrosive paint solution over surface-activated aluminum 6, 64

CNTs/sa-Al carbon nanotubes over a surface-activated aluminum 6

CVD Chemical Vapor Deposition 11

MWCNTs Multi-Wall Carbon Nanotubes 9

NPs nanoparticles xiv, 27

S-W Stone-Wales structural defects 10

SEM Scanning Electron Microscopy x, 6, 32, 48, 64

SWCNTs Single-Wall Carbon Nanotubes 9

VA-CNTs Vertically Aligned Carbon Nanotubes 16

XPS X-ray Photoelectron Spectrometer x, 6, 32, 48, 64